

Aus der
Universitätsklinik für Anaesthesiologie und Intensivmedizin

Inaugural-Dissertation

**Multidimensional suppression of acute pulmonary
inflammation by the leukotriene modifiers Montelukast and
Zileuton**

**zur Erlangung des Doktorgrades
der Medizin**

**der Medizinischen Fakultät
der Eberhard Karls Universität
zu Tübingen**

vorgelegt von

Zhang, Yi

2023

Dekan: Professor Dr. B. Pichler

1. Berichterstatter Privatdozentin Dr. F. Konrad
2. Berichterstatter: Professor Dr. T. Bakchoul

Tag der Disputation: 11.07.2023

Contents

CONTENTS.....	I
LIST OF FIGURES	IV
LIST OF TABLES	VI
LIST OF ABBREVIATIONS	VII
1 INTRODUCTION	1
1.1 ACUTE RESPIRATORY DISTRESS SYNDROME (ARDS).....	1
1.1.1 Definition of ARDS	1
1.1.2 Epidemiology.....	2
1.1.3 Etiology	3
1.1.4 Pathophysiology and clinical presentation.....	4
1.1.5 Therapy.....	5
1.1.5.1 Non-pharmacological treatments	5
1.1.5.2 Pharmacological treatments.....	6
1.1.6 Animal models of acute respiratory distress syndrome (ARDS).....	6
1.2 ROLE OF NEUTROPHILS IN ACUTE RESPIRATORY DISTRESS SYNDROME (ARDS).....	7
1.2.1 Migration of neutrophils	7
1.2.2 Platelet–neutrophil complexes (PNCs).....	10
1.2.3 Neutrophil oxidative stress	11
1.3 ROLE OF LEUKOTRIENES IN NEUTROPHIL ACTIVITY	11
1.3.1 Chemotaxis of neutrophils by leukotrienes.....	12
1.3.2 Leukotrienes enhance neutrophil adhesion to the endothelium	13
1.3.3 Leukotriene pathway and reactive oxygen species (ROS).....	13
1.4 LEUKOTRIENE MODIFIERS	14
1.5 QUESTIONS.....	14
2 MATERIALS AND METHODS	15
2.1 OVERVIEW	15
2.2 ANIMAL MODEL	16
2.2.1 Mice.....	16
2.2.2 Pulmonary inflammation model	16
2.3 GROUPING AND TREATMENTS	17
2.4 PMN COUNTS AND ADHESION MOLECULES	18
2.4.1 Sampling and preparation	18
2.4.2 Flow cytometry	22
2.5 PNC DETERMINATION	23
2.6 PMN TRAFFICKING IN EACH COMPARTMENT	24
2.6.1 Bone marrow.....	24
2.6.2 Blood.....	25
2.6.3 Lung.....	26

2.7	LEUKOTRIENE AND CYTOKINE DETERMINATION.....	26
2.7.1	Gene expression investigation by RT-qPCR.....	26
2.7.1.1	RNA isolation from murine lung.....	26
2.7.1.2	RNA concentration measurement.....	27
2.7.1.3	cDNA synthesis.....	27
2.7.1.4	RT-qPCR.....	28
2.7.2	ELISA.....	30
2.7.3	Immunofluorescence assay.....	31
2.8	IMMUNOHISTOCHEMISTRY.....	34
2.9	ROS DETECTION.....	35
2.10	MICROVASCULAR PERMEABILITY DETERMINED BY THE BCA ASSAY.....	35
2.11	PHAMTARGET AND SEARCH TOOL FOR THE RETRIEVAL OF INTERACTING GENES/PROTEINS (STRING) ANALYSIS.....	36
2.12	PLATELET ISOLATION.....	37
2.13	STATISTICS.....	38
2.14	LIST OF MATERIALS.....	39
2.14.1	Chemicals and reagents.....	39
2.14.2	Biochemical supplies.....	40
2.14.3	Enzyme.....	40
2.14.4	Solutions.....	40
2.14.5	Primer for the RT-qPCR.....	41
2.14.6	FACS-Antibody.....	42
2.14.7	Immunofluorescence staining.....	43
2.14.8	Materials.....	43
2.14.9	Devices.....	45
2.14.10	Software.....	46
3	RESULTS.....	47
3.1	MIGRATION OF NEUTROPHILS WAS DAMPENED BY MONTELUKAST AND ZILEUTON.....	47
3.1.1	Neutrophils were decreased in each pulmonary compartment.....	47
3.1.2	Neutrophil release was restrained in bone marrow.....	49
3.2	ADHESION MOLECULES WERE AFFECTED BY MONTELUKAST AND ZILEUTON..	52
3.3	INFLAMMATORY RESPONSES WERE INHIBITED BY MONTELUKAST AND ZILEUTON	56
3.3.1	Platelet–neutrophil complex formation was blocked by montelukast and zileuton.....	56
3.3.2	Reactive oxygen species production was reduced by montelukast and zileuton.....	57
3.3.3	Inflammatory chemokines were suppressed by montelukast and zileuton.....	58
3.4	LEUKOTRIENE PATHWAY WAS REPRESSED BY MONTELUKAST AND ZILEUTON	59
3.5	PHARMACOLOGICAL FINDINGS OF MONTELUKAST AND ZILEUTON.....	63

3.5.1	<i>Potential target proteins interaction network of montelukast and zileuton.....</i>	63
3.5.2	<i>Biological processes and molecular functions involved with montelukast and zileuton.....</i>	66
3.5.3	<i>Signaling pathway of montelukast and zileuton.....</i>	68
3.5.4	<i>Platelet activation is inhibited by montelukast and zileuton.....</i>	74
3.5.5	<i>Other features of montelukast and zileuton.....</i>	76
4	<i>DISCUSSION</i>	78
4.1	<i>MONTELUKAST AND ZILEUTON IMPAIR NEUTROPHIL MIGRATION MECHANISMS</i>	78
4.1.1	<i>Adhesion patterns</i>	78
4.1.2	<i>SDF-1/CXCR4 and bone marrow neutrophil release</i>	83
4.2	<i>MONTELUKAST AND ZILEUTON WEAKEN INFLAMMATORY RESPONSES</i>	84
4.2.1	<i>Chemokine release</i>	84
4.2.2	<i>PNC formation.....</i>	88
4.2.3	<i>ROS production.....</i>	89
4.3	<i>APPLICATION OF MONTELUKAST AND ZILEUTON.....</i>	89
5	<i>SUMMARY</i>	91
6	<i>ZUSAMMENFASSUNG</i>	93
7	<i>BIBLIOGRAPHY.....</i>	95
8	<i>DECLARATION OF CONTRIBUTIONS.....</i>	109
9	<i>ACKNOWLEDGEMENTS.....</i>	110

List of figures

FIGURE-1: TRANS-ENDOTHELIAL MIGRATION OF NEUTROPHILS (SIMPLIFIED).....	8
FIGURE-2: INTERACTIONS WITHIN AND BETWEEN PLATELET–NEUTROPHIL COMPLEXES (PNCs) AND THE ENDOTHELIUM.	10
FIGURE-3: LEUKOTRIENE SYNTHESIS.	12
FIGURE-4: OVERVIEW OF THE METHODS USED IN THIS DISSERTATION.	15
FIGURE-5: LPS INHALATION PROCESS.	17
FIGURE-6: GATING STRATEGY OF THE POLYMORPHONUCLEAR NEUTROPHIL (PMN) ANALYSIS.....	23
FIGURE-7: GATING STRATEGY OF THE PLATELET–NEUTROPHIL COMPLEX (PNC) ANALYSIS.....	24
FIGURE-8: BLOOD SMEAR PREPARATION.	25
FIGURE-9: TEMPERATURE CYCLE OF REAL-TIME QUANTITATIVE POLYMERASE CHAIN REACTION (RT-QPCR).	28
FIGURE-10: PRINCIPLE OF A SANDWICH ENZYME-LINKED IMMUNOSORBENT ASSAY (ELISA).	30
FIGURE-11: OVERVIEW OF IMMUNOFLUORESCENCE PROCESS.	32
FIGURE-12: FLOW CHART OF TARGET PROTEIN ANALYSIS.	36
FIGURE-13: IMMUNOHISTOCHEMICAL STAINING OF THE PULMONARY TISSUE AT INDICATED CONDITIONS.	47
FIGURE-14: THE EFFECTS OF MONTELUKAST AND ZILEUTON ON THE MIGRATION OF NEUTROPHILS INTO DIFFERENT COMPARTMENTS.	49
FIGURE-15: NEUTROPHIL RELEASE WAS SIGNIFICANTLY RESTRAINED BY MONTELUKAST AND ZILEUTON IN BONE MARROW	51
FIGURE-16: IMPACT OF MONTELUKAST AND ZILEUTON ON THE EXPRESSION OF ADHESION MOLECULES ON PMNS IN LUNG COMPARTMENTS.	54
FIGURE-17: THE ROLES OF MONTELUKAST AND ZILEUTON IN PLATELET–NEUTROPHIL COMPLEX (PNC) FORMATION.	56
FIGURE-18: THE ROLES OF MONTELUKAST AND ZILEUTON IN REACTIVE OXYGEN SPECIES (ROS) PRODUCTION.....	57
FIGURE-19: THE EFFECTS OF MONTELUKAST AND ZILEUTON ON INFLAMMATORY CHEMOKINE RELEASE.....	58
FIGURE-20: EFFECTS OF MONTELUKAST AND ZILEUTON ON THE EXPRESSION OF LEUKOTRIENE PATHWAY–RELATED GENES.	59
FIGURE-21: EXPRESSION OF THE LEUKOTRIENE RECEPTORS CysLTR1 AND LTB4R1 ON MURINE LUNG PMNS.	60
FIGURE-22: EXPRESSION OF THE LEUKOTRIENE RECEPTORS CysLTR1 AND LTB4R1 ON MURINE ENDOTHELIUM.	61

FIGURE-23: EXPRESSION OF THE LEUKOTRIENE RECEPTORS CysLTR1 AND LTB4R1 ON THE MURINE EPITHELIUM.	62
FIGURE-24: TWO-DIMENSIONAL (2D) AND THREE-DIMENSIONAL (3D) STRUCTURES OF MONTELUKAST AND ZILEUTON.	63
FIGURE-25: THE PROTEIN–PROTEIN INTERACTION (PPI) NETWORK OF MONTELUKAST AND ZILEUTON.	65
FIGURE-26: VISUAL REPRESENTATION OF PROTEIN–PROTEIN INTERACTIONS (PPIs) FOR PHARMTARGET NETWORKS.	66
FIGURE-27: GENE ONTOLOGY (GO) FUNCTIONAL CLASSIFICATION OF MONTELUKAST.	67
FIGURE-28: GENE ONTOLOGY (GO) FUNCTIONAL CLASSIFICATION OF ZILEUTON.	68
FIGURE-29: SIGNALING PATHWAY INVOLVED WITH MONTELUKAST.	69
FIGURE-30: SIGNALING PATHWAY INVOLVED WITH ZILEUTON.	70
FIGURE-31: CHEMOKINE SIGNALING PATHWAY FROM THE KYOTO ENCYCLOPEDIA OF GENES AND GENOMES (KEGG).	71
FIGURE-32: EXPRESSION OF THE ERK1/2 AND PCREB ON MURINE PMNs.	73
FIGURE-33: EXPRESSION OF THE PCREB ON MURINE LUNG ENDOTHELIUM AND EPITHELIUM.	74
FIGURE-34: GENE EXPRESSION OF TBXAS1 IN MURINE LUNG AND PROTEIN EXPRESSION OF P2Y12 ON ISOLATED PLATELETS.	76
FIGURE-35: GENE EXPRESSION OF MMP3 AND MMP9 AND PROTEIN LEVEL OF CASPASE-1 AND IL-1B ON MURINE PMNs.	77
FIGURE-36: ANTI-INFLAMMATORY FUNCTIONS OF MONTELUKAST AND ZILEUTON IN THIS STUDY.	90

List of tables

TABLE-1: KIGALI MODIFICATION OF THE BERLIN CRITERIA.....	2
TABLE-2: MEDICATION INFORMATION.....	17
TABLE-3: ANESTHETIC COMPOSITION.....	18
TABLE-4: COMPOSITION OF THE ENZYME SOLUTION FOR DIGESTING THE LUNG TISSUE.	19
TABLE-5: COMPOSITION OF THE STAINING BUFFER (FOR 1 LITER).	20
TABLE-6: COMPOSITION OF THE ERYTHROCYTE LYSIS BUFFER FOR ORGANS (FOR 1 LITER).	20
TABLE-7: ANTIBODY MIXES USED ON FLOW CYTOMETRIC ANALYSIS.....	21
TABLE-8: ANTIBODY MIXES USED FOR BONE MARROW ANALYSIS.	25
TABLE-9: MOUSE PRIMERS FOR REAL-TIME QUANTITATIVE POLYMERASE CHAIN REACTION AND THEIR MELTING TEMPERATURES (FOR SEQUENCES, SEE CHAPTER 2.14.5).	29
TABLE-10: ALCOHOL SERIES FOR DEWAXING IMMUNOFLUORESCENT SPECIMENS.....	32
TABLE-11: ANTIBODIES USED FOR IMMUNOFLUORESCENCE.	33
TABLE-12: OVERVIEW OF THE SIGNIFICANCES.....	38

List of abbreviations

12-HETE	Hydroxyeicosatetenoic acid
2D	Two-dimensional
3D	Three-dimensional
5-LO	5-lipoxygenase
AA	Arachidonic acid
ABTS	2,2'-Azino-bis(3-ethylbenzthiazoline-6-sulfonic acid)
ADCC	Antibody-dependent cellular cytotoxicity
AECC	American-European Consensus Conference
ALI	Acute lung injury
Alox5	Arachidonate 5-Lipoxygenase
ANOVA	Analysis of variance
ARDS	Acute respiratory distress syndrome
BAL	Bronchoalveolar lavage
BCA	Bicinchoninic acid
BP	Biological process
BSA	Bovines Serum albumin
cAMP	3',5'-cyclic adenosine monophosphate
cDNA	complementary DNA
Covid-19	Coronavirus disease 2019
COX1/2	Cyclooxygenase 1 and 2
CXCL1	C-X-C Motif Chemokine Ligand 1
CXCL2/3	C-X-C Motif Chemokine Ligand 2/3
CysLTR1	Cysteinyl Leukotriene Receptor 1
CysLTR2	Cysteinyl Leukotriene Receptor 2
CysLTs	Cysteinyl leukotrienes
DAD	Diffuse alveolar damage
DAVID	The Database for Annotation, Visualization, and Integrated Discovery
DHE	Dihydroacetylene
ECMO	Extracorporeal membrane oxygenation
ELISA	Enzyme-linked immunosorbent assay
ERK 1/2	Extracellular signal-regulated kinase 1/2
EVs	Extracellular vesicles
FACS	Fluorescence-activated cell sorting
FDA	Food and Drug Administration
FLIP	5-LO activating protein
FMO	Fluorescence minus one
FSC	Forward scattering
GO	Gene ontology
GRO α	Growth-related oncogene α
GSK3	Glycogen synthase kinase-3
H ₂ O ₂	Hydrogen peroxide
HPF	High-power fields
HRP	Horseradish Peroxidase
ICAM	Intercellular Adhesion Molecule
ICU	Intensive Care Unit
IL-1 β	Interleukin-1 β

IL-6	Interleukin-6
KC	Keratinocytes-derived chemokine
KEGG	The Kyoto Encyclopedia of Genes and Genomes
LFA-1	Lymphocyte function-associated antigen 1
LPS	Lipopolysaccharides
LT	Leukotriene
LTA4	Leukotriene A4
LTA4H	Leukotriene A4 Hydrolase
LTB4	Leukotriene B4
LTB4R1	Leukotriene B4 receptor 1
LTC4	Leukotriene C4
LTC4H	Leukotriene C4 hydrolase
LTC4S	Leukotriene C4 Synthase
LTD4	Leukotriene D4
Mac-1	Macrophage-1 antigen
MAPK	Mitogen-activated protein kinase
MF	Molecular function
MFI	Mean fluorescence intensity
MIP-2	Macrophage Inflammatory Protein-2
MMP	Matrix metalloproteinase
MPO	Myeloperoxidase
NADPH	Nicotinamide-adenine dinucleotide phosphate
NE	Neutrophil elastase
NETs	Neutrophil extracellular traps
NFW	Nuclease-free water
NTC	Non-template control
PAMPs	Pathogen-associated molecular patterns
PaO ₂ /FiO ₂	The ratio of arterial partial pressure to a fraction of inspired oxygen
PBS ⁻	Phosphate-buffered saline minus
PDE4B	Phosphodiesterase 4B
PDE4D	Phosphodiesterase 4D
PECAM-1	Platelet endothelial cell adhesion molecule-1
PEEP	Positive end-expiratory pressure
PGH2	Prostaglandin H2
PI3K	Phosphatidylinositol 3-kinase
PKA	Protein kinase A
PLA2	Phospholipase A2
PMN	Polymorphonuclear neutrophil
PNC	Platelet-neutrophil complex
PRRs	Pattern recognition receptors
PSGL-1	P-selectin glycoprotein ligand-1
ROS	Reactive oxygen species
RT-qPCR	Real-time quantitative polymerase chain reaction
SDF-1	Stromal cell-derived factor 1
SEM	Standard error of the mean
SSC	Side scattering
Tbxas1	Thromboxane A Synthase 1
TMP	Tetramethylbenzidine

TNF- α	Tumor necrosis factor α
TREM-1	Triggering receptor expressed on myeloid cells 1
TXA2	Thromboxane A2
VCAM-1	Vascular cell adhesion molecule 1
VEGF	Vascular endothelial growth factor
VLA-4	Very late antigen-4
WASP	Wiskott-Aldrich Syndrome protein

1 Introduction

1.1 Acute respiratory distress syndrome (ARDS)

1.1.1 Definition of ARDS

The concept of ARDS was first introduced in 1967 (Ashbaugh et al., 1967). It was initially described as a syndrome characterized by hypoxemia and unresponsive to common respiratory therapy.

In 1994, the definition of ARDS was revised by the American-European Consensus Conference (AECC) (Bernard et al., 1994); it was defined as hypoxemia of acute onset, a ratio of arterial partial pressure of oxygen to the fraction of inspired oxygen ($\text{PaO}_2/\text{FiO}_2$) ≤ 200 mmHg, bilateral pulmonary infiltrates, and no evidence of left atrial hypertension. At the same time, a new classification, acute lung injury (ALI), was introduced, which used similar diagnostic criteria but a slightly less stringent $\text{PaO}_2/\text{FiO}_2$ of ≤ 300 mmHg.

As this disease continues to be studied in-depth, the definition of ARDS has been described more clearly, and the Berlin definition, updated in 2012, has been widely adopted (ARDS Definition Task Force et al., 2012). It proposes three different classifications of ARDS according to the degree of hypoxemia: mild ($200 \text{ mmHg} < \text{PaO}_2/\text{FiO}_2 \leq 300 \text{ mmHg}$), moderate ($100 \text{ mmHg} < \text{PaO}_2/\text{FiO}_2 \leq 200 \text{ mmHg}$), and severe ($\text{PaO}_2/\text{FiO}_2 \leq 100 \text{ mmHg}$). Radiographic severity, positive end-expiratory pressure ($\geq 10 \text{ cmH}_2\text{O}$), respiratory system compliance ($\leq 40 \text{ ml/cmH}_2\text{O}$), and corrected expired volume per minute ($\geq 10 \text{ l/min}$) are four auxiliary diagnostic parameters for severe ARDS.

It has been argued that although the Berlin definition is a reliable and reproducible tool for identifying ARDS, the relatively demanding diagnostic indexes make it inapplicable in low-income countries, thus reducing the diagnostic rate of ARDS in these areas. Therefore, the ARDS diagnosis has been improved in medically underserved areas (Table-1) (Riviello et al., 2016).

Table-1: Kigali modification of the Berlin Criteria.

	Kigali Modification of the Berlin Criteria
Timing	Within one week of a new or worsening respiratory symptoms or known clinical insult.
Oxygenation	$SpO_2/FiO_2 \leq 315$
PEEP requirement	Positive end-expiratory pressure (PEEP) is not required.
Chest imaging	In chest radiographs or ultrasounds, bilateral opacities are not entirely explained by effusions, lobar/lung collapse, or nodules.
Origin of edema	Fluid overload or cardiac failure does not fully explain respiratory failure (echocardiography is needed to exclude hydrostatic edema if no risk factors are present).

1.1.2 Epidemiology

In addition to the high mortality rate of ARDS, it also has a very high incidence. In 1999, a prospective, population-based cohort study was conducted at 21 Washington, D.C. hospitals to identify patients who met consensus criteria for ALI and ARDS (Rubenfeld et al., 2005). Based on 15 months of follow-up of 1113 patients, the incidence of ARDS was 58.7 per 100,000 people per year. The in-hospital mortality rate was 38.5%. The incidence of ARDS increased with age, from 16 per 100,000 people per year aged 15–19 years to 306 per 100,000 people per year aged 75–84 years. The mortality rates increased with age, from 24% in patients aged 15–19 years to 60% in patients ≥ 85 years.

A multicenter joint study was completed in 2016 with 29,144 patients in 50 countries (Bellani et al., 2016). Approximately 10%–15% of inpatients and up to 23% of mechanically ventilated patients in the intensive care unit (ICU) fulfilled the ARDS criteria. The concurrent prevalence of mild ARDS in the ICU was 30.0%, 46.6% for moderate ARDS, and 23.4% for severe ARDS. The in-hospital mortality rate was 34.9% for mild ARDS patients, 40.3% for moderate ARDS patients, and 46.1% for severe ARDS patients (Bellani et al., 2016).

This syndrome appears to be under-recognized and under-treated, resulting in high mortality. These findings suggest a necessity for improvement in the treatment of patients with ARDS.

1.1.3 Etiology

ARDS is a heterogeneous-cause syndrome. Over 60 causes of ARDS have been identified (Siegel, 2016). Nevertheless, the vast majority of ARDS arises from some of the most common causes listed below.

Sepsis – Sepsis is a severe and widespread bloodstream infection and the primary cause of ARDS (Doyle et al., 1995; Fein et al., 1983; Hudson et al., 1995; Pepe et al., 1982), which accounts for 32% of ARDS cases (Bersten et al., 2002).

Aspiration pneumonia or community-acquired pneumonia – There is evidence that nearly one-third of hospitalized patients with pulmonary aspiration of gastric contents develop ARDS (Fowler et al., 1983; Pepe et al., 1982; Tietjen et al., 1994). Community-acquired pneumonia represents a widespread risk for developing ARDS outside of the hospital (Mannes et al., 1991).

Coronavirus disease 2019 (Covid-19) – To date, Covid-19 has resulted in 512 million infections and 6.24 million deaths (World Health Organization, 2022). Almost all of these deaths share the same characteristics: their deaths almost always started, progressed to, or ended in ARDS. In 2020, a report of 17 studies of 2486 hospitalized patients with Covid-19 from five countries found that approximately one-third had ARDS. Of the patients with Covid-19 transferred to the ICU, three-fourths had ARDS. The incidence of ARDS in non-surviving patients was 90% (Tzotzos et al., 2020).

Severe trauma – A 30-year historical retrospective study analyzing 43 clinical studies showed that the incidence of ARDS after severe trauma is about 10% (Pfeifer et al., 2017). Bilateral lung contusions or extensive tissue injuries may predispose or contribute to ARDS (Moore et al., 1993; Sutyak et al., 2007).

Other risk factors – Include but are not limited to transfusion-related acute lung injury (Bux and Sachs, 2007), severe acute pancreatitis (Zhou et al., 2010), smoking, and alcohol consumption (Iribarren et al., 2000).

1.1.4 Pathophysiology and clinical presentation

The pathology of ARDS is characterized by alveolar capillary permeability, pulmonary edema formation, reduced compliance, decreased alveolar clearance, and alveolar collapse (Swenson and Swenson, 2021). It is pathologically divided into three clinical stages (Tomashefski, 1990), named exudative, proliferative, and fibrotic phases.

Exudative phase – The early stage is characterized by diffuse alveolar damage (DAD) within 7–10 days. The first three days show significant protein-rich alveolar edema followed by alveolar type II cell hyperplasia and the pulmonary hyaline membrane begins to develop (Katzenstein and Askin, 1982; Katzenstein et al., 1986). However, diffuse alveolar damage is not specific, and more studies are needed to confirm whether this damage could be used to predict prognosis or determine treatment strategies (Siegel, 2019). The clinical presentation at this stage is hypoxemia requiring moderate-to-high oxygen concentrations and positive end-expiratory pressure. Imaging shows bilateral alveolar infiltrates and diffuse crackles (Rubenfeld et al., 1999).

Proliferative phase – This phase occurs after about 7–10 days, with apparent interstitial inflammation, fibrosis, and healing dysfunction: Pulmonary edema disappears, but along with type II alveolar cell hyperplasia, neutrophil and macrophage immigration, squamous epithelial metaplasia, myofibroblastic interstitial infiltration, and early collagen deposition. This phase lasts about 2–3 weeks. Clinically, it presents with increasing hypoxemia, low pulmonary compliance, high dead space, and sometimes progressive pulmonary hypertension. Imaging shows the progression from diffuse crackles to rough reticular pulmonary infiltrates (Siegel, 2019).

Fibrotic phase – Patients who survive the proliferative phase progress to a prolonged fibrotic stage with varying degrees of fibrosis of the lung tissue, occlusion of typical lung structures, and cyst formation. Clinical symptoms of hypoxemia and pulmonary infiltrate gradually improve over weeks to months.

1.1.5 Therapy

Therapy for ARDS is generally aimed at providing respiratory support, improving blood oxygen levels, and attempting to correct the causes of the disease (Standiford and Ward, 2016). The therapy for ARDS can be divided into non-pharmacological supportive treatment and pharmacological treatment.

1.1.5.1 Non-pharmacological treatments

Ventilation – One of the underlying causes of death in ARDS is hypoxia, so providing adequate blood oxygen is a fundamental need in treating ARDS. But simply high oxygen concentration does not solve the problem, while high oxygen levels can also cause lung damage (American lung association, 2020). Mechanical ventilation strategies for ARDS are broad and diverse (Liaqat et al., 2022). Pulmonary protective ventilation, optimal PEEP, appropriate driving pressure and recruitment maneuvers, and prone position ventilation are strongly recommended by many medical societies (Fan et al., 2017; Griffiths et al., 2019). The goal is to use a tidal volume as low as 6 ml/kg body weight with a low PEEP of 5 cmH₂O able to meet a pH of 7.30-7.45, PaO₂ 55-80 mmHg or SpO₂ 88-95% oxygenation (ARDS network et al., 2000; Roy and Paul, 2004).

Fluids Management – The proper amount of fluid in the body is crucial. Adequate fluid management, pulmonary capillary wedge pressure (PWCP) < 8 mmHg, helps reduce pulmonary edema and facilitates recovery from the disease. The fluid restriction that is too strict can affect the normal function of other organs, such as the heart and kidneys, leading to shock (Casey et al., 2019).

Extracorporeal membrane oxygenation (ECMO) – ECMO is one of the extracorporeal blood circulation methods used to direct blood oxygenation and remove carbon dioxide from the blood. ECMO is initiated as salvage therapy in patients with severe gas exchange abnormalities when mechanical ventilation fails to maintain adequate oxygenation or carbon dioxide excretion to sustain life. ECMO facilitates lung-protective ventilation by directly removing carbon dioxide from the blood.

These non-pharmacological treatments can only provide supportive treatment, relieve symptoms, and delay disease progression, but they rarely intervene deeply in the disease process.

1.1.5.2 Pharmacological treatments

ARDS was identified more than 50 years ago. Many medications have been or are being investigated in the treatment of ARDS, such as the immunomodulatory agents dexamethasone and vitamin C; the related specific pathway inhibitors, diltiazem and bevacizumab; the vascular dysfunction inhibitor, Haptoglobin; the anticoagulant, heparin. Despite our increased understanding of its pathophysiology and the biological mechanisms of lung injury, no medication has been clinically proven effective in modifying mortality.

Researchers are working on different elements of ARDS, but there are no satisfactory therapeutic medications yet. Since ARDS is not a homogeneous clinical disease with a wide range of underlying causes, it is difficult to find a perfect pharmacological agent for this heterogeneous clinical state (Araz, 2020). Our understanding of ARDS mechanisms is still inadequate, and new therapeutic approaches remain to be explored.

1.1.6 Animal models of acute respiratory distress syndrome (ARDS)

In human ARDS, alveolar neutrophilia, micro thrombosis, and hyaline membrane deposition are the main pathological features. All three pathological features are significantly characterized. These three pathological features correspond to inflammation, endothelial/epithelial damage, and alveolar/capillary barrier disruption, respectively (Matute-Bello and Matthay, 2008).

Ideally, an ARDS animal model should be a model that reproduces this pathological triad. However, there are many experimental models of ARDS, and none can fully reproduce all the characteristics of human ARDS to the same intensity. Only one or two characteristic dominates in most experimental models of ARDS: alveolar neutrophilia is most prominent in the lipopolysaccharides (LPS) inhalation model; protein deposition and alveolar neutrophilia are

highlighted in the bacterial inhalation model; Epithelial damage is most pronounced in the acid inhalation model. Therefore, no single animal model is perfect. The best animal model is the one that can reproduce the character required to test the investigator's hypothesis (Matute-Bello and Matthay, 2008).

1.2 Role of neutrophils in acute respiratory distress syndrome (ARDS)

Neutrophils activate adaptive immunity. Neutrophils are the first immune cells recruited to the inflammatory site by chemokines released from the endothelium, epithelium, or resident macrophages (Aulakh, 2018). Neutrophil-specific receptors recognize both exogenous and endogenous inflammatory stimuli and activate the cells. Activated neutrophils produce several cytotoxic products, including neutrophil extracellular traps (NETs), granzymes, reactive oxygen species (ROS), and various pro-inflammatory cytokines (Yang et al., 2018). These cytokines further promote neutrophil recruitment and activation. Proper innate immunity helps with organismal protection, but this excessive neutrophil activation leads to surrounding tissue damage and pulmonary dysfunction (Aulakh, 2018).

1.2.1 Migration of neutrophils

Neutrophils are produced in the bone marrow. The stromal cell-derived factor (SDF-1)/chemokine (CXC motif) receptor 4 (CXCR4) chemokine axis facilitates the retention of mature neutrophils in the bone marrow. When the immune system becomes inflamed or infected, the release of neutrophils from bone marrow reserves is markedly increased, and this is mediated by the synergistic action of cytokines and chemokines.

A hallmark of ARDS is neutrophil infiltration into the inflamed lung (Zemans and Matthay, 2017). The classical leukocyte transendothelial cascade in the lung consists of the following steps: capture, rolling, arrest, crawling, and diapedesis (Figure-1) (Kolaczkowska and Kubes, 2013). Neutrophil recruitment is initially motivated by changes in endothelial cells stimulated by inflammatory mediators (Ley et al., 2007). Upon stimulation, endothelial cells rapidly upregulate P-selectin and E-selectin expression (Sadik et al., 2011). Endothelium-expressed P-selectin

and E-selectin bind to P-selectin glycoprotein ligand-1 (PSGL1, also known as CD162) on the surface of circulating neutrophils, causing free-flowing neutrophils to tether (capture) to the endothelial surface, where they are subsequently rolling along the vascular direction of blood flow (Zarbock et al., 2011).

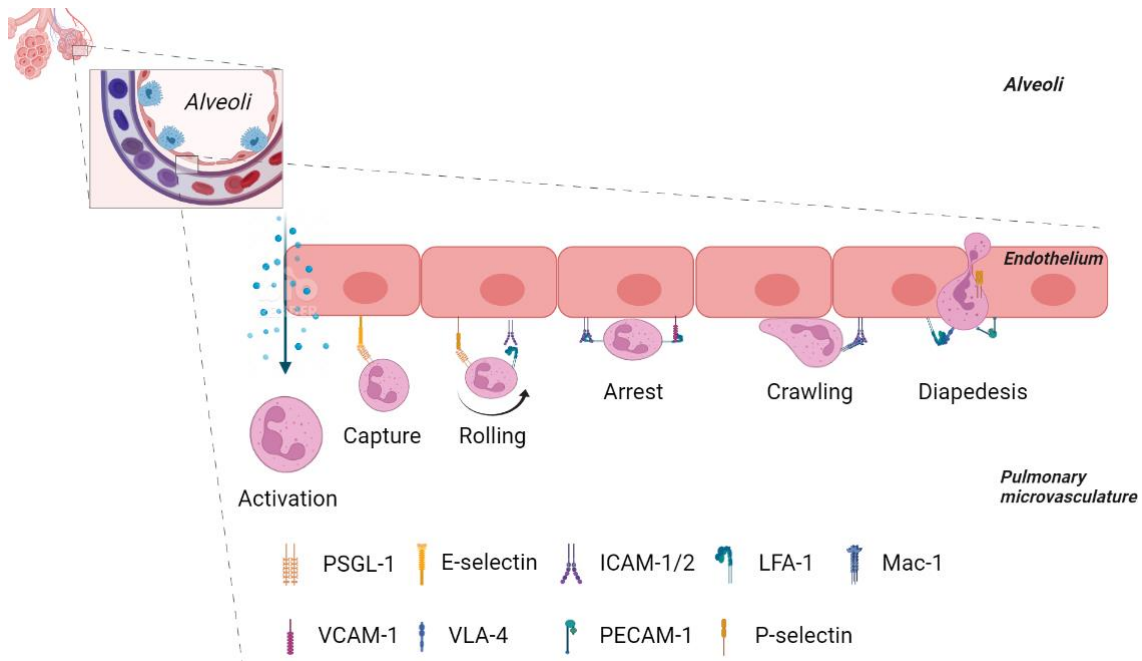


Figure-1: Trans-endothelial migration of neutrophils (simplified).

A simplified representation of polymorphonuclear neutrophil (PMN) migration. Chemokines activate PMNs. Selectin-mediated tethering leads to rolling over the endothelium. Interactions with integrins strengthen the binding of PMNs to the endothelium and ensures that they are arrested and crawl. Diapedesis is the last step and is done with the help of very late antigen-4 (VLA-4), platelet endothelial cell adhesion molecule 1 (PECAM-1). ICAM 1/2 = intercellular adhesion molecule 1/2; LFA-1 = lymphocyte function-associated antigen 1; Mac-1 = macrophage antigen 1; PSGL-1 = P-selectin glycoprotein ligand-1; VCAM-1 = vascular cell adhesion molecule 1. The figure was created with Edrawsoft (version 12.0.1).

Due to an increased blood flow rate, the neutrophils are exposed to shear stress. The selectin bonds are too weak to hold the neutrophils. Therefore, arrest and closer crawling become necessary steps. These phenomena are mainly dependent on intercellular adhesion molecule 1 (ICAM-1, also known as CD54), intercellular adhesion molecule 2 (ICAM-2, also known as CD102), platelet endothelial cell adhesion molecule 1 (PECAM-1, also known as CD31) and vascular cell adhesion molecule 1 (VCAM-1) expressed by endothelial cells, and macrophage-1 antigen (Mac-1, also known as CD11b/CD18), lymphocyte function-associated antigen 1 (LFA-1, also known as CD11a/CD18), and very late

antigen-4 (VLA-4, also known as CD49d/CD29) expressed by neutrophils (Filippi, 2019; Phillipson et al., 2006). After arrest, the neutrophils become flattened and deformed and adhere to the lumen surface of the endothelium in search of a suitable site for diapedesis (Phillipson et al., 2006; Schenkel et al., 2004).

Neutrophil extravasation usually occurs by the paracellular pathway and, in rare cases, happens by the transcellular route. Paracellular diapedesis requires a programmed multi-step articulation mediated by neutrophils and endothelial cells. Finally, leukocytes dissociate from the endothelium and cross the pericytes and basement membrane. Cross-cell migration usually occurs in relatively thin portions of the endothelium; thus, neutrophils migrate over shorter distances.

After penetrating the endothelium, neutrophils need to cross a layer of pericytes and the extracellular matrix (Filippi, 2019). Migration through the endothelial basement membrane and extracellular matrix occurs in the interstitial space between adjacent pericytes and low protein deposition areas in the extracellular matrix. This response needs to be catalyzed by $\alpha 6 \beta 1$ -integrin and related proteases, such as neutrophil elastase (NE) and matrix metalloproteinases (MMPs).

Neutrophil trans-epithelial migration can be divided into three phases. In the first stage, neutrophils in the lung interstitium interact with adhesion molecules, such as ICAM-1, expressed on the basolateral lung epithelium. In this process, some of the apical side neutrophils release chemokines, such as CXCL8, forming a concentration gradient from high to low across the apical to basolateral side (Metzemaekers et al., 2020). In the second stage, neutrophils migrate between lung epithelial cells along the paracellular zone, crossing a series of intercellular junctions through intermediate target chemoattractant and terminal target chemoattractant take-up and receptor-ligand interactions (Brazil and Parkos, 2016). In the final stage, neutrophils reach the apical surface of the epithelium and enter the alveolar lumen, where they can bind adhesion molecules expressed at the apical epithelial end and terminal chemokines in the alveolar lumen and participate in immune activity, releasing inflammatory factors and amplifying the inflammatory loop (Metzemaekers et al., 2020).

1.2.2 Platelet–neutrophil complexes (PNCs)

PNCs have been proved to increase neutrophil recruitment at sites of inflammation (Rossaint et al., 2014; Zarbock et al., 2006). In some inflammatory model studies, this cell-cell interaction has even been considered a prerequisite for neutrophil recruitment (Zarbock et al., 2006). During normal vascular physiology, red blood cells flow in the center of the vessel due to the fluidic nature of blood flow, while smaller platelets are pushed toward the periphery of the blood flow. These movements increase contact between neutrophils attached to the vessel wall and platelets (Goldsmith and Spain, 1984a). Many PNCs have been observed in normal *in vivo* blood vessels. However, these complexes are only temporarily present in healthy people (Goldsmith and Spain, 1984b).

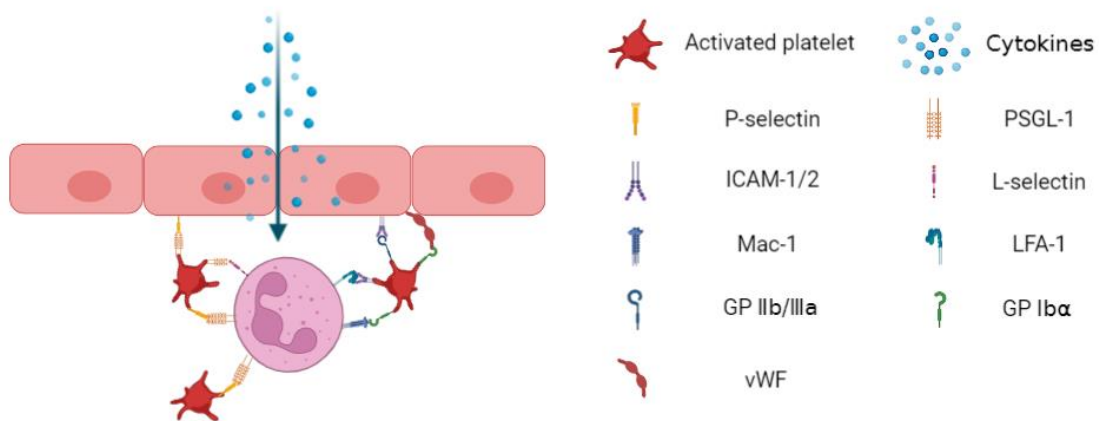


Figure-2: Interactions within and between platelet–neutrophil complexes (PNCs) and the endothelium.

GP 1ba = glycoprotein Iba; *GP IIb/IIIa* = glycoprotein IIb/IIIa; *ICAM 1/2* = intercellular adhesion molecule 1/2; *LFA 1* = lymphocyte function-associated antigen 1; *Mac-1* = macrophage antigen 1; *vWF* = von Willebrand Factor. The figure was created with Edrawsoft (version 12.0.1).

As shown in Figure-2, The formation of PNCs depends on P-selectin on platelets and PSGL-1 on the surface of neutrophils (Hamburger and McEver, 1990). After stimulation by inflammatory factors, neutrophils further express Mac-1 (Page and Pitchford, 2013). LFA-1 binds to platelet surface-expressed glycoprotein Iba (Simon et al., 2000) and ICAM-2 (Diacovo et al., 1994), further stabilizing the complexes. Meanwhile, platelets can bind to P-selectin, von Willebrand factor (vWF), and ICAM-1 on endothelial cells through surface PSGL-1, glycoprotein

Ib α , and glycoprotein IIb/IIIa (Page and Pitchford, 2013) to enhance neutrophil–endothelial cell interaction and thus accelerate the neutrophil extravasation process.

1.2.3 Neutrophil oxidative stress

In a reductive oxidation reaction, molecular oxygen is converted from molecular oxygen to water, generating free radical intermediates. Reactive oxygen species (ROS) is a general name for these intermediates (Kellner et al., 2017). An excessive ROS response termed oxidative burst can contribute to host defense and may also cause damage to surrounding tissue.

Neutrophils can produce ROS during phagocytosis and respond to soluble agonists (Chen and Junger, 2012). ROS can decrease the integrity of the endothelial barrier by causing the breakdown of endothelial junctions combined with increased cytoskeleton contraction and microtubular instability (Kellner et al., 2017). Additionally, increasing evidence suggests that PMN extravasation is regulated by oxidative stress and that ROS produced in injured tissues act as chemoattractants for immune cells (Griffin et al., 2012; Ku et al., 2015; Zhou et al., 2012).

1.3 Role of leukotrienes in neutrophil activity

The term leukotriene was first introduced in 1980 by Bengt I. Samuelsson (Samuelsson et al., 1980). Its root words are “leuko” and “triene”. “leuko” stands for leukocyte, and “triene” refers to the three conjugated double bonds of the compounds.

Leukotrienes are mainly secreted by inflammatory cells such as polymorphonuclear neutrophils (Brock et al., 1996), mast cells (Ramos et al., 1991), and dendritic cells (Hedi and Norbert, 2004), and activated macrophages (Chensue and Kunkel, 1983). These cells express 5-lipoxygenase (5-LO, also known as Alox5) and 5-LO activating protein (FLIP), which are essential for leukotriene biosynthesis. As shown in Figure-3, leukotrienes are primarily derived from the enzymatic release of arachidonic acid (AA) from membrane phospholipids by phospholipase A2 (PLA2).

Alox5 converts AA to leukotriene A4 (LTA4), an unstable epoxide. Cells containing leukotriene A4 hydrolase, such as neutrophils, convert LTA4 into leukotriene B4 (LTB4), a dihydroxy acid leukotriene. Cells that express leukotriene C 4 synthase, such as mast cells, produce cysteine leukotriene C4 (LTC4) by binding to glutathione tripeptides. Extracellularly, LTC4 can be converted to leukotriene D4 (LTD4) and leukotriene E4 (LTE4) by leukotriene C4 hydrolase. Since LTA4 is unstable, leukotrienes are categorized into LTB4, containing dihydroxy groups, and cysteinyl leukotrienes (CysLTs), including LTC4, LTD4, and LTE4, which contain amino acids. Leukotrienes bind to specific receptors: The high-affinity receptor for LTB4 is leukotriene B4 receptor 1 (LTB4R1), and the high-affinity receptors for LTC4 and LTD4 are cysteinyl leukotriene receptor 1 (CysLTR1) and cysteinyl leukotriene receptor 2 (CysLTR2), and the high-affinity receptor for LTE4 is G protein-coupled receptor 99 (GPR99) (Sasaki and Yokomizo, 2019).

1.3.1 Chemotaxis of neutrophils by leukotrienes

Several in vitro experiments have demonstrated that LTB4 (Afonso et al., 2012; Krauss et al., 1994; Yokomizo et al., 2018) and LTD4 (Krauss et al., 1994) have potent chemotaxis toward peripheral blood neutrophils. LTB4 is reported to be a

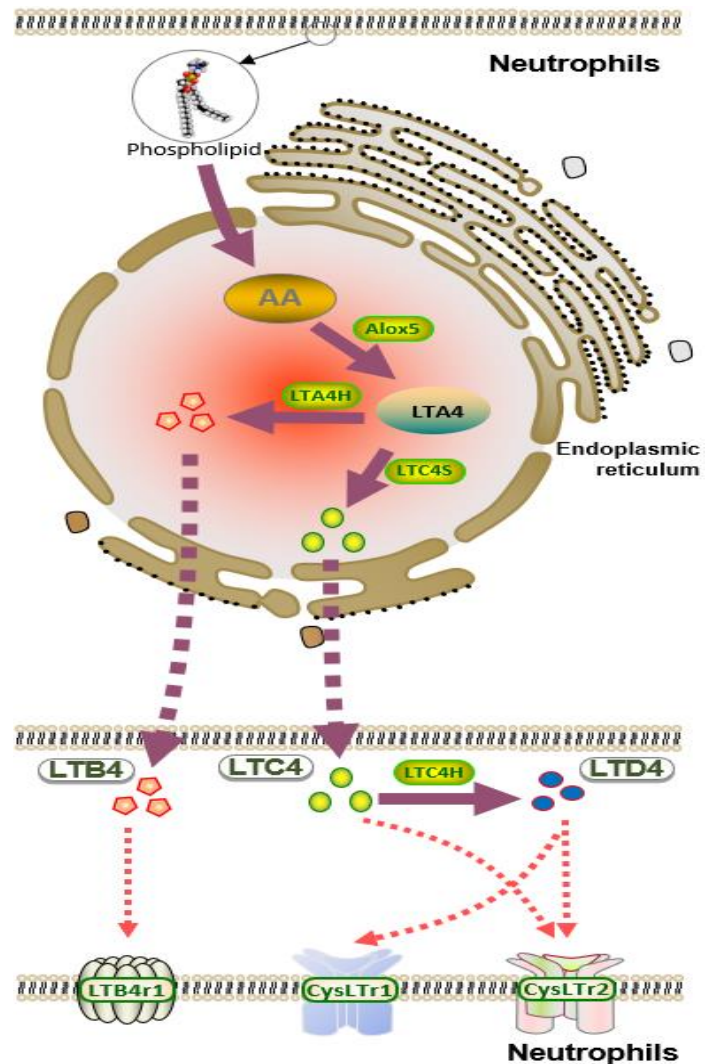


Figure-3: Leukotriene synthesis.

AA = arachidonic acid; Alox5 = arachidonate 5-lipoxygenase; CysLTR1 = cysteinyl leukotriene receptor 1; CysLTR2 = cysteinyl leukotriene receptor 2; LTA4 = leukotriene A4; LTA4H = leukotriene A4 hydrolase; LTB4 = leukotriene B4; LTB4R1 = leukotriene B4 receptor 1; LTC4 = leukotriene C4; LTC4H = leukotriene C4 hydrolase; LTC4S = leukotriene C4 synthase; LTD4 = leukotriene D4. The figure was created with Edrawsoft.

signaling relay molecule that masterfully regulates neutrophil chemotaxis to formylated peptides produced at the inflammatory core sites (Afonso et al., 2012). Two independent studies separately reported reduced chemotactic leukocytes in LTB4R1 knockout mice in a model of peritonitis (Haribabu et al., 2000; Tager et al., 2000).

Cysteinyl leukotrienes have been frequently reported in the pathogenesis of asthma. However, cysteinyl leukotrienes also have very potent pro-inflammatory activity and may play an essential role in inflammatory processes other than asthma. LTD4 induces an inflammatory response and airway remodeling in human airway epithelial cells, contributing to the promotion of neutrophil migration (Dholia et al., 2021). LTE4 has been shown to synergize with PGD2 to activate T helper 2 cells through different pathways, thereby promoting neutrophil migration and survival. (Xue et al., 2015)

1.3.2 Leukotrienes enhance neutrophil adhesion to the endothelium

Although the relevant adhesion mechanisms have not been fully characterized, several studies suggest that leukotriene-triggered leukocyte-endothelial cell adhesion may be caused mainly by a direct effect on endothelial cells (Hoover et al., 1984; Palmblad et al., 1994; Patricia et al., 1999).

According to a previous study (Pedersen et al., 1997), cysteinyl leukotrienes, such as LTC4 and LTD4, induce P-selectin expression in human endothelium through a non-CysLTR1 mediated mechanism. LTC4 and LTD4 stimulate human endothelial cells to synthesize platelet-activating factor and promote their binding to neutrophils (McIntyre et al., 1986).

Flow cytometry studies demonstrate that LTB4 triggers the upregulation of $\beta 2$ integrins on neutrophil surfaces, which promotes the arrest step of neutrophils to endothelial cells (Showell et al., 1998; Vaddi and Newton, 1994).

1.3.3 Leukotriene pathway and reactive oxygen species (ROS)

ROS production is normally derived from Nicotinamide-adenine dinucleotide phosphate (NADPH) oxidase and mitochondria (Haendeler et al., 2004).

However, other sources of cellular ROS, such as Alox5, catalyze arachidonic acid, generating leukotrienes and ROS (Soberman and Christmas, 2003). In T lymphocytes, CD28-induced production of ROS is dependent on the activation of Alox5 (Los et al., 1995). Leukotriene B4 plays a vital role in tumor necrosis factor α (TNF- α) induced ROS (Woo et al., 2000). Investigators have observed that LTB4 promotes ROS production in rat mesentery and increases leukocyte adhesion (Steiner et al., 2001).

It has also been reported that LTC4 is one of the primary mediators of endoplasmic reticulum stress activation, triggering ROS accumulation and DNA damage (Dvash et al., 2015).

1.4 Leukotriene modifiers

Leukotriene modifiers are the generic term for leukotriene receptor antagonists and leukotriene synthesis inhibitors, a class of medications that block the effect of leukotrienes in the body or block their synthesis.

Currently, the leukotriene receptor antagonists which have passed phase 4 clinical trials and are approved for clinical use in humans are montelukast, zafirlukast, and pranlukast. Among them, the most widely used is montelukast, while the only leukotriene synthesis inhibitor approved for human application is zileuton.

1.5 Questions

Despite decades of efforts to understand the pathogenesis and treatment of ARDS, its mortality on the ICU has not significantly improved, and most treatment strategies remain supportive. There are still no medications that have satisfactory efficacy in treating ARDS.

As a new perspective on ARDS treatment, leukotrienes have been demonstrated to play an integral role in acute and chronic inflammation (Nakamura and Shimizu, 2011). So, are the leukotriene receptor inhibitor montelukast and the leukotriene receptor inhibitor zileuton practical approaches to control ARDS? What are the similarities and differences in the performance of the two agents?

2 Materials and Methods

2.1 Overview

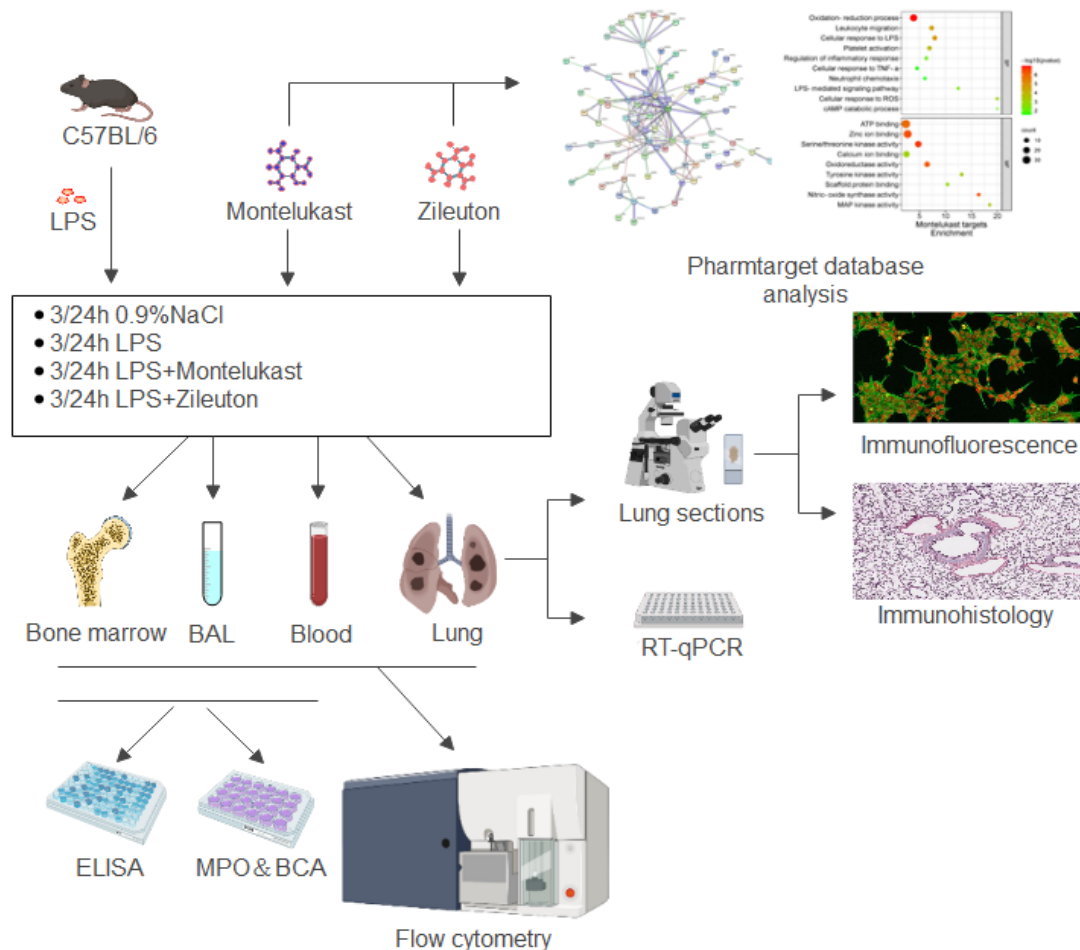


Figure-4: Overview of the methods used in this dissertation.

A murine acute pulmonary inflammation model was generated by lipopolysaccharide (LPS) inhalation. Lung tissue single-cell suspensions, bone marrow, bronchoalveolar lavage (BAL), and blood were used for flow cytometry. Chemokine levels in plasma, BAL supernatant, and bone marrow supernatant were determined by enzyme-linked immunosorbent assay (ELISA). Myeloperoxidase (MPO) and bicinchoninic acid (BCA) assays detected the oxidative burst and protein concentration, respectively, BAL cells in the supernatant. Immunofluorescence and immunohistochemistry images were generated from the lung tissue. Real-time quantitative polymerase chain reaction (RT-qPCR) examined intrapulmonary gene expression of inflammatory mediators and leukotriene synthesis key enzymes. The Pharmtarget database was used to analyze potential targets of montelukast and zileuton. The figure was created with Edrawsoft.

Based on a murine model of acute pulmonary inflammation induced by nebulized inhalation of LPS (Reutershan et al., 2005), we investigated several effects of montelukast and zileuton related to neutrophil migration and activation. We used

flow cytometry to quantify the number of neutrophils and PNCs in each compartment and the expression of neutrophil adhesion molecules. We used enzyme-linked immunosorbent assay (ELISA) to detect the release of cytokines in plasma, bronchoalveolar lavage (BAL) supernatant, and bone marrow supernatant. We utilized myeloperoxidase (MPO) and bicinchoninic acid (BCA) assays to evaluate BAL cells' oxidative burst and protein concentration. Real-time quantitative polymerase chain reaction (RT-qPCR) determined gene expression in pulmonary tissue. We employed immunofluorescence to detect protein expression in lung tissue and applied immunohistochemistry to explore neutrophil migration and the inflammatory status of the lung. And we used the Pharmtarget database to analyze montelukast and zileuton potential targets (Figure-4).

2.2 Animal model

2.2.1 Mice

Eight to twelve weeks old wild-type C57BL/6 mice were obtained from Jackson Laboratory (Bar Harbor, ME). Male mice were used for this project. All animal experiments were approved by the University of Tuebingen Animal Care and Use Committee. The animals were kept in cages at 22°C and humidity of 50%–60% and a 12-hour photoperiod, with up to four mice per cage.

2.2.2 Pulmonary inflammation model

Since we focused on neutrophil migration during acute lung inflammation, we chose a murine LPS inhalation pulmonary inflammation model with significant alveolar neutrophilia, accompanied by the expression of multiple adhesion molecules and abundant inflammatory factor release (Lorenz et al., 2001), which can be stably repeated. For LPS inhalation, LPS was dissolved in 7.5 ml sterile 0.9% NaCl at a concentration of 500 µg/ml. Up to 4 mice were placed in an inhalation chamber connected to a nebulizer on one side and a vacuum ejector on the other side. It ensures a continuous flow of air within the chamber. With the help of the nebulizer, the LPS solution is evaporated, and by the suction of the vacuum ejector, it is delivered into the chamber, and the vapor is inhaled by the mice (Figure-5). The inhalation was stopped after 30 minutes.

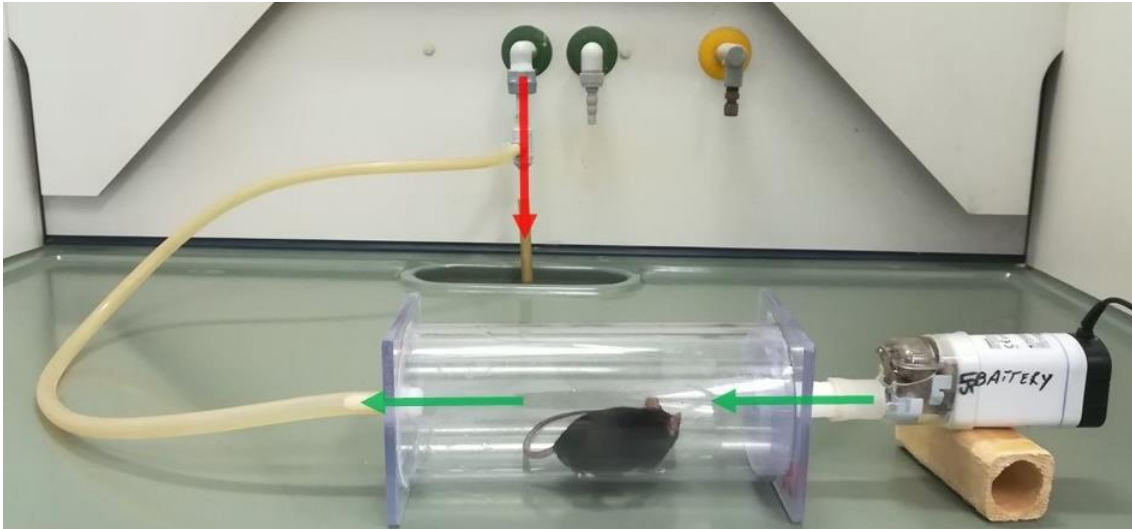


Figure-5: LPS inhalation process.

The nebulizer (right, white) is connected to an inhalation chamber where the mice are located. At the other end, a vacuum ejector continuously generates suction through which nebulized LPS constantly flows through the chamber, where the mice inhale it. Green arrows = LPS steam path. Red arrow = water path. Own picture.

2.3 Grouping and treatments

The mice were divided into four groups: control group, stimulation group, montelukast treatment group, and zileuton treatment group. The control group inhaled 0.9% NaCl. The stimulation group was subjected to LPS inhalation. The montelukast group was intraperitoneally injected with 0.1 $\mu\text{g}/\mu\text{l}$ montelukast at 1 $\mu\text{g}/\text{g}$ body weight 1 hour after LPS inhalation. The zileuton group was intraperitoneally injected with 0.1 $\mu\text{g}/\mu\text{l}$ zileuton at 1 $\mu\text{g}/\text{g}$ body weight 1 hour after LPS inhalation. Medication information is shown in Table-2.

Table-2: Medication information.

Medications	Stock concentration	Article number; Manufacturer; Place	Work concentration
Montelukast	10 $\mu\text{g}/\mu\text{l}$	10008318; Cayman chemical company; Michigan, USA	0.1 $\mu\text{g}/\mu\text{l}$
Zileuton	10 $\mu\text{g}/\mu\text{l}$	10006967; Cayman chemical company; Michigan, USA	0.1 $\mu\text{g}/\mu\text{l}$

2.4 PMN counts and adhesion molecules

2.4.1 Sampling and preparation

Organ harvest took place 3 or 24 hours after LPS inhalation, depending on the cohort. Preoperatively, the mice received 10ul/g per bodyweight of intraperitoneal injection of anesthetics. The anesthetic composition is shown in Table-3.

Table-3: Anesthetic composition.

Medications	Ingredients	Concentration	ID; Manufacturer; Place	Quantity
Ketamine	Ketamine hydrochloride	50 mg/ml	03760898; Hameln Pharma Plus GmbH; Hameln, DE	1,2 ml
Sedaxylan	Xylazine	20 mg/ml	1906602; Dechra Pharmaceuticals; Northwich, GB	0,4 ml
NaCl	Sodium chloride	0,9 %	02737756; Braun; Melsungen, DE	8,4 ml
Total				10 ml

After the mice were unresponsive to pain at the extremities of the limbs, they were placed on their back and fixed at their limbs and head. The skin was incised starting from the submandibular region and opening toward the pelvic area until the peritoneum was exposed. The muscle layer was incised along the saber and rib arch, and then a diaphragmatic incision was made, resulting in the collapse of both lungs. The thorax was opened on both sides lateral to the pectoral muscles, and the thorax shield was fixed upward so that the thoracic site was accessible. With a syringe wetted with heparin, at least 500 µl of blood was taken from the right ventricle, transferred to a 1.5-ml Eppendorf tube, and immediately placed in a water bath at 37°C. The large sub-hepatic abdominal vessels were then severed. The right ventricle was punctured again, and the pulmonary circulation was flushed with 3 mL of phosphate-buffered saline minus (PBS⁻) to wash away the circulating PMNs from the pulmonary vessels. The trachea was exposed and punctured with a catheter. The lung was lavaged with phosphate-buffered saline

minus (PBS⁻) to obtain 2 ml of BAL, which was stored in a tube on ice. Finally, the cardiopulmonary pouch was dissected from the pulmonary hilum. The right upper and lower lung lobes were transferred to cryotubes and rapidly frozen in liquid nitrogen. Subsequently, they were stored at -80°C so the samples could be used later for RT-qPCR. The right middle lung lobe and the left lung were mechanically dissected and placed in a 50-ml Falcon tube that contained 2.5 ml of enzyme solution (Table-4). Tissues were digested enzymatically in an incubation shaker at 70 rpm and 37°C for 30 minutes.

Table-4: Composition of the enzyme solution for digesting the lung tissue.

Enzyme	ID; Manufacturer; Place	Quantity/mouse
Collagenase XI from <i>Clostridium histolyticum</i>	C7657; Sigma-Aldrich; St. Louis, USA	2,5 µl
DNAse from bovine pancreas	DN25; Sigma-Aldrich; St. Louis, USA	2,5 µl
Hyaluronidase from bovine testes	H3506; Sigma-Aldrich; St. Louis, USA	2,5 µl
PBS ⁻	Gibco; Carlsbad, USA	2,4925 ml
Total		2,5 ml

The leukocyte count of the blood samples was determined by using a light microscope. The counting occurred in a 1:10 dilution with Türk's solution in a Neubauer counting chamber. For each mouse, 25 µl of blood was taken for fluorescence-activated cell sorting (FACS) staining, and the remaining blood was then centrifuged at 13,000 rpm for 10 minutes at room temperature to preserve plasma. Plasma was stored at -80°C for further investigations.

BAL was centrifuged at 1,300 rpm for 10 minutes at 4°C, and 2 ml of the supernatant was aliquoted for ELISA, MPO, and BCA assay. The aliquots were stored at -80°C. The cell pellet was resuspended with 200–500 µl of staining buffer (Table-5), depending on how many cells were expected. The leukocyte count was determined according to the same scheme as the blood samples. The sample was diluted or concentrated so that there were 200,000 cells per 100 µl.

After the lung tissue had been incubated in an enzyme cocktail at 37°C for 30 minutes on a horizontal shaker, it was pressed through a cell strainer with 70 µm pores and rinsed with 15 ml of PBS⁻. The resulting cell suspension was centrifuged at 1,300 rpm for 10 minutes at 4°C, and the supernatant was discarded. To lyse the erythrocytes, the cell pellet was resuspended in 2.5 ml of lysis buffer (Table-6) and incubated for 10 minutes on ice. The lysis was stopped with 17.5 ml of staining buffer, and the suspension was centrifuged again at 1,300 rpm for 10 minutes at 4°C. The supernatant was discarded, and the pellet was resuspended in 500–1000 µl of staining buffer, depending on how many cells were expected. The leukocyte count was determined, and the suspension was adjusted to 200,000 cells per 100 µl by dilution or concentration.

Table-5: Composition of the staining buffer (for 1 liter).

Substance	Article number	Manufacturer	Place	Quantity
Aqua dest		Own production	Tübingen, DE	1 Liter
PBS ⁻	18912014	Thermo Fisher Scientific	Waltham, USA	2 Tablets
Bovines Serum albumin	A3294	Sigma-Aldrich	St. Louis, USA	10 g
NaN ₃	08591	Sigma-Aldrich	St. Louis, USA	5 ml

Table-6: Composition of the erythrocyte lysis buffer for organs (for 1 liter).

Substance	Article number	Manufacturer	Place	Quantity
Aqua dest		Own production	Tübingen, DE	1 Liter
NH ₄ Cl	3J002532	AppliChem	Darmstadt, DE	8,024 g
NaHCO ₃	K10720529	Merck KGaA	Darmstadt, DE	0,84 g
Disodium EDTA	ED4S	Sigma-Aldrich	St. Louis, USA	0,372 g

Fluorescently labeled monoclonal antibodies were used for flow cytometry to identify different cell populations and to quantify the surface expression of different proteins. The antibodies used were divided into two antibody mixes (Table-7). A FACS sample for each antibody mix was prepared for blood,

pulmonary single-cell suspension, and BAL from each test animal. One unstained tube and fluorescence minus one (FMO) control were prepared for each sample type. In addition, one single-stained sample was prepared for each antibody.

Table-7: Antibody mixes used on flow cytometric analysis.

Antibody mix1	Article number	Manufacturer	Fluorescence	Stock Con.	Work Con.
CD45	103130	BioLegend	PerCP	0.2mg/ml	2µg/µl
Ly6G	127618	BioLegend	PE/Cyanine 7	0.2mg/ml	2µg/µl
CD42b	0401-D	Emfret Analytics	FITC	0.2mg/ml	2µg/µl
CD162	555306	BD Biosciences	PE	0.2mg/ml	2µg/µl
CD62L	104424	BioLegend	Pacific Blue	0.2mg/ml	2µg/µl
CD62P	148304	BioLegend	APC	0.2mg/ml	2µg/µl
Antibody mix2	Article number	Manufacturer	Fluorescence	Stock Con.	Work Con.
CD45	103130	BioLegend	PerCP	0.2mg/ml	2µg/µl
Ly6G	127618	BioLegend	PE/Cyanine 7	0.2mg/ml	2µg/µl
CD42b	0401-D	Emfret Analytics	FITC	0.2mg/ml	2µg/µl
CD11a	141006	BioLegend	PE	0.2mg/ml	2µg/µl
CD11b	101224	BioLegend	Pacific Blue	0.2mg/ml	2µg/µl
CD49d	103614	BioLegend	APC	0.2mg/ml	2µg/µl

CD45 is a general leukocyte marker, and lymphocyte antigen 6 complex locus G6D (Ly6G) was used to specifically identify neutrophils. CD42b was used to identify activated platelets. The remaining antibodies bind to cell adhesion molecules, and the mean fluorescence intensity (MFI) was determined to quantify the corresponding protein expression.

Fifty microliters of staining buffer (unstained control), FMO mix, or antibody mix was pipetted into each FACS tube. Then, 25 µl of whole blood or 100 µl of the BAL or pulmonary single-cell suspension was added. The blood samples were incubated in the dark for 20 minutes at room temperature. One milliliter of 10% BD FACS lysing solution was added and incubated for 10 minutes. Then, 1 ml of staining buffer was appended. The BAL and lung samples were incubated in the

dark for 30 minutes at room temperature, and then 2 ml of staining buffer was added to each. All samples were centrifuged at 1,3000 rpm for 10 minutes at 4°C, and the supernatant was discarded. This washing step was repeated twice with 2 ml of staining buffer, and then the cells were fixed with 400 µl of 2% formaldehyde diluted in staining buffer. The samples were analyzed within 24 hours.

2.4.2 Flow cytometry

Samples were measured with a FACS Canto II flow cytometer (BD Biosciences, Franklin Lakes, NJ, USA). The FACS measurement data were recorded using the BD FACS Diva software (version 9 from BD Biosciences). The FlowJo software (version 7.2.5 from FlowJo LCC, Ashland, OR, USA) was used for the subsequent analysis of the data.

After the measurement, compensation is necessary for multiple fluorescence signals. In flow cytometry, bandpass filters select the appropriate range of excitation and emission wavelengths. However, fluorescence from more than one fluorochrome is detected when emission spectra overlap. Therefore, fluorescence compensation is required to correct for such spectral overlap. This process ensures that the fluorescence detected by a particular detector comes only from the target fluorochrome. If cells have only come into contact with one dye, emission must involve this dye (positive area). If there is no emission, then the cells are in negative territory. A matrix can be generated from these positive and negative values placed over each cell population to be analyzed. Therefore, we applied single-staining tubes and unstained tubes to build fluorescence compensation matrixes for each specimen type and antibody mix by FlowJo 7.

A flow cytometer analyzes the size and granularity of the cells and allows identifying many cells within a short period of time. The nozzle creates tiny droplets with single cells, which flow past lasers. Firstly, two signals are shown: the intensity of the light scattered at small angles (FSC; forward scattering) and the intensity of the light scattered at large angles (SSC; side scattering). FSC identifies the size of a cell and SSC indicates its granularity. If we plot these two values against each other in a dot-plot diagram, we can identify individual cell

populations—granulocytes, monocytes, and lymphocytes—and differentiate them from one another.

With specific surface markers, a cell population was divided into subpopulations. A gating strategy was used to identify individual cell populations. The blood sample analysis illustrates the procedure (Figure-6). First, in the FSC-SSC dot-plot diagram, a gate was set for morphological leukocytes, which depended on their granularity and cell size (Figure-6A). In the morphological leukocyte population, the CD45-positive cells were determined (Figure-6B). The proportion of Ly6G-positive cells that are PMN was then determined from the CD45-positive cells (Figure-6C).

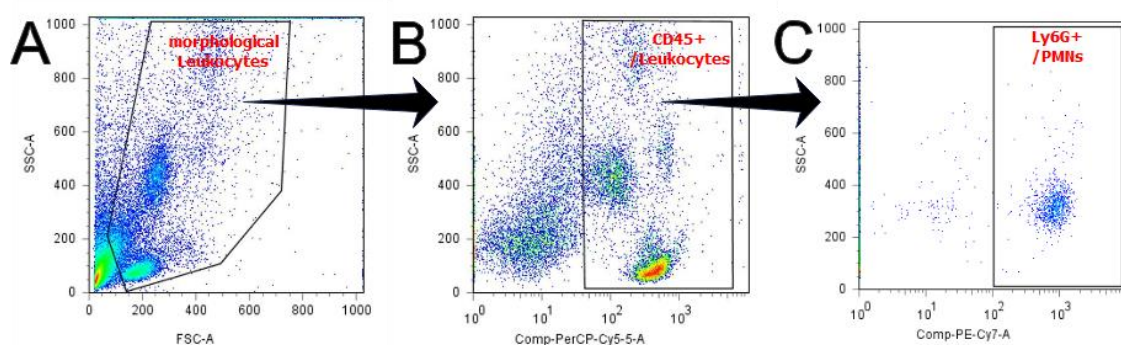


Figure-6: Gating strategy of the polymorphonuclear neutrophil (PMN) analysis.

A First, a gate for leukocytes was created from all detected events in the Forward scattering/ Side scattering diagram. **B** The Compensated-CD45-positive cells from the morphological leukocyte population were gated in the Compensated-PerCP/ Side scattering diagram. **C** In the Compensated-PE-Cy7/Side scattering diagram, the Compensated -Ly6G-positive cells (PMNs) were gated from the population of Compensated-CD45-positive cells. Own picture.

The percentage of the selected subpopulation concerning the total cell population was indicated in the individual gates. From these percentages and the total number of cells previously determined with the Neubauer counting chamber, absolute numbers for the PMNs could be determined.

2.5 PNC determination

After neutrophils have been identified, PNCs can also be determined with the help of fluorescence minus one (FMO) (Figure-7).

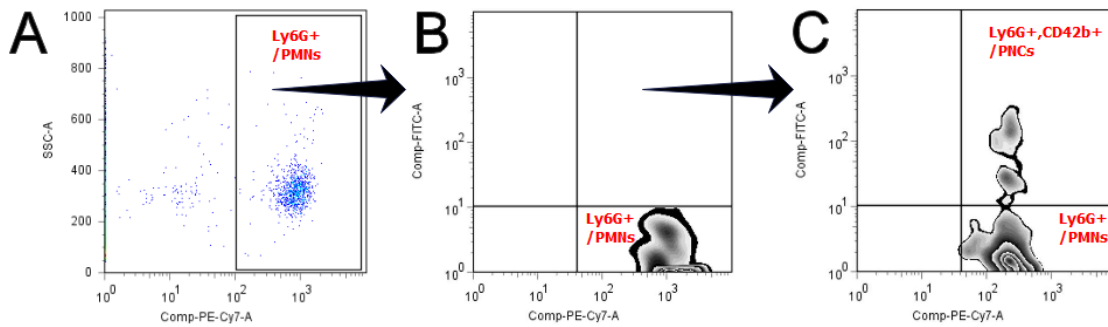


Figure-7: Gating strategy of the platelet–neutrophil complex (PNC) analysis.

A Identified neutrophils. **B** In the Compensated-PE-Cy7/Compensated-FITC diagram, FMO-stained cells do not contain Compensated-FITC-CD42b antibodies, allowing the determination of the Compensated-FITC negative versus positive boundary. **C** A distinction was made between PNCs and PMNs. Compensated-FITC-CD42b-positive marks the platelets, PNCs are Compensated-PE-Cy7 and Compensated-FITC positive, and PMNs are Compensated -PE-Cy7 positive and Compensated-FITC negative. Own picture.

2.6 PMN trafficking in each compartment

2.6.1 Bone marrow

The skin of the thigh and calf was separated. The tibia was cut with scissors, and the hip joint was moved to determine its position. A wedge-shaped incision was made above the hip joint to separate the intact joint, and the severed limb was placed in 37°C PBS⁻ for 5 minutes. The thigh muscles were separated, the knee and hip joints were dissected, and the intact femur was removed. With a 25G needle and a 5-ml syringe, each femur was rinsed of all bone marrow with 2 ml of PBS⁻, and bone marrow from each mouse was collected in a 15-ml tube and set aside on ice. The solution was centrifuged at 1,3000 rpm for 10 minutes at 4°C. The supernatant was used for the ELISA, and the bone marrow was stained with antibody mix3 (Table-8).

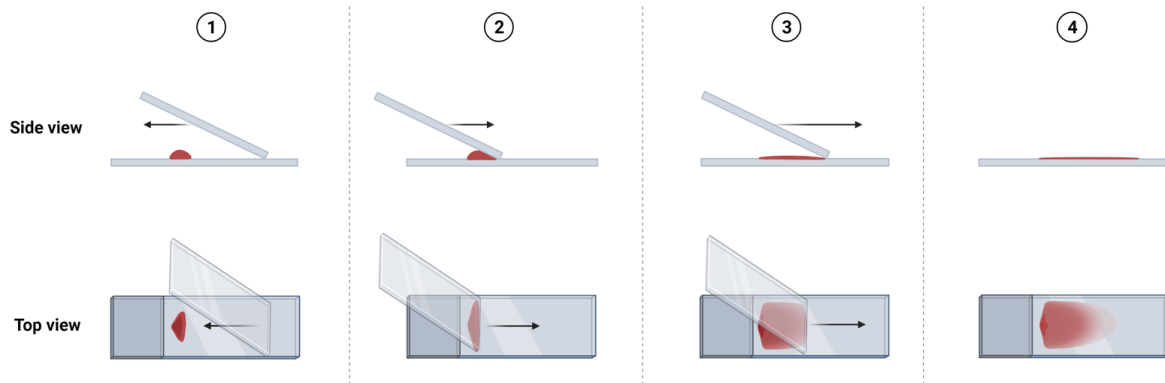
Table-8: Antibody mixes used for bone marrow analysis.

Antibody mix3	Article number	Manufacturer	Fluorescence	Stock Con.	Work Con.
CD45	103130	BioLegend	PerCP	0.2mg/ml	2µg/µl
Ly6G	127618	BioLegend	PE/Cyanine 7	0.2mg/ml	2µg/µl
CXCR4	146508	BioLegend	APC	0.2mg/ml	2µg/µl
CXCR2	149304	BioLegend	PE	0.2mg/ml	2µg/µl

2.6.2 Blood

Blood smears were prepared to determine whether the neutrophils released into the blood were more mature/segmented or immature/band neutrophils (n = 2; Figure-8).

Blood Smear Preparation Wedge Method

**Figure-8: Blood smear preparation.**

① Take 4 µl of blood from the right ventricle and place a drop on one end of a clean, grease-free slide. Then, hold the slide in one hand and take another slide with smooth edges in the other hand as a pusher. Afterward, place the edge of the pushing slide in front of the blood drop and then pull it backward. The blood will be evenly attached between the two slides when it comes in contact with the blood drop. ② Push the slide forward smoothly to the other end at about 30–45 degrees. ③ The angle should be consistent when pushing, and the force should be even so that a smooth blood smear can be made (the blood smear should not be too thick or too thin). ④ Dry the prepared blood smear without heating. The figure was prepared with Edrawsoft (version 12.0.1).

Blood smears were stained by following a modified Giemsa staining protocol using Diff Quik (Dade Behring, Newark, DE, USA). (1) Dip each slide in the fixative solution (5 × 1 second), then let it drain well. (2) Immerse the slide in staining solution I (red) for 5 × 1 second, then allow it to drain. (3) Immerse the

slide in staining solution II (blue) for 5 × 1 second, then allow it to drain. (4) Rinse the slide with Aqua Dest and let it dry. Differential counts were conducted under a 40× immersion objective lens by counting 100 leukocytes in randomly selected fields of view.

2.6.3 Lung

APC-labeled rat anti-mouse Ly6G (10 µl) + 240 µl of 0.9% saline antibody solution was injected via the tail vein to bind intravascular PMN. Mice were then euthanized. Blood, lung tissue, and BAL were obtained as described in chapter 2.4.1. Samples were then stained with PerCP-labeled CD45 and PE/Cy7-labeled Ly6G. It allows differentiation between neutrophils attached to the endothelium (APC-Ly6G+/PECy7-Ly6G+) and neutrophils in the pulmonary interstitium (APC-Ly6G-/PECy7-Ly6G+).

2.7 Leukotriene and cytokine determination

2.7.1 Gene expression investigation by RT-qPCR

2.7.1.1 RNA isolation from murine lung

RNA isolation by TRIzol™ reagent (Thermo Fisher Scientific, Waltham, MA, USA) was performed according to the manufacturer's instructions. The lungs, stored at -80°C, were brought to room temperature, and the right upper lobe was placed in a Precellys tube with 1 ml of TRIzol™ reagent and ceramic beads. TRIzol™ contains phenol and guanidine isothiocyanate, both of which denature proteins. The samples were then homogenized at 5000 rpm for 2 × 20 seconds and then left to stand at room temperature for 5 minutes. Then, 200 µl of chloroform was added, and the samples were vortexed until they were homogeneously milky. The homogenate was incubated for 10 minutes at room temperature and then centrifuged at 12,000 g and room temperature for 5 minutes, whereupon it separated into three phases. The upper phase contains the RNA dissolved by phenol and chloroform, the interphase contains DNA, and the lower phase has organic residues from proteins and DNA. The upper phase was transferred to a new RNase-free 1.5-ml Eppendorf tube, and 500 µl of isopropanol was added to precipitate the RNA. The tube was shaken by hand and then incubated on ice for

30 minutes. After subsequent centrifugation at 12,000 *g* for 10 minutes at 4°C, an RNA pellet was visible at the bottom of the Eppendorf tube. The isopropanol supernatant was discarded, and 1 ml of 75% ethanol was added. The pellet was loosened by vortexing and then centrifuged at 12,000 *g* for 10 minutes at 4°C. This washing step was repeated. The Eppendorf tubes were then left under a fume hood for 10 minutes, to allow the remaining alcohol to evaporate. The pellet was resuspended in 40 µl of nuclease-free water (NFW) or 2 µl of NFW for tiny amounts of RNA. In the last step, the samples were briefly centrifuged and then heated at 55°C for 10 minutes on Thermomixer5436 to improve the RNA solubility. If the RNA was not used immediately, it was stored at -80°C.

2.7.1.2 RNA concentration measurement

The entire workplace was cleaned with RNase-Away. The RNA samples were thawed and placed on ice. The RNA concentration of the samples was measured using the Nanodrop spectrophotometer. It should be 400–600 ng/µl to ensure good complementary DNA (cDNA) synthesis. If this was not the case, the sample was diluted to a suitable concentration with NFW.

2.7.1.3 cDNA synthesis

cDNA was reverse transcribed from mRNA. The RNA concentration was used to calculate which sample volume contained exactly 1 µg of RNA, which was pipetted into an RNase-free 0.2-ml Eppendorf tube. Next, 5 µl of the iScript™ Synthesis Mix (iScript™ cDNA Synthesis Kit, Bio-Rad, Munich, DE) was added, and the volume was adjusted to 20 µl with NFW. The synthesis mix consisted of 1 µl reverse transcriptase and 4 µl of the reaction mix.

A thermal cycler (T100 Thermal Cycler, Bio-Rad) was used for the transcription: annealing at 25°C for 5 minutes, followed by reverse transcription at 46°C for 20 minutes. The reverse transcriptase was inactivated by heating at 95°C for 1 minute, and the samples were then cooled down to 4°C. Then, 140 µl of NFW was added to each sample so that the volume was now 160 µl. The cDNA was stored at -80°C.

2.7.1.4 RT-qPCR

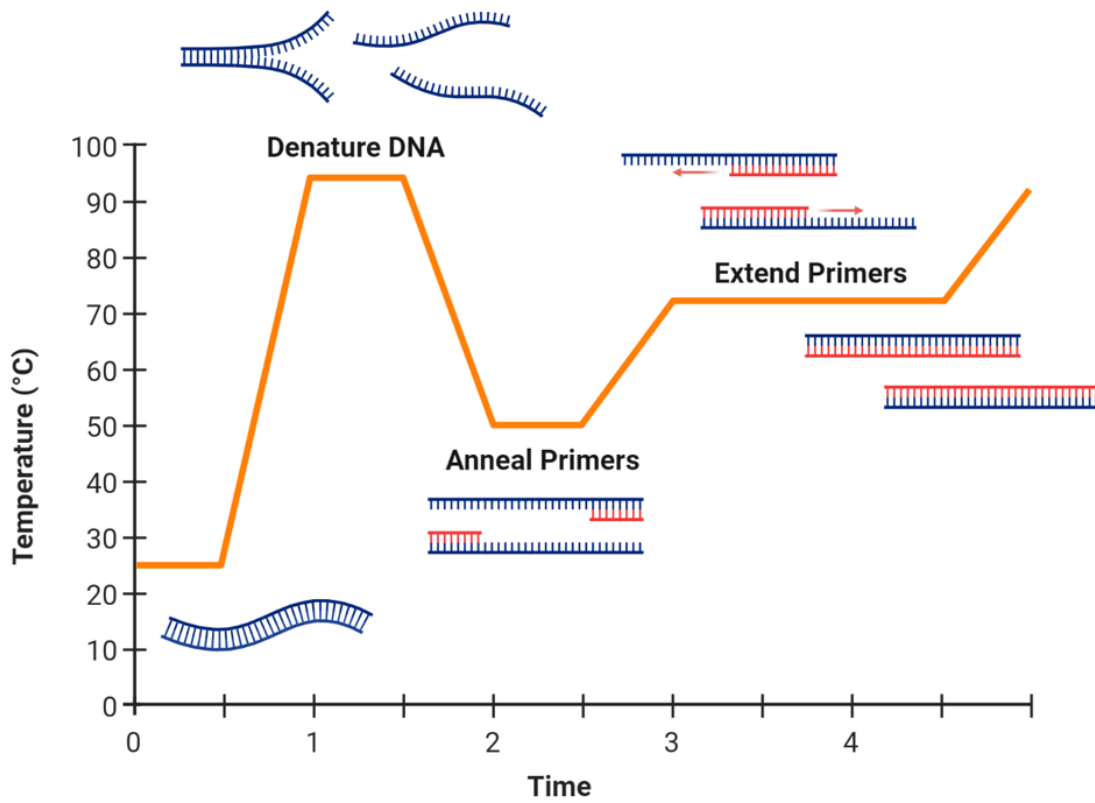


Figure-9: Temperature cycle of real-time quantitative polymerase chain reaction (RT-qPCR).

At 95°C, complementary DNA (cDNA) is denatured so that it is a single strand. Depending on the primer, the primer and DNA strand are hybridized at 57–66°C, and the Taq polymerase synthesizes the complementary DNA strand. This denaturation, annealing, and primer extension protocol are repeated 40 times. After each cycle, the fluorescence intensity is measured; it is proportional to the amount of synthesized double-stranded DNA (dsDNA). The figure was created with Edrawsoft (version 12.0.1).

PCR is used to amplify nucleic acids. In addition to primers and deoxyribonucleotide triphosphates, PCR requires thermostable DNA polymerase of the thermophilic, gram-positive bacterium *Thermus aquaticus* (Taq polymerase). The amplification consists of three successive steps. It is repeated 40 times, with the amount of nucleic acid growing exponentially with each cycle. In the first step, cDNA is denatured at 95°C. It is single-stranded. Depending on the primer in the investigation (Table-9), the primer attaches to the single strand of DNA at 57–66°C, known as annealing (Figure-9). Starting at the 5' end of the single strand, Taq polymerase synthesizes the complementary strand to

synthesize double-stranded DNA (dsDNA). The specific selection of primers enabled the expression of the corresponding genes to be investigated.

Table-9: Mouse primers for real-time quantitative polymerase chain reaction and their melting temperatures (for sequences, see chapter 2.14.5).

Primer	Melting temperature	Primer	Melting temperature
TNF- α	65.5°C	Alox5	63 °C
IL-6 (Interleukin-6)	65.5 °C	LTA4H	60 °C
CXCL1 (C-X-C Motif Chemokine Ligand 1)	65°C	LTC4S	65,5°C
CXCL2/3 (C-X-C Motif Chemokine Ligand 2/3)	63,8°C	MAPK1 (Mitogen-activated protein kinase 1)	61°C
LTB4R1	66°C	MAPK3 (Mitogen-activated protein kinase 3)	66°C
CysLTR1	61.3°C	Tbxas1 (Thromboxane A Synthase 1)	61 °C
CysLTR2	57 °C		

The iTaq Universal SYBR Green Supermix (Bio-Rad) was used to quantify the expression of the genes of interest. In addition to the ingredients required for the PCR, this mix contains a fluorescent dye with a high binding affinity for dsDNA. When it binds to dsDNA, there is a structural change, and the DNA–dye complex absorbs blue light (wavelength $\lambda_{\max} = 497$ nm) and emits green light ($\lambda_{\max} = 520$ nm). The gene expression level can now be quantified based on the fluorescence intensity.

Four microliters of the cDNA sample was pipetted into each well of a PCR plate, followed by 5 μ l of NFW, 10 μ l of SYBR Green, and 1 μ l of the primer mix. For negative controls (no template control [NTC]), the sample was replaced with NFW. A dilution series of cDNA was used to generate a standard curve: 1:2, 1:4, and 1:8. A primer that binds to the ribosomal 18s RNA was used as a reference value because its expression should be constant regardless of the treatment.

A thermal cycler was used for the amplification cycles and fluorescence measurement (C1000 Thermal Cycler CFX96 Real-Time System, Bio-Rad, Munich, DE). The evaluation was performed using the CFX Manager software

(version 3.1, Bio-Rad). The CFX Manager software carried out the corresponding calculation.

2.7.2 ELISA

ELISA was used to detect specific cytokines in the BAL, blood plasma, and bone marrow. ELISA uses enzyme-coupled antibodies that bind to the cytokine to be detected. This enzyme catalyzes a reaction that produces a colored product, and there is a positive correlation between the cytokine concentration and the speed of the color reaction. ELISA kits for TNF- α , IL-6, CXCL1, CXCL2/3, and SDF-1 were used (R&D Systems, Minneapolis, MN, USA). These kits are so-called sandwich ELISAs (Figure-10).

First, the reaction plates are coated with a capture antibody, which binds to the target antigen. According to the manufacturer's instructions, the

capture antibody was dissolved in a special ELISA-PBS, and 100 μ l was pipetted into each well. The plate was incubated overnight at room temperature so the antibody could bind to the surface of the well. The next day, the plate was washed with 400 μ l of ELISA washing buffer (ELISA-PBS with 0.05% Tween). This procedure is subsequently referred to as washing. Nonspecific protein binding sites were blocked by pipetting 300 μ l of reagent diluent into each well and incubating for 1 hour at room temperature. The standard solution was serially diluted seven times at the indicated concentrations provided by the manufacturer to generate a standard concentration curve. After another washing step, 100 μ l

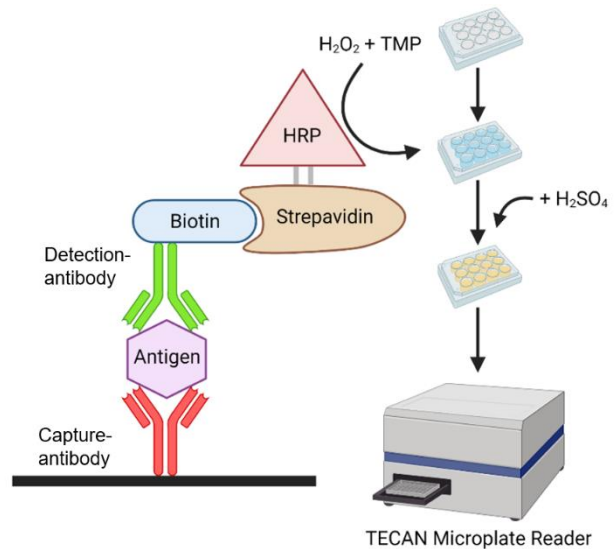


Figure-10: Principle of a sandwich enzyme-linked immunosorbent assay (ELISA).

The reaction plate is coated with the capture antibody. The antigen binds to the capture antibody. The biotin-conjugated detection antibody binds the antigen. Streptavidin binds to biotin and reduces hydrogen peroxide (H₂O₂) to H₂O. 3,3',5,5'-Tetramethylbenzidine (TMB) is oxidized and turns blue. The redox reaction is stopped with sulfuric acid (H₂SO₄), which simultaneously changes the solution to yellow. The color intensity is measured immediately with the TECAN Microplate Reader. The figure was created with Edrawsoft (version 12.0.1).

of the standards or samples was pipetted into each well; there were duplicates for each standard or sample. The plate was incubated for 2 hours at room temperature. Then, 100 μl of the biotin-conjugated detection antibody dissolved in Reagent Diluent, according to the manufacturer's instructions, was added to each well and incubated again for 2 hours at room temperature.

Biotin serves as a binding partner for streptavidin. One hundred microliters of streptavidin-conjugated horseradish peroxidase (HRP) was pipetted into each well. HRP catalyzes the color reaction, and because the conjugated streptavidin has a high affinity for the biotin bound to the detection antibody, the intensity of the color reaction is proportional to the amount of bound antigen. After incubation for 20 minutes in the dark and washing again, 100 μl of a 1:1 mix of hydrogen peroxide (H_2O_2) and 3,3',5,5'-tetramethylbenzidine (TMB) was added to each well incubated for 20 minutes, protected from light. The HRP reduces H_2O_2 to water (H_2O), whereby the tetramethylbenzidine (TMB) serves as a reducing agent and turns light blue due to oxidation. The redox reaction was stopped by adding a 50 μl of ELISA stop solution (sulfuric acid [H_2SO_4]), which turned the samples yellow. The absorbance was immediately read at 570 nm with a TECAN Microplate Reader (Infinite M200 Pro). Magellan (version 7.2) was used to perform linear regression analysis based on the standard.

2.7.3 Immunofluorescence assay

The trachea and lung tissue were exposed, as described in chapter 2.4.1. The lungs were filled with 4% formaldehyde via a tracheostomy cannula and fixed for 10 minutes. The lungs were removed, and the right and left lungs were transferred to separate embedding cassettes and stored in 4% formaldehyde for at least 6 hours.

After fixing in formaldehyde, the specimens were dehydrated by feeding them into a series of increasing ethanol concentrations (50%–100%) using a Leica TP1020 embedding carousel. In the penultimate step, the ethanol was replaced with xylene, and finally, the preparations were immersed in liquid paraffin. With the help of the EG1150H embedding system from Leica, the organs were embedded in paraffin blocks, and then 3–4- μm -thick sections were cut with a

microtome (Leica RM2235), placed on a microscope slide, and dried overnight at 42°C on a paraffin stretching table. Figure-11 provides an overview of immunofluorescence.

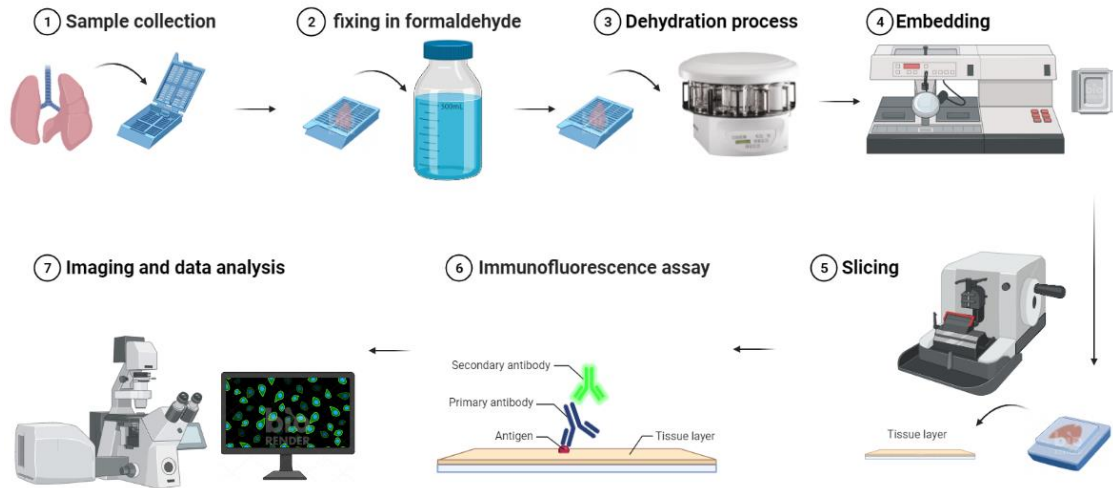


Figure-11: Overview of immunofluorescence process.

① Lung tissue was collected after 10 minutes of fixation in 4% formaldehyde and placed in cassettes. ② Lung tissue was fixed in 4% formaldehyde for 6 hours. ③ Lung tissue was dehydrated by the TP1020 embedding carousel. ④ Lung tissue was embedded by using the EG1150H embedding system. ⑤ Tissue was sliced with a Leica RM2235. ⑥ Slices were stained with various combinations of antibodies. ⑦ Slices were imaged and analyzed by the Leica SP8 system. The figure was created with Edrawsoft (version 12.0.1).

Before staining, the specimens first had to be dewaxed. For this purpose, they were transferred to an alcohol series, as shown in Table-10.

Table-10: Alcohol series for dewaxing immunofluorescent specimens.

Alcohol	Duration
3x Xylol	3x 5 minutes
2x Ethanol 100%	2x 5 minutes
1x Ethanol 96%	5 minutes
1x Ethanol 70%	5 minutes
1x Ethanol 50%	5 minutes

After dewaxing, the sections were washed for 3 × 5 minutes in PBS⁻. It was necessary to unmask the antibodies to allow successful binding to the antigens. This was accomplished by boiling the slices for 10 minutes in a citrate buffer-based unmasking solution (diluted 1:100, Vector Laboratories H3300,

Burlingame, CA, USA). The sections were naturally cooled to room temperature for 1 hour and then washed with PBS⁻ 2 × 5 minutes.

The sections were then fixed with 4% formaldehyde for 10 minutes, and then permeabilized in PBS⁻ containing 0.1% Triton X-100 for 10 minutes. The sections were then washed for 2 × 5 minutes in PBS⁻. For blocking nonspecific antigen-antibody binding, the sections were incubated with 5% bovine serum albumin (BSA) for 60 minutes, then washed for 2 × 5 minutes with PBS⁻. The primary antibody was added to a mixture containing 1% BSA and 1% secondary antibody serum, and the sections were incubated for 1 hour at room temperature or overnight at 4°C. The IgG from the secondary antibody host was used for IgG control, and no primary antibody was added for the negative control.

After washing, fluorescently labeled secondary antibody was added to a mixture containing 1% BSA and 1% secondary antibody serum, and the sections were incubated for 1 hour at room temperature in the dark. Cell nuclei were stained with 4',6-diamidino-2-phenylindole (DAPI; ROTI Mount FluorCare, HP20.1) and then covered with a coverslip. The panel for antibody application is detailed in Table-11.

Table-11: Antibodies used for immunofluorescence.

Primary antibody	Work Concentration	Secondary antibody	Work Concentration
Ly6G (rat anti-mouse)	1:100	Goat anti-rat(A647)	1:500
CysLTR1 (rabbit anti-mouse)	1:200	Goat anti-rabbit(A488)	1:500
LTB4R1 (rabbit anti-mouse)	1:200	Donkey anti-rabbit(A546)	1:500
ERK1/2 (rabbit anti-mouse)	1:200	Goat anti-rabbit(A594)	1:500
p-CREB (mouse anti-mouse)	1:200	Donkey anti-mouse(A488)	1:500
Caspase-1 (rat anti-mouse)	1:200	chicken anti-rat (A594)	1:500
CD41 (rabbit anti-mouse)	1:100	Donkey anti-rabbit(A488)	1:500
P2Y12 (goat anti-mouse)	1:200	Donkey anti-goat(A594)	1:500

Images of the stained sections were taken with Leica's SP8 light confocal microscope. The images were analyzed by Leica Application Suite X (version 5.0.3, Leica, Wetzlar, DE).

2.8 Immunohistochemistry

The steps for dewaxing are the same as described in chapter 2.7.3. Endogenous peroxidase activity was blocked with 30% hydrogen peroxide and methanol. The same unmasking step as in section 2.7.3 was performed to ensure the antibody would successfully bind to the antigen. The sections were incubated with the avidin-blocking mix for 60 minutes to block endogenous avidin. Each 900 µl of avidin-blocking mix contained 1 ml of 1% BSA in PBS⁻, 100 µl of normal rabbit serum, and 4 drops of Avidin block solution.

The primary antibody was rat anti-mouse Ly6G antibody diluted 1:500. A normal rat IgG antibody diluted 1000-fold was used as a positive control; the negative controls had no primary antibodies. They were all diluted with a biotin-blocking mix. Each 1 ml of biotin-blocking mix contained 900 µl of 1% BSA in PBS⁻, 100 µl of normal rabbit serum, and 4 drops of Biotin block solution. The sections were incubated by indicated antibodies at 4°C overnight.

The secondary antibody used was biotinylated rabbit anti-rat IgG. Each secondary antibody mix contained 1 ml of 1% BSA in PBS⁻, 100 µl of rabbit serum, and 10 µl of secondary antibody. After being rinsed with 1% BSA for 5 minutes, the sections were incubated with the secondary antibody mix for 60 minutes.

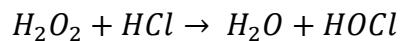
The ABC kit reagents prepared avidin-biotin complexes conjugated with HRP. After another 5-minute PBS⁻ rinse, the slices were incubated with this solution for 30 minutes so that the avidin-biotin complex could bind to the secondary antibody. It was then rinsed again for 5 minutes with PBS⁻. The sections were incubated in a 3,3'-diaminobenzidine (DAB)-containing solution for 5 minutes. DAB was oxidized as a substrate for HRP, creating a water-insoluble brown dye so that the neutrophils were colored brown. The preparations were then rinsed with PBS⁻ for 5 minutes. Finally, the cell nuclei were counterstained with FastNuclearRed for 5 minutes and then rinsed under running tap water for 5 minutes. The alcohol series in Table-10 was used in reverse order to dehydrate the preparations, and then they were covered with Eukitt and a cover slip.

The DM IRB light microscope and the AxioCam MRc camera from Zeiss and Axiovision software (version 4.8.2.0, Zeiss, Oberkochen, DE) was used to take images of the stained sections.

2.9 ROS detection

ROS were detected in both the interstitium and BAL. ROS in the lung interstitium was assayed with dihydroacetylene (DHE), and ROS in BAL was determined using the MPO assay. DHE has specificity for superoxide and H₂O₂. It was used as a fluorescent probe to detect ROS production of PMNs. It displays blue fluorescence in the cytosol until it is oxidized and subsequently interacts with cellular DNA to stain the nucleus a bright fluorescent red. After incubation with CD45 and Ly6G antibodies, samples were permeated with Permashield buffer and then incubated with 1 ml of staining buffer containing 5 µl of DHE and incubated for 20 minutes, followed by the usual washing and fixation procedure.

MPO is an enzyme that occurs in azurophilic granules of neutrophilic granulocytes (Kinkade et al., 1983). It catalyzes the formation of hypochlorous acid (HOCl) from H₂O₂ (hydrogen peroxide) (Winterbourn et al., 2006):



2,2'-Azino-bis(3-ethylbenzthiazoline-6-sulfonic acid) (ABTS), an MPO substrate, was used to evaluate MPO activity. During the enzymatic conversion of ABTS by MPO, the greenish-turquoise ABTS cation is created. For the reaction, 50 µl of sample, 50 µl of citrate buffer, and 100 µl of ABTS solution were pipetted into each well, and the plate was incubated at 37°C for 30 minutes. The intensity of the color reaction was then determined photometrically using the TECAN Microplate Reader (Infinite M200 Pro) at 405 nm.

2.10 Microvascular permeability determined by the BCA assay

Using a BCA protein assay kit, extravasation of protein in BAL was detected as an indication of capillary leakage. The BCA method was first described in 1985 (Smith et al., 1985). The method is based on proteins reducing Cu²⁺ to Cu⁺ in an alkaline medium. Cu⁺ forms a complex with BCA, which turns purple and can be

detected photometrically at 562 nm. For this assay, 25 μ l of supernatant from each BAL was incubated with 200 μ l of BCA solution for 30 minutes at 37°C. The albumin standard (2 mg/ml) included with the kit was used as a reference. The TECAN Microplate Reader (Infinite M200 Pro) was used for the photometric measurement of the color reaction.

2.11 Phamtarget and Search Tool for the Retrieval of Interacting Genes/Proteins (STRING) analysis

A pharmacological target network analysis was performed to understand the pharmacological similarities and differences between montelukast and zileuton and the potential pharmacological functions (Figure-12).

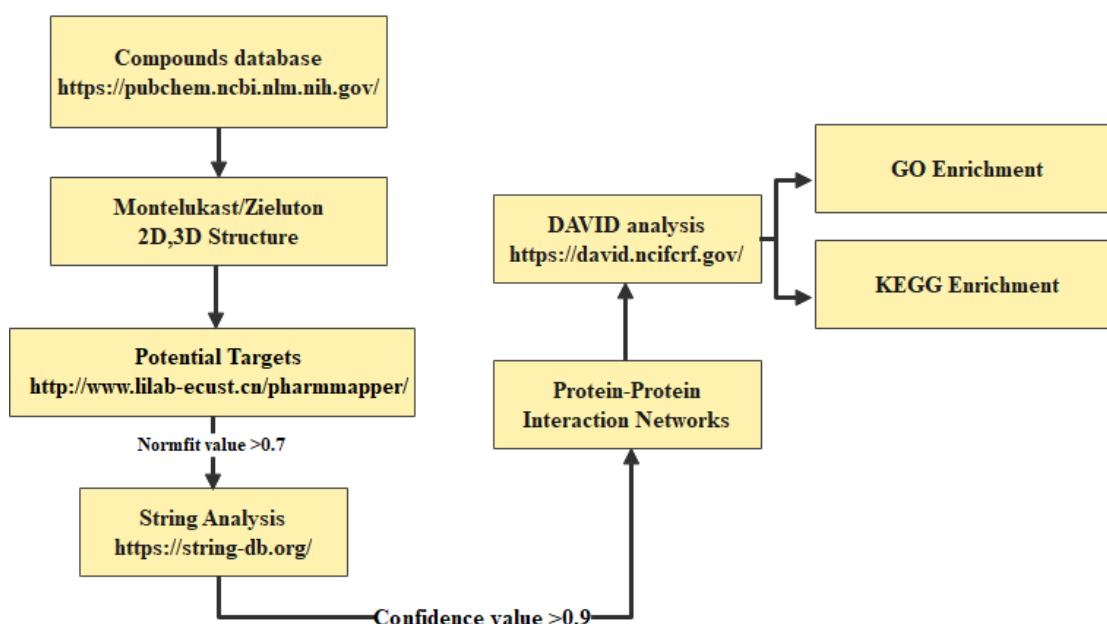


Figure-12: Flow chart of target protein analysis.

DAVID=The Database for Annotation, Visualization, and Integrated Discovery.
GO= Gene ontology. KEGG= the Kyoto Encyclopedia of Genes and Genomes.
The figure was created with Edrawsoft.

The two-dimensional (2D) structural formulae and three-dimensional (3D) pharmacophore models of montelukast and zileuton were downloaded from PubChem (<https://pubchem.ncbi.nlm.nih.gov/>), a large, free, public database of chemical information.

The PharmMapper server (<http://www.lilab-ecust.cn/pharmmapper/>) is an open-source web tool that identifies potential targets for a given probe small molecule using a pharmacophore mapping approach (Liu et al., 2010; Wang et al., 2017). By sending the 3D pharmacophore models from PubChem, we obtained information on potential drug targets for montelukast and zileuton. The information includes the name of the target protein and the number of hydrophobic groups in its potential binding site, positive and negative charge content, binding capacity (Norm Fit value), and gene name.

An interface to the STRING database (<https://string-db.org/>) provides information about known and predicted interactions among proteins. The STRING protein–protein interaction (PPI) analysis includes a group of highly bound proteins (Norm Fit > 0.7).

Cytoscape is a convenient, open-source software for visualizing biological pathways and PPI networks. The STRING analysis selected proteins with a high confidence value (> 0.9) to construct the PPI network plot. Cytoscape (Version 3.9.0) contributed to this endeavor.

The Database for Annotation, Visualization, and Integrated Discovery (DAVID) is a comprehensive molecular function annotation tool that represents an essential reference for researchers to understand the biological significance behind many molecules. DAVID (<https://david.ncifcrf.gov/>) investigated those proteins included in the PPI network. The outcomes from the DAVID analysis were plotted by using <https://www.bioinformatics.com.cn>, a free online data analysis and visualization platform.

Pathview (Version 3.15) is a pathway-based data integration and visualization toolset. It plots and displays various biological data on a graph of related pathways (Luo, 2022).

2.12 Platelet isolation

Human whole blood was separated for *ex vivo* experiments according to the following steps. Ten milliliters of blood was collected in a citrate anticoagulation

tube. It was centrifuged at 900 *g* for 5 minutes at 16°C. After the first centrifugation, the whole blood was divided into three layers. The upper layer contains mainly platelets and a few leukocytes. The thin middle layer is the buffer layer, which is rich in leukocytes. The bottom layer consists mainly of red blood cells. The upper layer was transferred into sterile tubes and centrifuged at 1000 *g* for 10 minutes at 16°C. Then, the upper two thirds of the plasma were discarded, and the lower one third was gently mixed to obtain platelet-rich plasma (PRP). It was then placed on ice for 5 minutes to allow sufficient homogenization before use in *ex vivo* experiments.

2.13 Statistics

Statistical evaluation of the data collected was carried out with GraphPad Prism (Version 9.1 from GraphPad Software, Inc., San Diego, USA). The data were checked for a normal distribution using the Shapiro–Wilk and Kolmogorov–Smirnov tests. A one-way analysis of variance (ANOVA) with the Bonferroni post hoc test was used for normally distributed data, and the Kruskal–Wallis test was used for non-normally distributed data. The underlying significance level was $\alpha = 5\%$. The significance is marked in figures with asterisks, which are described in Table-12.

Table-12: Overview of the Significances.

Symbol	p-Value
*	$p \leq 0,05$
**	$p \leq 0,01$
***	$p \leq 0,001$
****	$p \leq 0,0001$

2.14 List of materials

2.14.1 Chemicals and reagents

Chemicals	Article number	Manufacturer	Place
ABTS	A1888-2G	Sigma-Aldrich	St. Louis, USA
Ammonium chloride (NH ₄ Cl)	3J002532	AppliChem	Darmstadt, DE
Ammonium persulfate 10% (APS)	9592.3	Carl Roth GmbH	Karlsruhe, DE
Aqua dest		Own production	Tübingen, DE
Avidin/Biotin Blocking Kit	SP-2001	Vector Laboratories	Burlingame, USA
Bovines Serum Albumin	A3294	Sigma-Aldrich	St. Louis, USA
Chloroform	C2432	Sigma-Aldrich	St. Louis, USA
DAB Peroxidase Substrate Kit	SK-4100	Vector Laboratories	Burlingame, USA
Disodium-EDTA 0,5 M	E-7889	Sigma-Aldrich	St. Louis, USA
Ethanol for molecular biology	A3678	AppliChem GmbH	Darmstadt, DE
Eukitt Quick-hardening mounting medium	03989	Sigma Aldrich	St. Louis, USA
Formaldehyde (4%)	100496	Merck KGaA	Darmstadt, DE
Glycerin	G5516	Sigma-Aldrich	St. Louis, USA
Histogreen HRP-Substrate Kit	E109	Linaris	Dossenheim, DE
Isopropanol	I9516	Sigma-Aldrich	St. Louis, USA
iTaq™ Universal SYBR® Green Supermix	1725124	Bio-Rad	München, DE
Methanol	32213	Honeywell	Morristown, USA
Sodium azide (NaN ₃)	S8032	Sigma-Aldrich	St. Louis, USA
Sodium chloride (NaCl)	52455	Sigma-Aldrich	St. Louis, USA
Sodium hydrogen carbonate (NaHCO ₃)	1063290500	Merck KGaA	Darmstadt, DE
NP-40 (IGEPAL® CA-630)	I8896	Sigma-Aldrich	St. Louis, USA
Mayer's hemalum solution	A0884	AppliChem GmbH	Darmstadt, DE
Nuclease Free Water	A7398	AppliChem GmbH	Darmstadt, DE
PBS ⁻	18912014	Sigma-Aldrich	St. Louis, USA
RNase Away	7002	Molecular BioProducts Inc.	San Diego, USA
Sodium dodecyl sulfate(SDS)	L4509	Sigma-Aldrich	St. Louis, USA
Triton® X-100	A9779	AppliChem GmbH	Darmstadt, DE

TRIZOL™ Reagent	15596026	Thermo Fisher Scientific	Waltham, USA
Turk's solution	93770	Merck KGaA	Darmstadt, DE
Tween 20	A4974	AppliChem GmbH	Darmstadt, DE
Unmasking Solution	H-3300	Vector Laboratories	Burlingame, USA
Vectastain ABC Kit HRP	PK-4000	Vector Laboratories	Burlingame, USA
Hydrogen peroxide (30%)	H1009	Merck KGaA	Darmstadt, DE
Xylene	131769	AppliChem GmbH	Darmstadt, DE

2.14.2 Biochemical supplies

Items	Article number	Manufacturer	Place
Montelukast	151767-02-1	Cayman chemical company	Michigan, USA
Zileuton	111406-87-2	Cayman chemical company	Michigan, USA
Ketamine hameln	03760898	Hameln Pharma Plus GmbH	Hameln, DE
Sedaxylan	615906	Dechra Pharmaceuticals	Northwich, GB
Heparin	059872	Leo Pharma GmbH	Neu-Isenburg, DE
LPS	L6011	Sigma-Aldrich	St. Louis, USA
NaCl	2350748	B. Braun	Melsungen, DE

2.14.3 Enzyme

Enzyme	Article number	Manufacturer	Place
iScript cDNA Synthesis Kit	1708891	Bio-Rad	München, DE
Collagenase from Clostridium histolyticum	C7657	Sigma-Aldrich	St. Louis, USA
DNAse from bovine pancreas	DN25	Sigma-Aldrich	St. Louis, USA
Hyaluronidase from bovine testes	H3506	Sigma-Aldrich	St. Louis, USA
Streptavidin-HRP	DY998	R&D Systems	Minneapolis, USA

2.14.4 Solutions

Solution	Article number	Manufacturer	Place
----------	----------------	--------------	-------

ELISA PBS		own production	Tübingen, DE
Aqua dest.	1 L		
KCl	0,2 g		
KH ₂ PO ₄	0,2 g		
NaCl	8,0 g		
Na ₂ HPO ₄	1,4 g		
filter			
Adjust pH to 7.2 - 7.4			
ELISA stop solution:		own production	Tübingen, DE
Aqua dest.	68 ml		
H ₂ SO ₄ (18 M)	4 ml		
Erythrocyte Lysis Buffer (organs)		own production	Tübingen, DE
Aqua dest.	1 L		
NH ₄ Cl	8,024 g		
NaHCO ₃	0,84 g		
Disodium-EDTA	0,372 g		
FACS Lysing Solution (Erythrocyte lysis)	349202	BD Biosciences	Franklin Lakes, USA
FACS Flow	342003	BD Biosciences	Franklin Lakes, USA
FACS Shutdown Solution	334224	BD Biosciences	Franklin Lakes, USA
FACS Clean Solution	340345	BD Biosciences	Franklin Lakes, USA
FACS Rinse Solution	340346	BD Biosciences	Franklin Lakes, USA
FACS staining buffer:		own production	Tübingen, DE
Aqua dest.	1 L		
PBS ⁻	2 Tablets		
BSA	10 g		
NaN ₃	5 ml		
Substrate Reagent Pack (ELISA)	DY999	R&D Systems	Minneapolis, USA

2.14.5 Primer for the RT-qPCR

Primer	Sequence	Manufacturer	Place
m18s for	5'- gta acc cgt tga acc cca tt -3'	biomers.net	Ulm, DE
m18s rev	5'- cca tcc aat cgg tag tag cg -3'	biomers.net	Ulm, DE
mTNF α for	5'- cgt cgt agc aaa cca cca ag -3'	biomers.net	Ulm, DE
mTNF α rev	5'- gaa cct ggg agt aga caa gg -3'	biomers.net	Ulm, DE
mIL6 for	5'- gag gat acc act ccc aac ag -3'	biomers.net	Ulm, DE
mIL6 rev	5'- aac gca cta ggt ttg ccg ag -3'	biomers.net	Ulm, DE
mCXCL1 for	5'- aaa ccg aag tca tag cca cac -3'	biomers.net	Ulm, DE
mCXCL1 rev	5'- ggg gac acc ttt tag cat ctt -3'	biomers.net	Ulm, DE

mCXCL2/3 for	5'- atc cag agc ttg agt gtg acg -3'	biomers.net	Ulm, DE
mCXCL2/3 rev	5'- gcc ttg cct ttg ttc agt atc -3'	biomers.net	Ulm, DE
mLTB4R1 for	5'- ccg ccc ctt tat gtc cca aa-3'	biomers.net	Ulm, DE
mLTB4R1 rev	5'- gcc agc aga aaa gac acc ac -3'	biomers.net	Ulm, DE
mCysLTR1 for	5'- ggt ttc ttt ggc aat agc tt -3'	biomers.net	Ulm, DE
mCysLTR1 rev	5'- aac ata ata gac cac acg gag a -3'	biomers.net	Ulm, DE
mCysLTR2 for	5'- ctt ccg att ttc tat tca tca gc-3'	biomers.net	Ulm, DE
mCysLTR2 rev	5'- cca agt ccc caa ata tcc aa -3'	biomers.net	Ulm, DE
mAlox5 for	5'- cca ttg cca tcc agc tca acc a -3'	biomers.net	Ulm, DE
mAlox5 rev	5'- aag cca gtc gta ctt tga atc cg -3'	biomers.net	Ulm, DE
mLTA4H for	5'- tca agc cca att acg acg tga c-3'	biomers.net	Ulm, DE
mLTA4H rev	5'- atc ttc ctc ttt ggc agt aac cc- 3'	biomers.net	Ulm, DE
mLTC4S for	5'- aac tgc agc gag tac ttt ccg- 3'	biomers.net	Ulm, DE
mLTC4S rev	5'-aca ggt aga aca gtc cgc aca gg-3'	biomers.net	Ulm, DE
mTbxas1 for	5'- att ctg ccc aat aag aac cga g -3'	biomers.net	Ulm, DE
mTbxas1 rev	5'- tgg tcc cgt aag gca atc aca -3'	biomers.net	Ulm, DE
mMAPK1 for	5'- aat tgg tca gga caa ggg ctc -3'	biomers.net	Ulm, DE
mMAPK1 rev	5'- gag tgg gta agc tga gac gg -3'	biomers.net	Ulm, DE
mMAPK3 for	5'- agt ctc tgc cct cga aaa cc -3'	biomers.net	Ulm, DE
mMAPK3 rev	5'- act gtg atg cgc ttg ttt gg -3'	biomers.net	Ulm, DE

2.14.6 FACS-Antibody

FACS		Article number	Manufacturer	Place
Cytometer Setup and Tracking Beads		642412	BD Biosciences	Franklin Lakes, USA

Antibody	Fluorescence	Clone	Article number	Manufacturer	Place
CD42b	FITC	Xia.G5	M040-1	Emfret Analytics	Eibelstadt, DE
CD45	PerCP	RA3-6B2	103130	BioLegend	San Diego, USA
Ly6G	PE-Cy7	1A8	127618	BioLegend	San Diego, USA
Ly6G	APC	1A8	127614	BioLegend	San Diego, USA
CD62L	PB	MEL-14	104424	BioLegend	San Diego, USA
CD62P	APC	RMP-1	148304	BioLegend	San Diego, USA

CD162	PE	2PH1	555306	BD Biosciences	Franklin Lakes, USA
CD11b	PB	M1/70	101224	BioLegend	San Diego, USA
CD49d	APC	R1-2	103614	BioLegend	San Diego, USA
CD11a	PE	H155-78	141006	BioLegend	San Diego, USA
CXCR4	APC	L276F12	146508	BioLegend	San Diego, USA
CXCR2	PE	SA044G4	149304	BioLegend	San Diego, USA

2.14.7 Immunofluorescence staining

Product	Article number	Manufacturer	Place
ly6G(rat anti-mouse)	ab25377	Abcam	Cambridge, UK
CysLTR1(rabbit anti-mouse)	ABIN6260900	antibodies-online GmbH	Aachen, DE
LTB4R1(rabbit anti-mouse)	ABIN905202	antibodies-online GmbH	Aachen, DE
CD41(rabbit anti-mouse)	ab63983	Abcam	Cambridge, UK
ERK1/2 (rabbit anti-mouse)	0812019	Cell signaling	Danvers, USA.
p-CREB (mouse anti-mouse)	sc-81486	Santa cruz	Dallas, USA
Caspase-1 (rat anti-mouse)	14-983280	Invitrogen	Waltham,USA
P2Y12(goat anti-mouse)	sc-27152	Santa cruz	Dallas, USA
normal goat IgG	31245	Invitrogen	Waltham,USA
normal donkey IgG	ABIN5633226	antibodies-online GmbH	Aachen, DE
normal goat serum	sc-2043	Santa cruz	Dallas, USA
normal donkey serum	ab7475	Abcam	Cambridge, UK

2.14.8 Materials

Product	Article number	Manufacturer	Place
96-well plates for immunology (ELISA plates)	436110	Thermo Fisher Scientific	Waltham, USA
Cover glasses (24 x 60 mm)	01-2460/5	R. Langenbrinck GmbH	Emmendingen, DE
ROTILABO® embedding cassettes	K113.1	Carl Roth GmbH	Karlsruhe, DE
FACS Falcon 5 ml	352052	Corning Inc.	Corning, USA
Falcon 15 ml	188271	Greiner Bio-One GmbH	Frickenhausen, DE
Falcon 50 ml	10788561	Corning Inc.	Corning, USA
"Pap Pen" grease pencil	MKP-1	Kisker Biotech	Steinfurt, DE
Filter paper (10 cm)	CA20.1	Carl Roth GmbH	Karlsruhe, DE
Filter pipette tip 10 µl short	07-602-8300	nerbe plus GmbH	Winsen, DE
Filter pipette tip 10 µl long	07-612-8300	nerbe plus GmbH	Winsen, DE
Filter pipette tip 100 µl	07-642-8300	nerbe plus GmbH	Winsen, DE

Filter pipette tip 1000 µl	07-693-8300	nerbe plus GmbH	Winsen, DE
Filter pipette tip 20 µl	07-622-8300	nerbe plus GmbH	Winsen, DE
Filter pipette tip 200 µl	07-662-8300	nerbe plus GmbH	Winsen, DE
Gazin gauze compresses	18500	Lohmann & Rauscher GmbH	Rengsdorf, DE
Microlance cannula 3 (22G)	300900	BD Biosciences	Franklin Lakes, USA
Microlance cannula 3 (27G)	302200	BD Biosciences	Franklin Lakes, USA
Sterican cannula (20G)	4657519	Braun Medical	Melsungen, DE
Comb, 12, well, 1.0 mm	NC3012	Thermo Fisher Scientific	Waltham, USA
Nunc™ cryovials 1.8 ml	10674511	Thermo Fisher Scientific	Waltham, USA
Multi-channel pipette tips epT.I.P.S.® 10 ml	0030000811	Eppendorf	Hamburg, DE
Multi-channel pipette tips epT.I.P.S.® 200 µl	0030000870	Eppendorf	Hamburg, DE
Microtome Blade R35	0207500005	Feather	Osaka, JPN
Microseal 'B' PCR Plate Sealing Film	MSB101	Bio-Rad	München, DE
Multiplate® 96-Well PCR Plate	MLL9601	Bio-Rad	München, DE
Nitrile gloves	290419	Abena	Aabenraa, Denmark
Nitrile gloves	942202	Paul Hartmann AG	Heidenheim, DE
SuperFrost Plus slide (75 x 25 mm)	03-0060	R. Langenbrinck GmbH	Emmendingen, DE
Parafilm M sealing film	5170002	Omnilab	Bremen, DE
Paraplast Plus	X881.1	Leica	Wetzlar, DE
Pasteur pipette 3ml	LW4112	Alpha Laboratories Limited	Eastleigh, UK
Pipette tip 10 µl	701130600	Sarstedt	Nürnbrecht, DE
Pipette tip 20 µl	701116	Sarstedt	Nürnbrecht, DE
Pipette tip 200 µl	70760002	Sarstedt	Nürnbrecht, DE
Pipette tip 1000 µl	701181	Sarstedt	Nürnbrecht, DE
Reaction vessel 0.2 ml (RNase free)	XT87.1	Carl Roth GmbH	Karlsruhe, DE
Reaction vessel 1.5 ml	616201	Greiner Bio-One GmbH	Frickenhausen, DE
ROTILABO® reaction vessel (RNase free) 1.5 ml	EA84.1	Carl Roth GmbH	Karlsruhe, DE
1 ml syringe	300013	BD Biosciences	Franklin Lakes, USA
Syringe 10 ml Inject Luer Solo	4606108V	Braun Medical	Melsungen, DE

Syringe 2 ml Inject Luer Solo	4606027V	Braun Medical	Melsungen, DE
Syringe 5 ml Inject Luer Solo	4606051V	Braun Medical	Melsungen, DE
Stripette 10 ml	10608261	Corning Inc.	Corning, USA
Stripette 25 ml	10024420	Corning Inc.	Corning, USA
Stripette 5ml	10156420	Corning Inc.	Corning, USA
Trans-Blot® Turbo Midi 0.2 µm PVDF Transfer Pack	1704157	Bio-Rad	München, DE
ROTILABO® sealing film	EN76.1	Carl Roth GmbH	Karlsruhe, DE
Cell sieve (70 µm pore size)	542070	Greiner Bio-One GmbH	Frickenhausen, DE

2.14.9 Devices

Device	Description	Manufacturer	Place
Aqua dest. Manufacturing device	Purelab flex 2	Veolia Water Technologies	Paris, FR
Chemiluminescence reader	Fusion SL4	Vilber Lourmat	Eberhardzell, DE
Embedding system	EG1150H	Leica	Wetzlar, DE
ELISA Washer	hydro flex	Tecan	Männedorf, CH
Histocarousel	TP1020	Leica	Wetzlar, DE
Homogenizer	Precellys 24	Bertin technologies	Montigny-le-Bretonneux, FR
Inhalation chamber	Own production	Medical technology workshop at the University Hospital	Tübingen, DE
Incubation shaker	Infors HT Ecotron	Infors AG	Einsbach, DE
Microplate reader	Infinite M200 Pro	Tecan	Männedorf, CH
Microtome	RM2235	Leica	Wetzlar, DE
Incubator	Heraeus Oven	Thermo Fisher Scientific	Waltham, USA
Multichannel pipette 100 µl	Research plus	Eppendorf	Hamburg, DE
Multichannel pipette 300 µl	Research plus	eppendorf	Hamburg, DE
Microscope	Leitz DM IRB	Leica	Bensheim, DE
Microwave	Normal version	Bosch	Stuttgart, DE
Multi-pipette	Multi-pipette plus	Eppendorf	Hamburg, DE
Nanodrop	NanoDrop 2000 Spectrophotometer	Thermo Fisher Scientific	Schwerte, DE
Paraffin stretching bath	HI1210	Leica	Wetzlar, DE
Thermal cycler	C1000 Thermal Cycler CFX96 Real-Time System	Bio-Rad	München, DE
Paraffin stretching table	HI1220	Leica	Wetzlar, DE
Pipette 10 µl	Reference	Eppendorf	Hamburg, DE
Pipette 100 µl	Reference	Eppendorf	Hamburg, DE
Pipette 1000 µl	Reference	Eppendorf	Hamburg, DE

Thermal cycler	T100 Thermal Cycler	Bio-Rad	München, DE
Pipette 20 µl	Research plus	Eppendorf	Hamburg, DE
Pipette 200 µl	Research plus	Eppendorf	Hamburg, DE
Thermoblock	Thermomixer 5436	Eppendorf	Hamburg, DE
Table mixer	Vortex Genie 2	Scientific Industries	New York, USA
Benchtop centrifuge	Mini-Zentrifuge ROTILABO®	Carl Roth GmbH	Karlsruhe, DE
Nebulizer	MicroAir U100	OMRON Healthcare	Kyoto, JP
Scale	Mettler PK4800	Mettler	Gießen, DE
Rocker shaker	Speci-Mix 92641	Bioblock Scientific	Dubuque, USA
Scale	Kern ALS	Kern & Sohn GmbH	Balingen, DE
Western Blot Transfer System	Trans-Blot Turbo Blotting System	Bio-Rad	München, DE
Rocker shaker	Wippschüttler ST5	CAT	Ballrechten-Dottingen, DE
Centrifuge	Heraeus Fresco 17 Centrifuge	Thermo Fisher Scientific	Schwerte, DE
Centrifuge	Heraeus Megafuge 1.0R	Thermo Fisher Scientific	Schwerte, DE

2.14.10 Software

Software	Manufacturer	Place
Leica Application suite X	Leica	Wetzlar, DE
CFX Manager v3.1	Bio-Rad	München, DE
Excel 2016	Microsoft	Redmond, USA
FACSDiva Software v9	BD Biosciences	Franklin Lakes, USA
Flow Jo v7.2.5	FlowJo LCC	Ashland, USA
GraphPad Prism v9	GraphPad Software, Inc.	San Diego, USA
Magellan v7.2	Tecan	Männedorf, CH
Nanodrop 2000 v1.6	Thermo Fisher Scientific	Waltham, USA
PowerPoint 2016	Microsoft	Redmond, USA
Word 2016	Microsoft	Redmond, USA
Edraw V12.0.1	Edrawsoft	Shenzhen, China
Cytoscape V3.9.0	NIGMS	Bethesda, USA

3 Results

3.1 Migration of neutrophils was dampened by montelukast and zileuton

3.1.1 Neutrophils were decreased in each pulmonary compartment

As previously described, excessive neutrophil migration is a major contributor to the inflammatory response in the lung (Zemans and Matthay, 2017). We firstly performed immunohistochemistry to quantify PMN infiltration into the lung of mice.

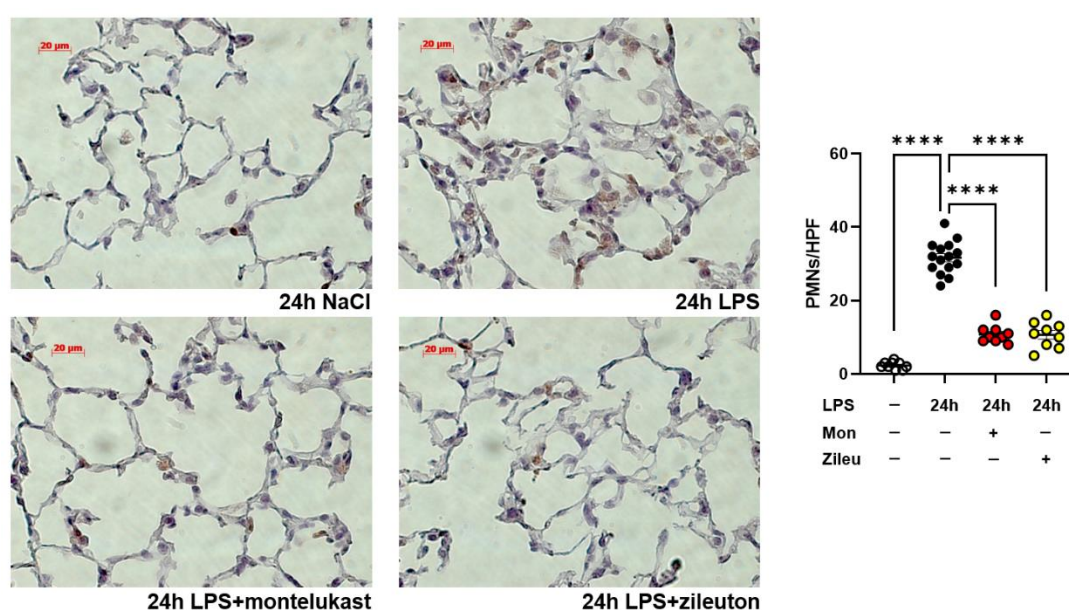


Figure-13: Immunohistochemical staining of the pulmonary tissue at indicated conditions.

Overview of lung histology and morphology by immunohistochemistry under indicated conditions. PMNs were stained with a specific marker Ly6G and appeared brown in histology (original magnification, 63x, one representative image of $n \geq 3$ is shown). Scaled bar = 20 μ m. PMNs from five representative pictures were enumerated from three different slides by light microscopy ($n=9-15$). Data are presented as mean \pm SEM; **** $p < 0.0001$. Multiple group comparison was analyzed by one-way ANOVA and Bonferroni post-hoc test. HPF=high power field.

PMNs were immunohistochemistry labeled with a specific antibody Ly6G, appearing brown in histology. Our acute pulmonary inflammation model showed that nebulized inhalation of LPS in mice successfully induced neutrophil migration into the lung and resulted in a significant increase of neutrophils in the lung tissue

24 hours after the onset of inflammation and could be significantly alleviated by montelukast and zileuton (Figure-13).

Since PMN counts from histological sections are relatively imprecise, we verified this and explored more detail with additional flow cytometry-based methods.

Neutrophil infiltration was evident at all three different pulmonary compartments (intravascular, lung tissue, and alveoli) 24 hours after the onset of inflammation. Leukotriene pathway blockers montelukast and zileuton significantly dampen neutrophil recruitment in all explored compartments (Figure-14a).

The blockade of inflammatory neutrophil migration into the lung induced by these agents appears to be all-encompassing. To confirm this, we investigated them in a more detailed pulmonary compartment model. A second different fluorescently conjugated Ly6G antibody (APC-Ly6G) was injected via the tail vein to distinguish between neutrophils attached to the pulmonary endothelium (APC-Ly6G+/PE-Cy7-Ly6G+) and neutrophils derived from the interstitium (APC-Ly6G-/PE-Cy7-Ly6G+). Consistent with the findings of montelukast and zileuton on neutrophil migration throughout the lung, there were reductions in neutrophils adhering to the pulmonary vasculature and neutrophils in the lung interstitium (Figure-14b).

These findings confirmed our conclusion based on Figure-14a that montelukast and zileuton suppress neutrophil aggregation in all compartments under inflammation.

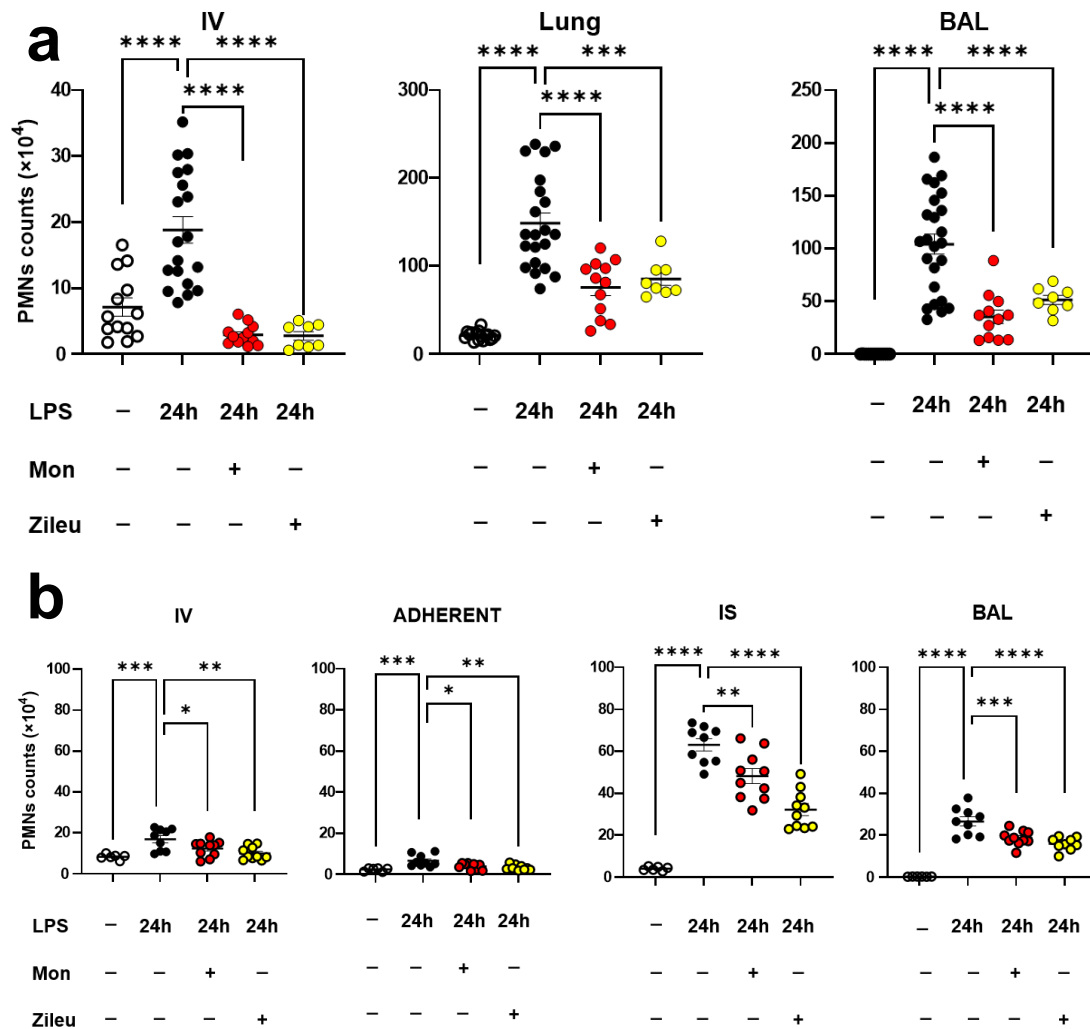


Figure-14: The effects of montelukast and zileuton on the migration of neutrophils into different compartments.

Flow cytometry was used to detect and quantify PMNs. CD45-positive and Ly6G-positive cells were identified as PMNs. Montelukast and zileuton inhibited LPS inhalation-induced migration of neutrophils in intravascular(IV) (Figure-14a,b), adherent to the pulmonary endothelium (ADHERENT) (Figure-14b), in the lung interstitium (IS) (Figure-14b) and Bronchoalveolar lavage (BAL) (Figure-14a,b). The data are presented as mean \pm standard error of the mean(SEM), $n \geq 8$; * $p < 0.05$; ** $p < 0.01$; *** $p < 0.001$; **** $p < 0.0001$. Multiple group comparisons were analyzed by one-way analysis of variance with the Bonferroni post hoc test, or with the Kruskal–Wallis test.

3.1.2 Neutrophil release was restrained in bone marrow

Since neutrophils were reduced in each compartment after montelukast or zileuton administration, leukocytes are generated in the bone marrow and then

released into the blood circulation. We asked whether the decrease in neutrophils outside the bone marrow is due to decreased neutrophil release from the bone marrow?

SDF-1 is a chemokine mainly in the bone marrow and has a strong neutrophil chemotactic capacity (Eash et al., 2010). We hypothesized that montelukast and zileuton reduce the release of bone marrow neutrophils by increasing the concentration of SDF-1 in the bone marrow. Bone marrow neutrophils express both CXCR2, a primary receptor for inflammatory factors, and CXCR4, a major receptor for SDF-1, during the transition from naive to mature. CXCR2 and CXCR4 are essential for the neutrophil life cycle (McKenna et al., 2021). As neutrophils progress from naive to mature, more CXCR2 and fewer CXCR4 are expressed.

To understand the link between SDF-1 in the bone marrow and PMNs released into the blood, we isolated neutrophils from whole bone marrow, analyzed CXCR4 and CXCR2 on them, and measured SDF-1 concentrations in the bone marrow and blood. Besides, we performed counts of mature neutrophils and band neutrophils using Diff-quick stained blood smears.

We observed that montelukast and zileuton increased the SDF-1 concentration in the bone marrow and kept PMNs in the bone marrow (Figure-15a,b). However, the SDF-1 concentration in the blood did not change (Figure-15c).

CXCR4-positive neutrophils are more likely to stay in the bone marrow than CXCR2-positive neutrophils. As far as we know, immature cells express more CXCR4, while mature neutrophils should express more CXCR2 (McKenna et al., 2021). So, we prepared blood smears from eight to twelve weeks old wild-type C57BL/6 mice and used the Diff Quik staining method. Both Segmented and banded PMNs in the blood were significantly lifted 24h after LPS stimulation and could be reduced by montelukast and zileuton. And the results showed that segmented PMNs were reduced to a greater extent than banded PMNs (Figure-15d).

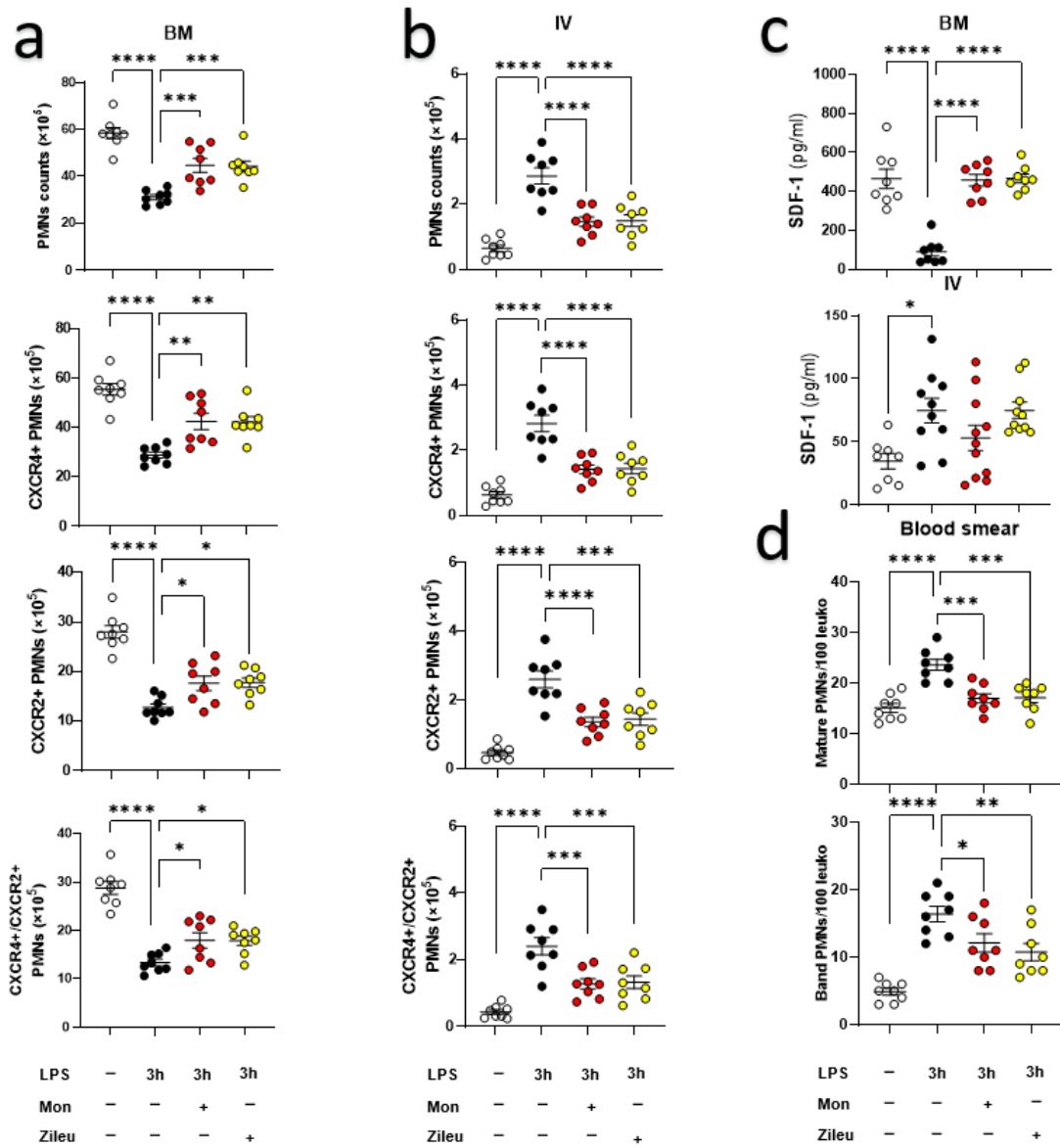


Figure-15: Neutrophil release was significantly restrained by montelukast and zileuton in bone marrow

CXCR4 and CXCR2 on neutrophils were detected by flow cytometry (Figure-15a,b). SDF-1 was measured by ELISA 3 hours following LPS exposure (Figure-15c). Blood smears were stained by modified Giemsa staining (Diff Quik) (Figure-15d). Differential counts were conducted under 40 \times magnification of the immersion objective by counting 100 leukocytes in randomly selected fields of view. The data are presented as mean \pm SEM, $n=8$; * $p < 0.05$; ** $p < 0.01$; *** $p < 0.001$; **** $p < 0.0001$. Multiple group comparisons were analyzed by one-way analysis of variance with the Bonferroni post hoc test, or by the Kruskal–Wallis test.

3.2 Adhesion molecules were affected by montelukast and zileuton

As presented in chapter 3.1.1, 24 hours after LPS inhalation and montelukast or zileuton administration, there were significantly fewer neutrophils in the blood, lung tissue, and alveoli compared with the inflammatory status (Figure-14). As described in chapter 1.2.1, neutrophils must sequentially cross the endothelial, interstitial, and epithelial barriers to enter the alveolar lumen during migration to the lung. These steps require the regulation of multiple molecules in different compartments to interact with the endothelium and epithelium to complete the adhesion cascade reaction. That leads to the question, what are the impacts of montelukast and zileuton on these adhesion molecules in different compartments?

Next, we investigated the expression of specific adhesion molecules on neutrophils as they migrate through the different lung compartments, namely P-selectin, L-selectin, PGSL-1, LFA-1, Mac-1, and VLA-4. Our previous studies revealed that these adhesion molecules show altered expression patterns during neutrophil migration and play distinct roles in different steps (Konrad et al., 2019).

CD62P – The CD62P signal on PMNs was low in the blood but increased 10-fold when PMNs reached lung tissue and alveoli. CD62P expression on neutrophils in the montelukast-treated group was significantly reduced 24 hours after inflammation onset in intravascular, lung tissue, and BAL. Zileuton decreased neutrophil CD62P expression significantly in the BAL (Figure-16a).

CD62L – There were no significant differences in CD62L expression on neutrophils after LPS induction in blood and lung tissue. Montelukast and zileuton significantly decreased CD62L expression only on BAL PMNs (Figure-16b).

CD162 – PMNs in the blood showed the highest CD162 expression. This expression was much less upon entry into lung tissue or adhesion to the pulmonary vascular endothelium. These findings suggest an essential role for CD162 at the first stage of the neutrophil migration process. Montelukast showed significant inhibition of CD162 on neutrophils in all three compartments

(intravascular, lung, and alveoli). Zileuton significantly decreased CD162 in blood and BAL (Figure-16c).

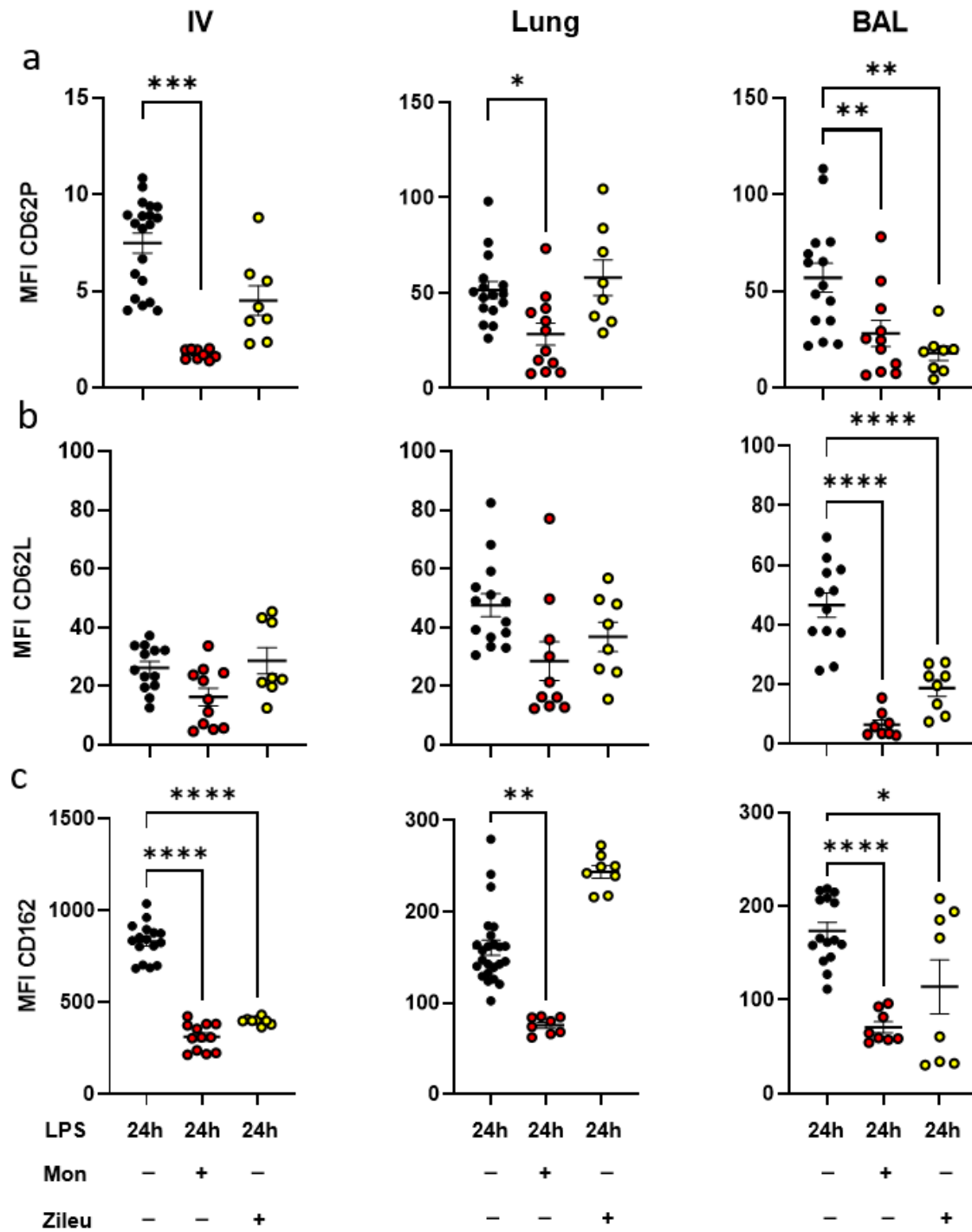


Figure-16. to be continued

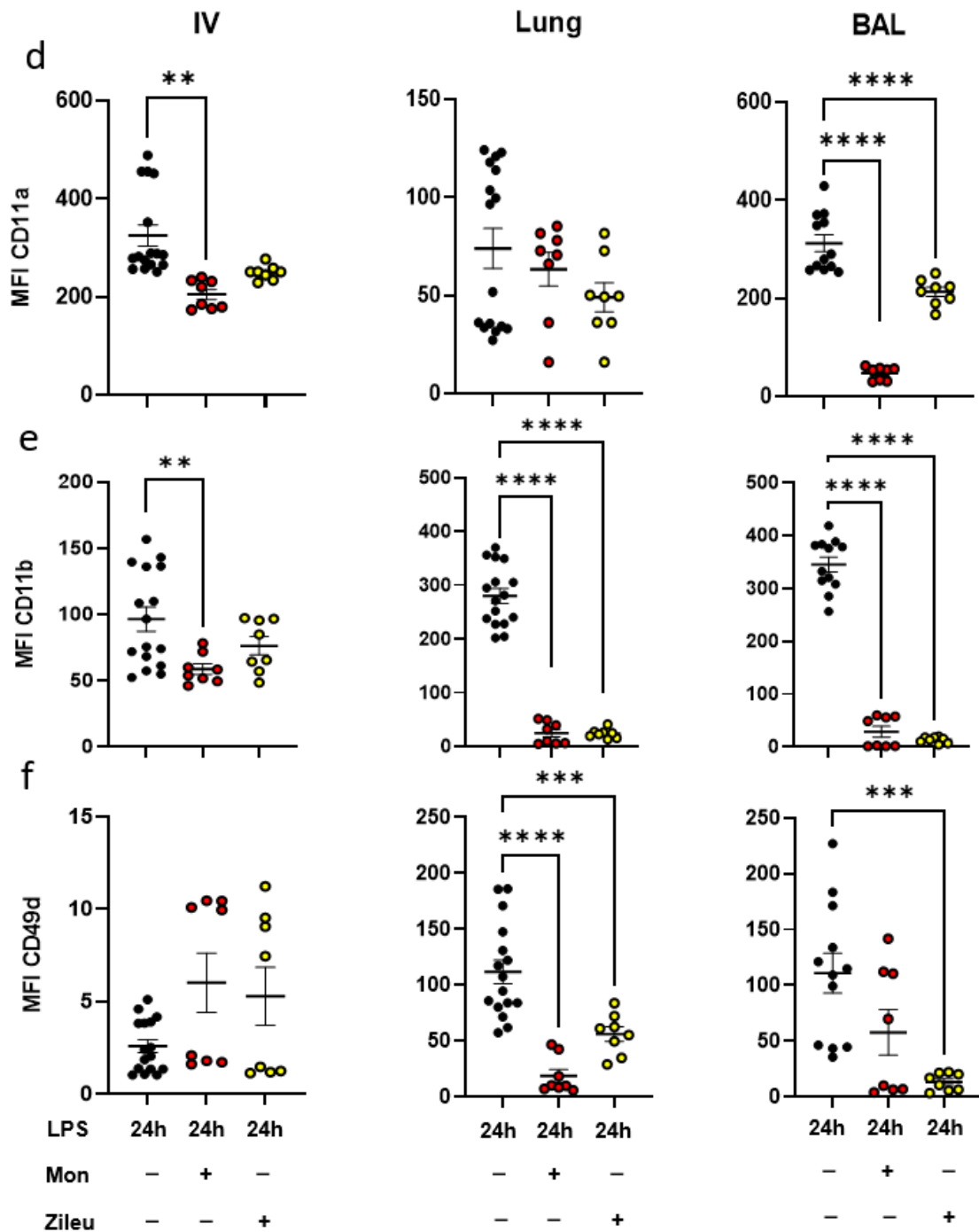


Figure-16: Impact of montelukast and zileuton on the expression of adhesion molecules on PMNs in lung compartments.

The expression of adhesion molecules was investigated by using flow cytometry 24 hours after the onset of inflammation. P-selectin (a), L-selectin (b), PGSL-1 (c), LFA-1 (d), Mac-1 (e), and VLA-4 (f) expressed on the PMNs of each compartment were detected by CD62P, CD62L, CD162, CD11a, CD11b, and CD49d antibodies, respectively. The mean fluorescence intensity (MFI) was analyzed for the adhesion molecules on PMNs in each compartment. The data are presented as mean \pm SEM, $n \geq 8$; * $p < 0.05$; ** $p < 0.01$; *** $p < 0.001$; **** $p < 0.0001$. Multiple group comparisons were analyzed by one-way analysis of variance with the Bonferroni post hoc test, or by the Kruskal–Wallis test.

CD11a – CD11a was highly expressed on blood vessel PMNs, and its expression diminished upon entering lung tissue, but it was elevated again in the alveoli. Both agents significantly reduced CD11a expression on BAL PMNs, and montelukast significantly inhibited CD11a expression in blood PMNs (Figure-16d).

CD11b – There was a substantial increase in CD11b expression on PMNs after they contacted lung tissue and reached alveoli. Both montelukast and zileuton were significantly resistant to this increase in transmigration activity in the lung tissue and alveoli. In addition, montelukast acted on it significantly in the blood (Figure-16e).

CD49d – CD49d was expressed at low levels on circulating PMNs, but upon migration to the lung tissue, expression increased sharply. Both agents significantly inhibited CD49d expression in the lung tissue, but only zileuton could significantly inhibit it in BAL (Figure-16f).

From a spatial perspective, for neutrophils in the blood, montelukast significantly inhibited CD11a, CD11b, CD62P, and CD162. In comparison, zileuton did not affect integrins but significantly inhibited CD162. Montelukast significantly inhibited both selectins and their ligand in lung tissue, namely CD62P, CD62L, and CD162, and the integrins CD49d and CD11b, but not CD11a. In contrast, zileuton did not affect the selectins part, CD62P, CD62L, and CD162, but had the same significant effect on integrins as montelukast.

In BAL, montelukast significantly inhibited CD62P, CD62L, CD162, and two integrins, CD11a and CD11b, but not CD49d. Zileuton showed significant inhibition of all investigated proteins.

Such spatial differences in the expression of selectins and integrins and their different inhibitory manifestations by the two agents provide clues to reveal the dynamic migration of neutrophils and the different pharmacological mechanisms of each agent.

3.3 Inflammatory responses were inhibited by montelukast and zileuton

3.3.1 Platelet–neutrophil complex formation was blocked by montelukast and zileuton

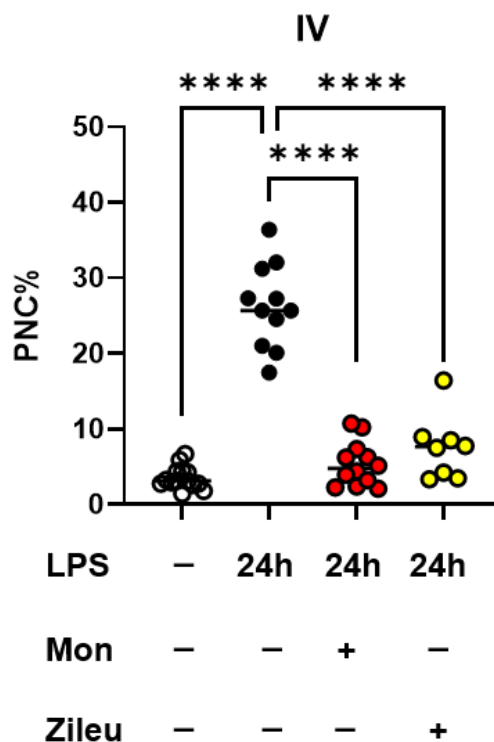


Figure-17: The roles of montelukast and zileuton in platelet–neutrophil complex (PNC) formation.

The formation of PNCs in intravascular was detected by flow cytometry (frequency of parents), which were Ly6G and CD42b double positive. The data are presented as mean \pm SEM, $n \geq 8$; **** $p < 0.0001$. Multiple group comparisons were analyzed by one-way analysis of variance with the Bonferroni post hoc test.

In addition to neutrophil recruitment, PNC formation is a factor that assists neutrophil migration after the inflammatory response (Kellner et al., 2017). To investigate the anti-inflammatory effects of montelukast and zileuton on PNC formation, we examined it in intravascular, lung tissue, and BAL based on flow cytometry.

This study did not observe significant changes in PNCs in lung tissue and BAL. But the PNC formation in the blood (Figure-17) was significantly lifted 24h after LPS stimulation and could be reduced by montelukast and zileuton.

3.3.2 Reactive oxygen species production was reduced by montelukast and zileuton

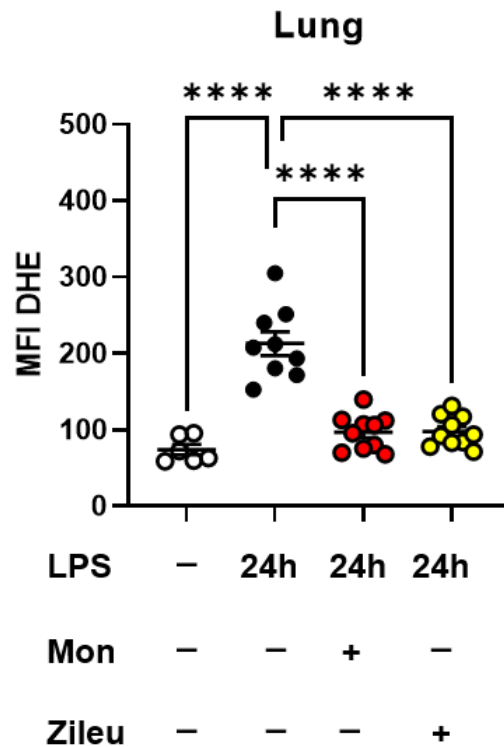


Figure-18: The roles of montelukast and zileuton in reactive oxygen species (ROS) production.

The mean fluorescence intensity (MFI) of dihydroethidium (DHE) determined ROS production. The data are presented as mean \pm SEM, $n \geq 8$; **** $p < 0.0001$. Multiple group comparisons were analyzed by one-way analysis of variance with the Bonferroni post hoc test.

Reactive oxygen species are thought to be involved in inflammation, delivering and regulating receptor signaling on the surface of activated cells, and promoting cell adhesion and migration (Hurd et al., 2012). To investigate the effects of montelukast and zileuton on ROS production, we examined it in intravascular, lung tissue, and BAL based on flow cytometry.

Results showed that the reactive oxygen species production of the lung, but not intravascular and BAL, was significantly lifted 24h after LPS stimulation and could be reduced by montelukast and zileuton (Figure-18).

3.3.3 Inflammatory chemokines were suppressed by montelukast and zileuton

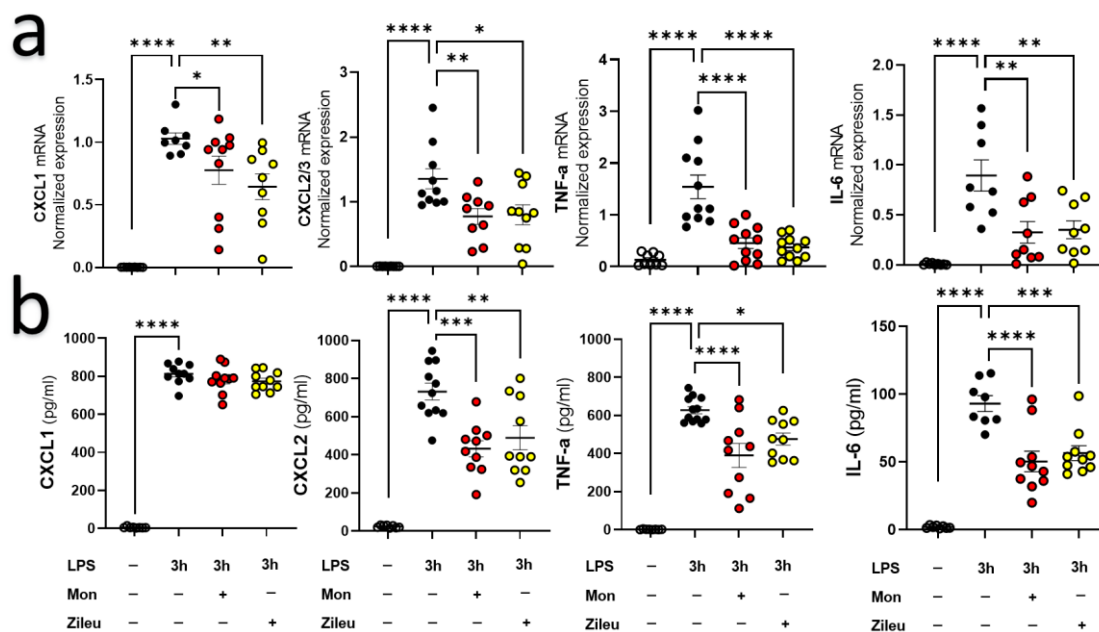


Figure-19: The effects of montelukast and zileuton on inflammatory chemokine release.

Gene expression of the inflammatory chemokines CXCL1, CXCL2/3, TNF- α , and IL-6 were detected by real-time quantitative polymerase chain reaction (RT-qPCR)(a). Enzyme-linked immunosorbent assay (ELISA) was used to determine the corresponding protein levels in bronchoalveolar lavage (BAL)(b). The data are presented as mean \pm SEM, $n \geq 8$; * $p < 0.05$; ** $p < 0.01$; *** $p < 0.001$; **** $p < 0.0001$. Multiple group comparisons were analyzed by one-way analysis of variance with the Bonferroni post hoc test, or by the Kruskal–Wallis test.

We determined the impact of montelukast and zileuton on the gene expression of several chemotactic factors three hours after LPS inhalation, namely CXCL1, CXCL2/3, TNF- α , and IL-6. Both agents significantly reduced the expression of these factors (Figure-19a).

To verify these findings, we examined them at the protein level by ELISA. Twenty-four hours after pharmacological administration, CXCL2, TNF- α , and IL-6 expression were decreased significantly in BAL by montelukast and zileuton compared to the stimulation group only with 24 hours of LPS stimulation. However, the CXCL1 protein was not significantly decreased (Figure-19b).

3.4 Leukotriene pathway was repressed by montelukast and zileuton

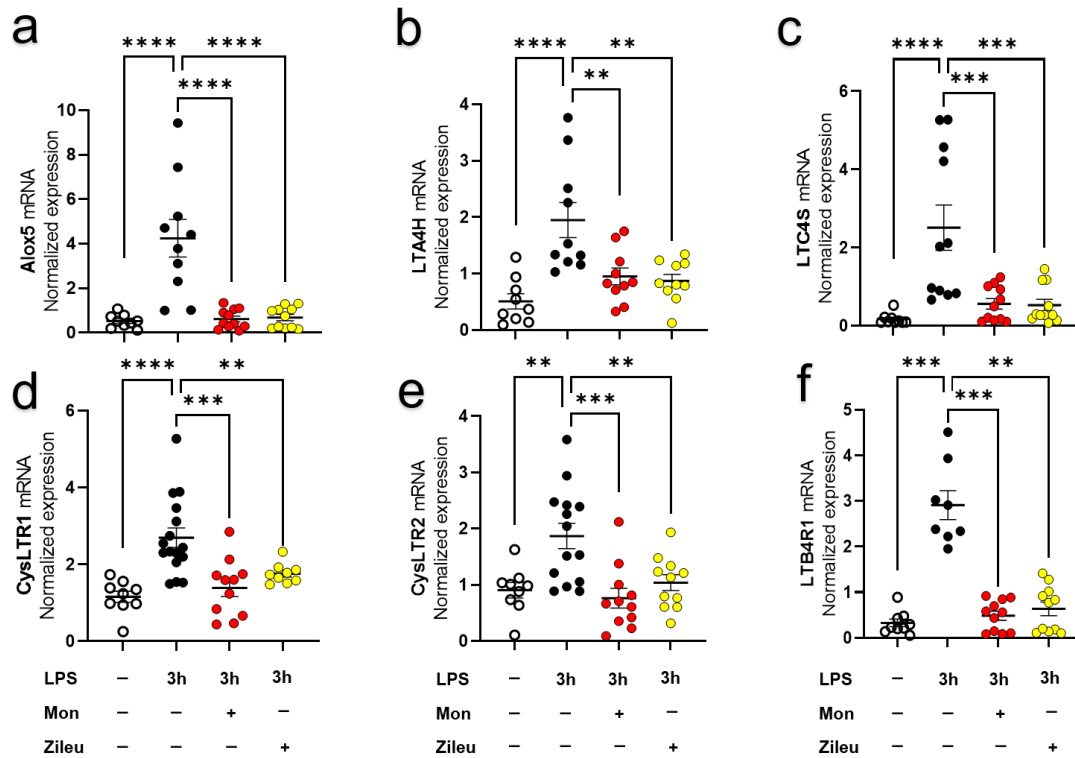


Figure-20: Effects of montelukast and zileuton on the expression of leukotriene pathway-related genes.

Gene expression of Alox5, CysLTR1, CysLTR2, LTA4H, LTC4S, and LTB4R1 was determined in lung tissue by real-time quantitative polymerase chain reaction (RT-qPCR) three hours after LPS exposure. The data are presented as mean \pm SEM, $n \geq 8$; ** $p < 0.01$; *** $p < 0.001$; **** $p < 0.0001$. Multiple group comparisons were analyzed by one-way analysis of variance with the Bonferroni post hoc test, or by the Kruskal–Wallis test.

As mentioned previously, montelukast and zileuton are leukotriene pathway inhibitors. How do they affect the expression of leukotriene pathway-related genes in this study?

We investigated the influence of montelukast and zileuton on leukotriene pathway-related genes in the lung. As inflammation progresses, the gene expression of the key leukotriene pathway enzymes Alox5, LTA4H, and LTC4S, and the receptor proteins CysLTR1, CysLTR2, and LTB4R1, increased significantly. Zileuton significantly reduced the expression of Alox5 and LTB4R1. The Expression of the downstream key enzymes LTA4H and LTC4S was also reduced. Montelukast, an inhibitor of cysteine leukotriene receptors, inhibited all

critical enzymes of the upstream synthesis pathway of leukotrienes, and the intensity of inhibition was not weaker than that of zileuton (Figure-20).

To verify these findings at the protein level, we evaluated the surface expression of CysLTR1 and LTB4R1 on murine lung tissue PMNs by immunofluorescence.

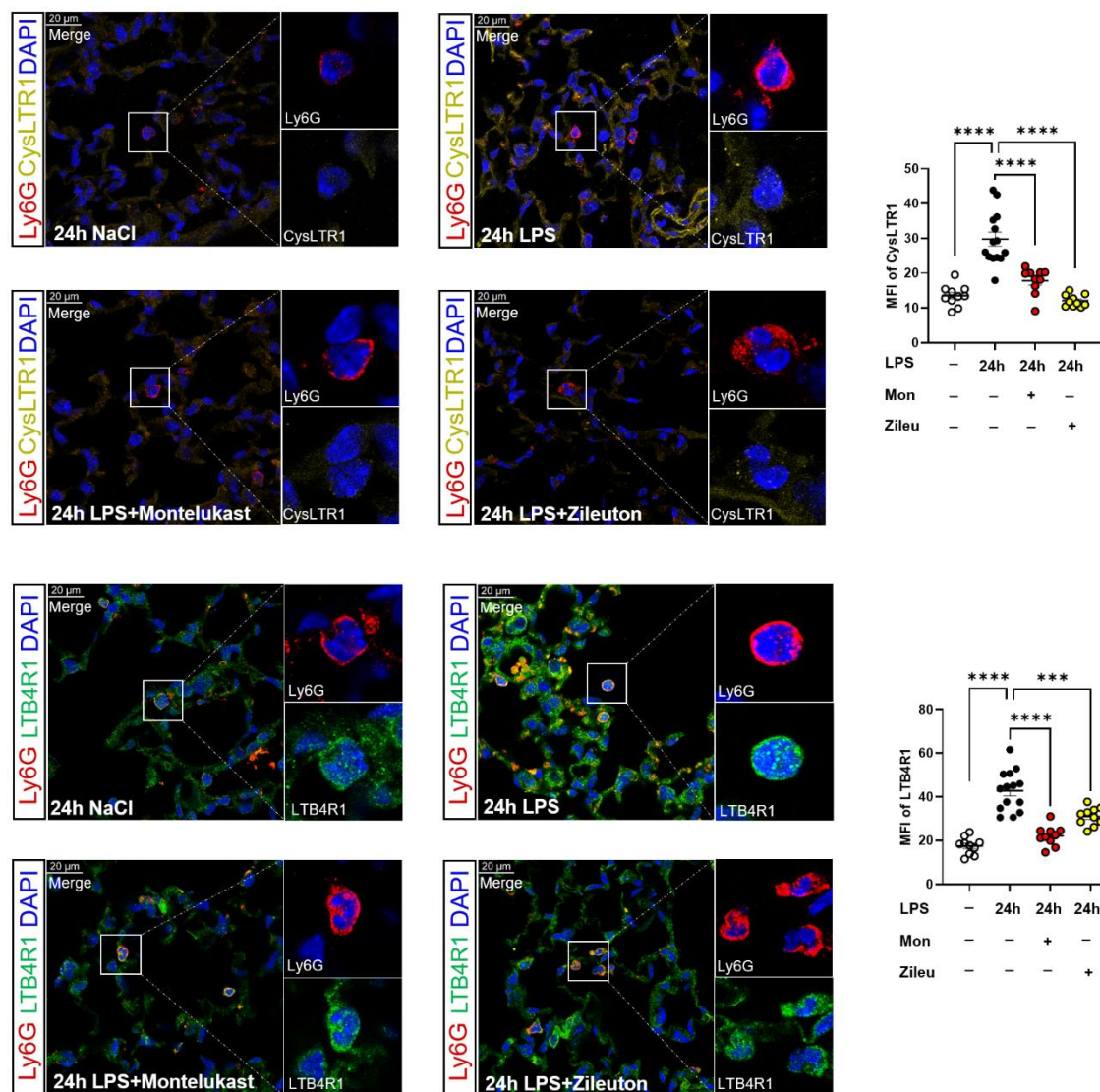


Figure-21: Expression of the leukotriene receptors CysLTR1 and LTB4R1 on murine lung PMNs.

Immunofluorescence staining of CysLTR1 (yellow) and LTB4R1 (green) on murine PMNs in the lung 24h after NaCl or LPS exposure with or without montelukast or zileuton (original magnification $\times 63$, cell zoomed; one representative image of five from two independent experiments is shown). Ly6G (red) was used as a PMN marker. DAPI (blue) was used as a DNA marker. The scale bar is $20 \mu\text{m}$. The mean fluorescence intensity (MFI) of CysLTR1 and LTB4R1 were measured at indicated conditions by ImageJ. The data are presented as mean \pm SEM, ($n = 10-14$); *** $p < 0.001$; **** $p < 0.0001$. Multiple group comparisons were analyzed by one-way analysis of variance with the Bonferroni post hoc test.

We measured the mean fluorescence intensity of CysLTR1 and LTB4R1 on murine lung PMNs at indicated conditions. Consistent with the gene expression results, the protein levels of both CysLTR1 and LTB4R1 decreased significantly by montelukast or zileuton after LPS stimulation (Figure-21).

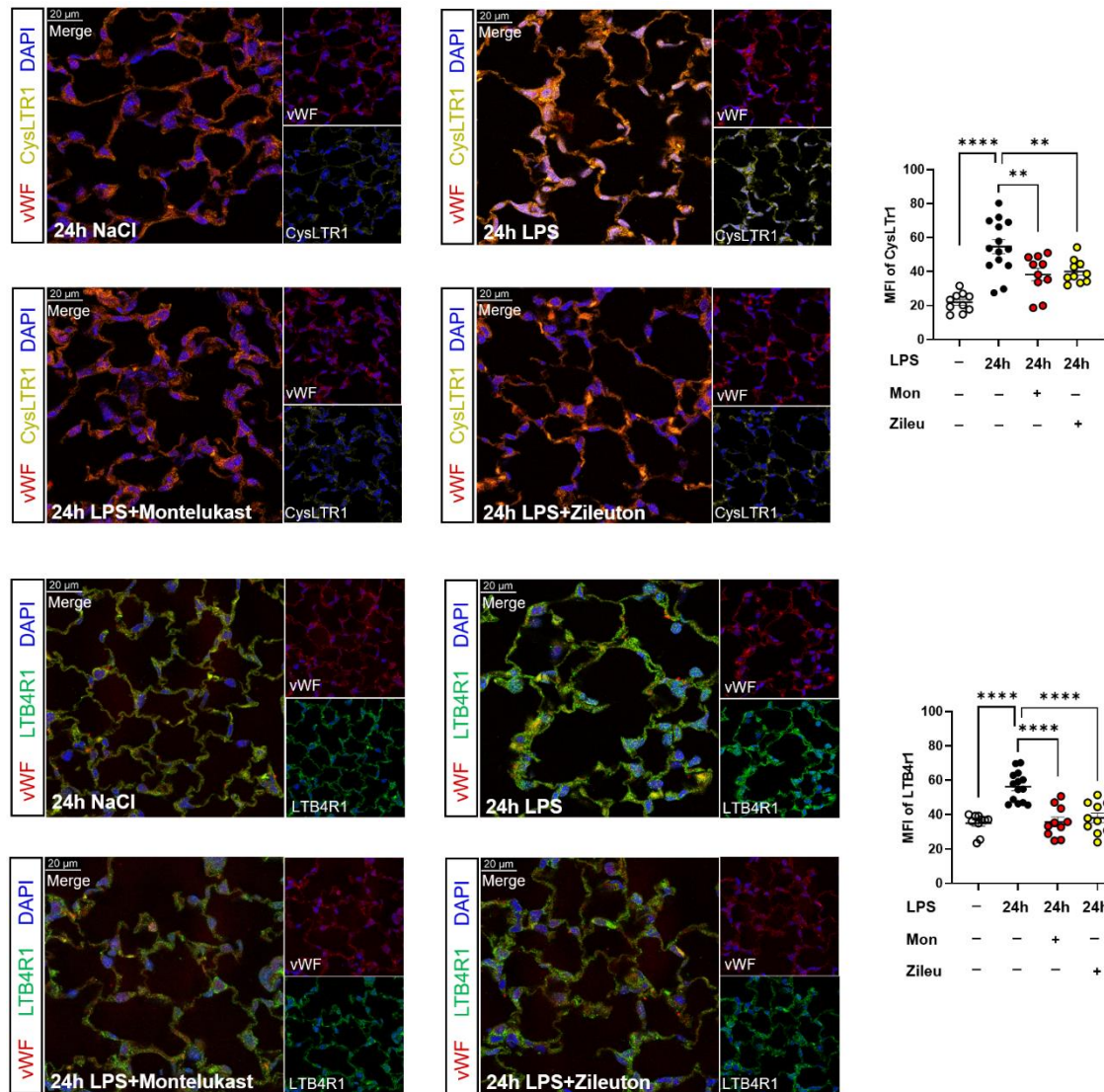


Figure-22: Expression of the leukotriene receptors CysLTR1 and LTB4R1 on murine endothelium.

Immunofluorescence staining of CysLTR1 (yellow) and LTB4R1 (green) on murine endothelium in the lung 24h after NaCl or LPS exposure with or without montelukast or zileuton (original magnification $\times 63$, cell zoomed; one representative image of five from two independent experiments is shown). vWF (red) was used as an endothelium marker. DAPI (blue) was used as a DNA marker. The scale bar is 20 μm . The mean fluorescence intensity (MFI) of CysLTR1 and LTB4R1 were measured at indicated conditions by ImageJ. The data are presented as mean \pm SEM, ($n = 10-14$); ** $p < 0.01$; **** $p < 0.0001$. Multiple group comparisons were analyzed by one-way analysis of variance with the Bonferroni post hoc test.

At the same time, we found that CysLTR1 and LTB4R1 appeared to be expressed on endothelium or epithelium. So, we continued to verify the expression of CysLTR1 and LTB4R1 on murine lung endothelium and epithelium by immunofluorescence.

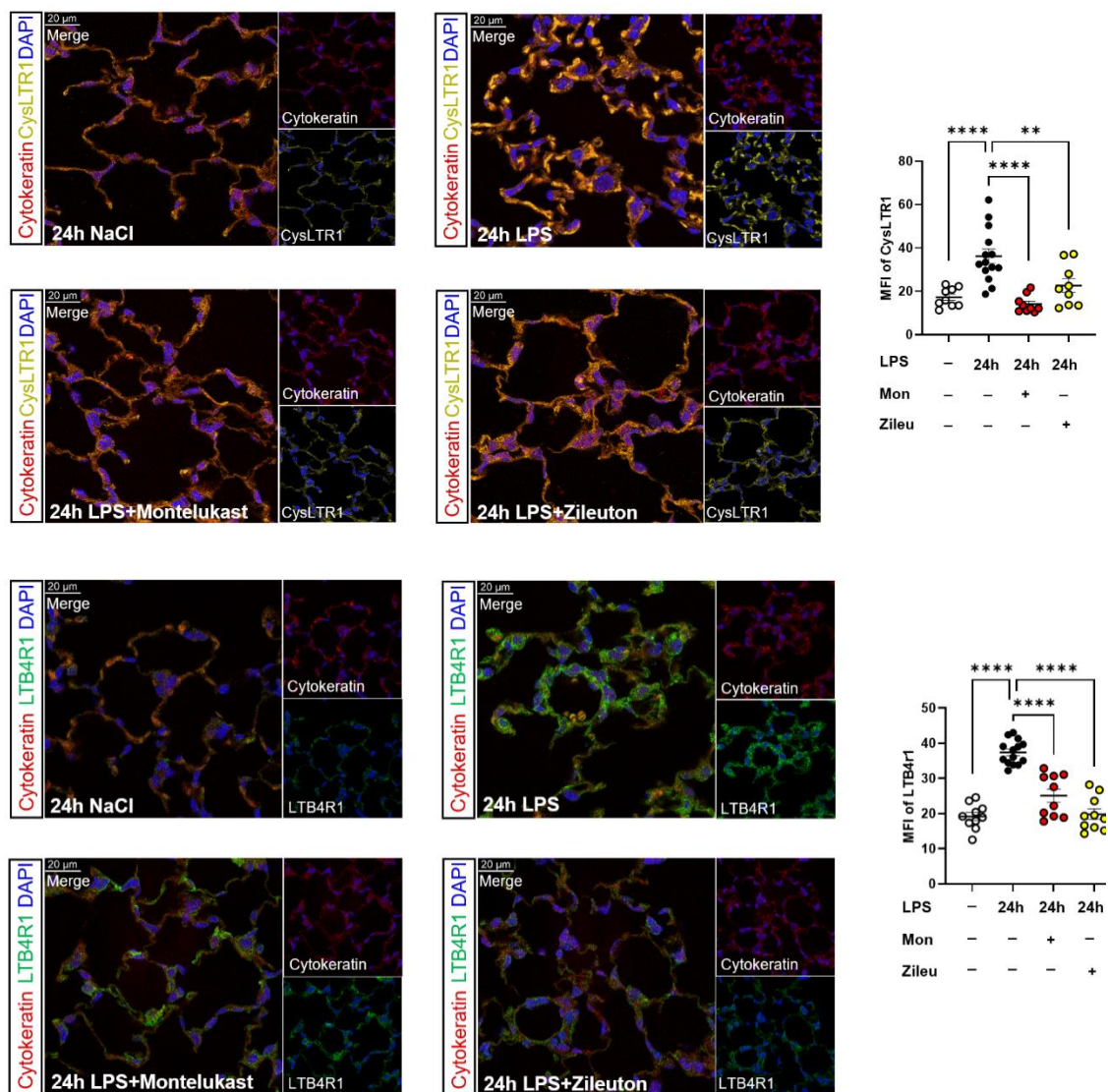


Figure-23: Expression of the leukotriene receptors CysLTR1 and LTB4R1 on the murine epithelium.

Immunofluorescence staining of CysLTR1 (yellow) and LTB4R1 (green) on the murine epithelium in the lung 24h after NaCl or LPS exposure with or without montelukast or zileuton (original magnification $\times 63$, cell zoomed; one representative image of five from two independent experiments is shown). Cytokeratin (red) was used as an epithelium marker. DAPI (blue) was used as a DNA marker. The scale bar is 20 μm . The mean fluorescence intensity (MFI) of CysLTR1 and LTB4R1 were measured at indicated conditions by ImageJ. The data are presented as mean \pm SEM, ($n = 10-14$); ** $p < 0.01$; **** $p < 0.0001$. Multiple group comparisons were analyzed by one-way analysis of variance with the Bonferroni post hoc test.

We measured the mean fluorescence intensity of CysLTR1 and LTB4R1 on murine lung endothelium and epithelium at indicated conditions. It confirmed that the protein CysLTR1 and LTB4R1 were expressed on both murine endothelium and epithelium and could be decreased significantly by montelukast or zileuton after LPS stimulation (Figure-22,23).

3.5 Pharmacological findings of montelukast and zileuton

3.5.1 Potential target proteins interaction network of montelukast and zileuton

As shown above, montelukast performed excellently, inhibiting not only the cysteine leukotriene receptor but also the upstream key enzyme for leukotriene synthesis. Furthermore, apart from the differences in the effect on adhesion molecules, the improvement of acute pulmonary inflammation in mice produced by montelukast and zileuton was very similar.

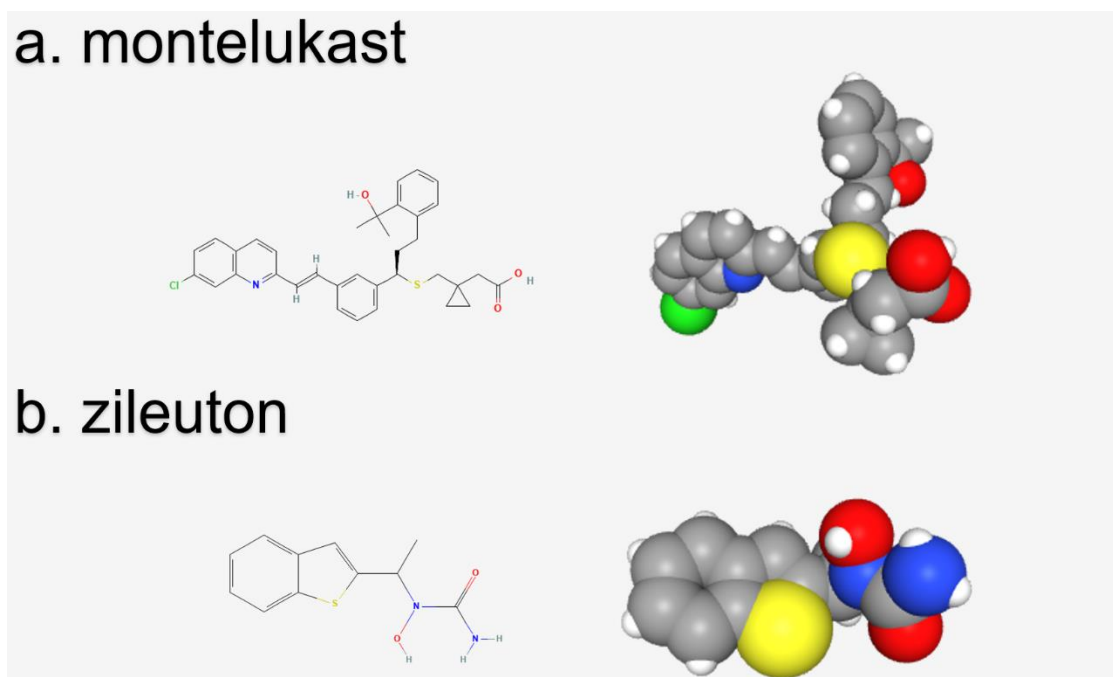


Figure-24: Two-dimensional (2D) and three-dimensional (3D) structures of montelukast and zileuton.

Compound structures were obtained from PubChem (<https://pubchem.ncbi.nlm.nih.gov>, 21.10.2021). The colors indicate the following: gray for carbon atoms, blue for nitrogen atoms, green for chlorine atoms, red for oxygen atoms, and white for hydrogen atoms.

Therefore, we examined the drug structure and potential targets of montelukast to investigate its potential broad-spectrum anti-inflammatory effects and its similarities to and differences from zileuton.

Montelukast has three benzene rings, three oxygen atoms, one sulfur atom, one nitrogen atom, and one chlorine atom (Figure-24a), while zileuton has one benzene ring, two oxygen atoms, two nitrogen atoms, and one sulfur atom (Figure-24b). Montelukast has a richer chemical structure. Compared with Zileuton, Montelukast has a more complex structure and binding sites. By sending their 3D structures to the PharmMapper Server, we obtained information on the potential targets of the agents.

More than 300 target proteins are shown in our obtained dataset. A Norm-Fit-value can represent the magnitude of the likelihood of a target protein binding to an agent, and we selected target proteins with high confidence values (Norm-Fit-values > 0.7) for inclusion in the subsequent analysis. A total of 171 montelukast targets and 81 zileuton targets were included in the analysis.

We wanted to know the similarities and differences between montelukast and zileuton in terms of protein function. STRING is a network tool that shows direct and indirect connections between proteins based on pre-existing connections. To obtain the network of drug targets and the similarities, differences, and associations between two agents, we included the target proteins with a Norm-Fit-value greater than 0.7 in the STRING protein interaction analysis.

After this step, we obtained the network interaction map between montelukast and zileuton target proteins. We show only the target protein networks with a high confidence value, which were not less than 0.9, and A total of 84 proteins were included in the protein–protein interaction network. The results are shown in Figure-25.

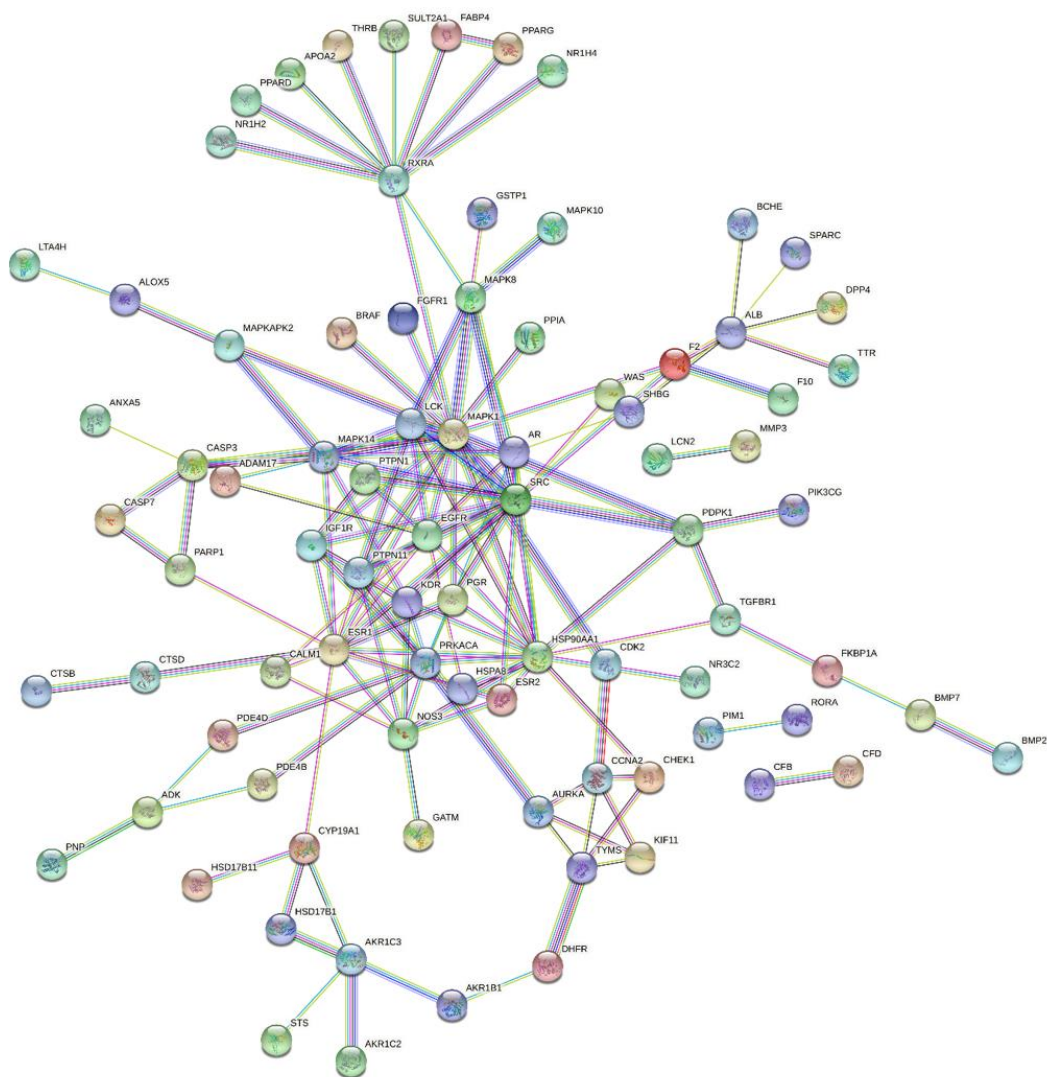


Figure-25: The protein–protein interaction (PPI) network of montelukast and zileuton.

Each node represents all proteins produced by a single protein-coding gene locus. The cyan line represents interactions from curated databases. The purple line represents interactions that have been experimentally determined. The green line represents interactions originating from the gene neighborhood. The red line represents gene fusion. The blue line represents gene co-occurrence. The yellow line originates from text mining. The black represents gene co-expression. The light blue represents a protein homology. Confidence value ≥ 0.9 . The figure was created with <https://string-db.org/>, 21.10.2021.

With Cytoscape (Version 3.9.0), we visualized these data to show better agent–protein and protein–protein interactions (Figure-26).

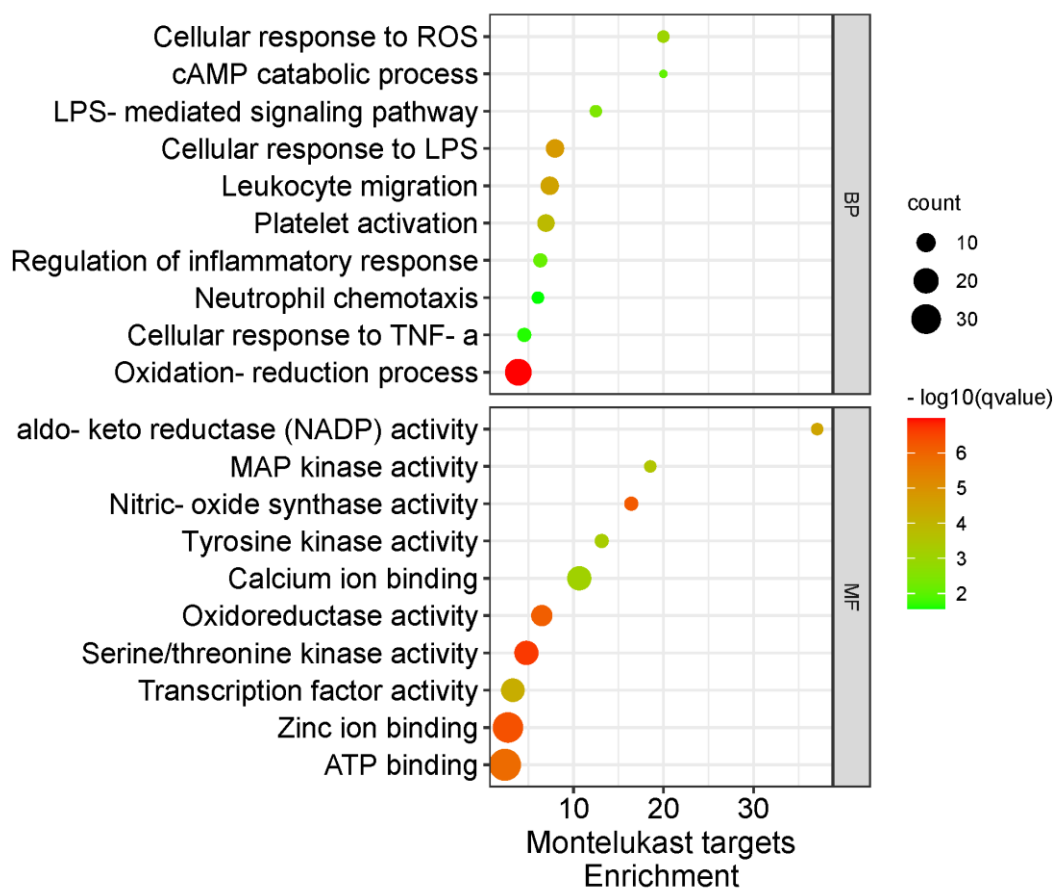


Figure-27: Gene Ontology (GO) functional classification of montelukast.

The enriched functional classification was summarized in two main categories: biological process (BP) and molecular function (MF). The x-axis indicates the number of genes in each category, and the y-axis indicates different GO terms. The q-value is a corrected p-value ranging from 0 to 1. The color and size of the dots represent the range of the q-value and the number of targets mapped to the indicated pathways, respectively. The heatmap was plotted by <https://www.bioinformatics.com.cn>, a free online data analysis and visualization platform.

The enrichment results found that montelukast and zileuton may directly affect biological processes related to inflammation, such as leukocyte migration, neutrophil chemotaxis, cellular response to LPS, and ROS synthesis. These findings explain, to some extent, the results of our *in vivo* migration assay and ROS detection (Figure-27 and Figure-28).

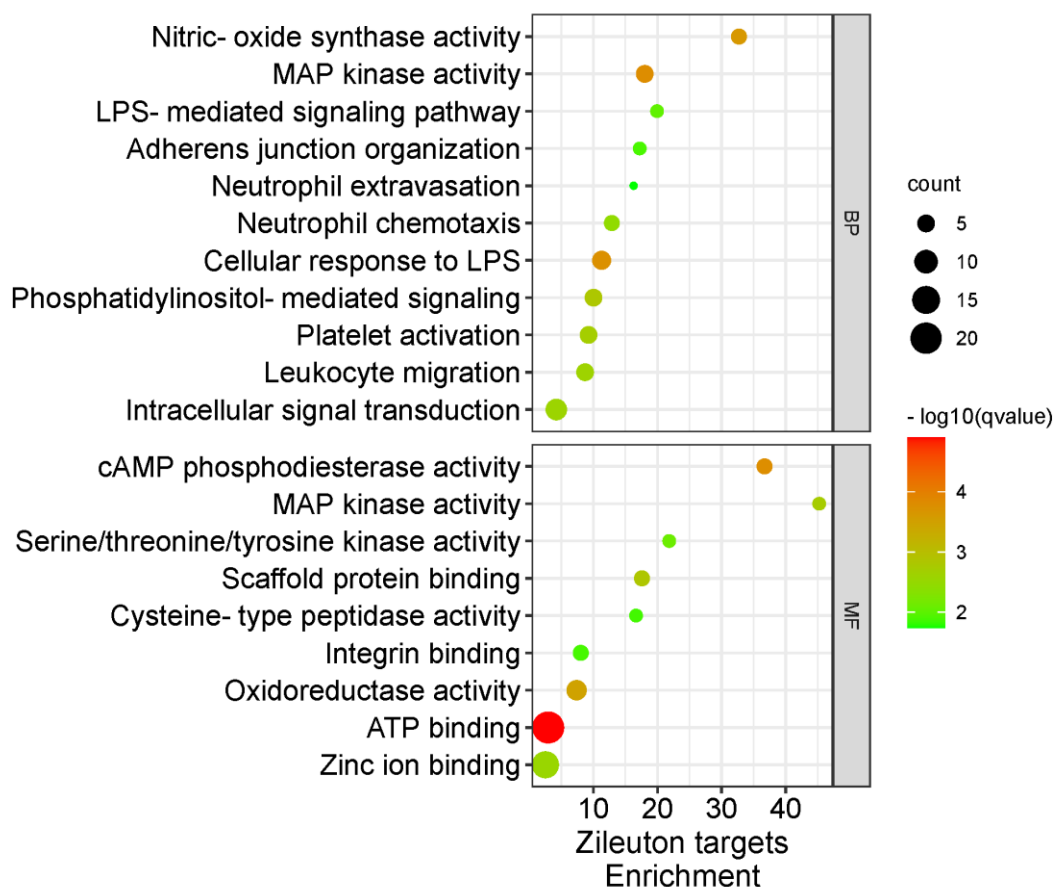


Figure-28: Gene Ontology (GO) functional classification of zileuton.

The enriched functional classification was summarized in two main categories: biological process (BP) and molecular function (MF). The x-axis indicates the number of genes in each category, and the y-axis indicates different GO terms. The q-value is a corrected p-value ranging from 0 to 1. The color and size of the dots represent the range of the q-value and the number of targets mapped to the indicated pathways, respectively. The heatmap was plotted by <https://www.bioinformatics.com.cn>, a free online data analysis and visualization platform.

Furthermore, the enrichment scatter dots provide information on the molecular functions involved, such as calcium-binding, transcription factor activity, 3',5'-cyclic adenosine monophosphate (cAMP) metabolic processes, and MAP enzyme activity, which provide insight into the mechanism of pharmacological actions.

3.5.3 Signaling pathway of montelukast and zileuton

Based on the Kyoto Encyclopedia of Genes and Genomes (KEGG) database, we evaluated the involved signaling pathway of potential targets using by DAVID web

tool. According to KEGG mapping, several signaling pathways are highly enriched, such as the FoxO pathway (Figure-29 and Figure-30), the phosphatidylinositol 3-kinase (PI3K)-Akt pathway (Figure-29 and Figure-30), the chemokine pathway (Figure-29), the MAPK pathway (Figure-29 and Figure-30), and leukocyte trans-endothelial migration (Figure-30).

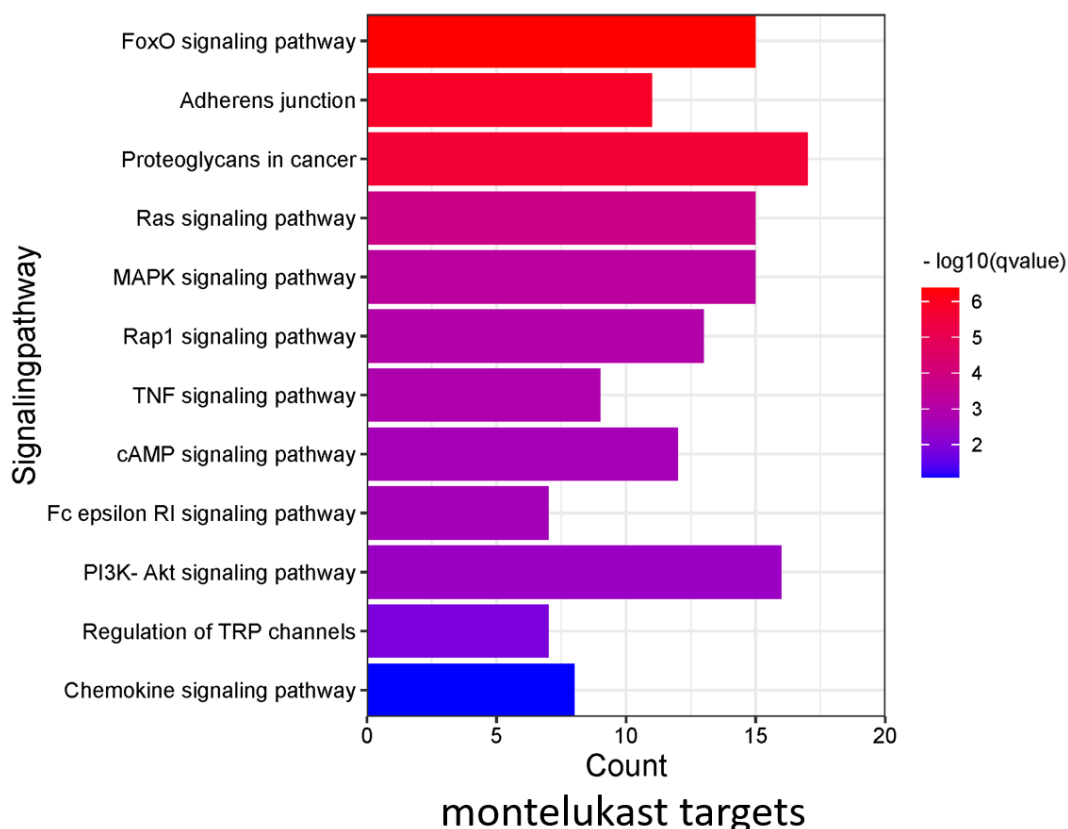


Figure-29: Signaling pathway involved with montelukast.

The x-axis indicates the number of genes in each category, and the y-axis indicates different signaling pathways. The q-value is a corrected p-value ranging from 0 to 1. The color of the bars represents the range of the q-value mapped to the indicated pathways. The heatmap was plotted by <https://www.bioinformatics.com.cn>, a free online data analysis and visualization platform.

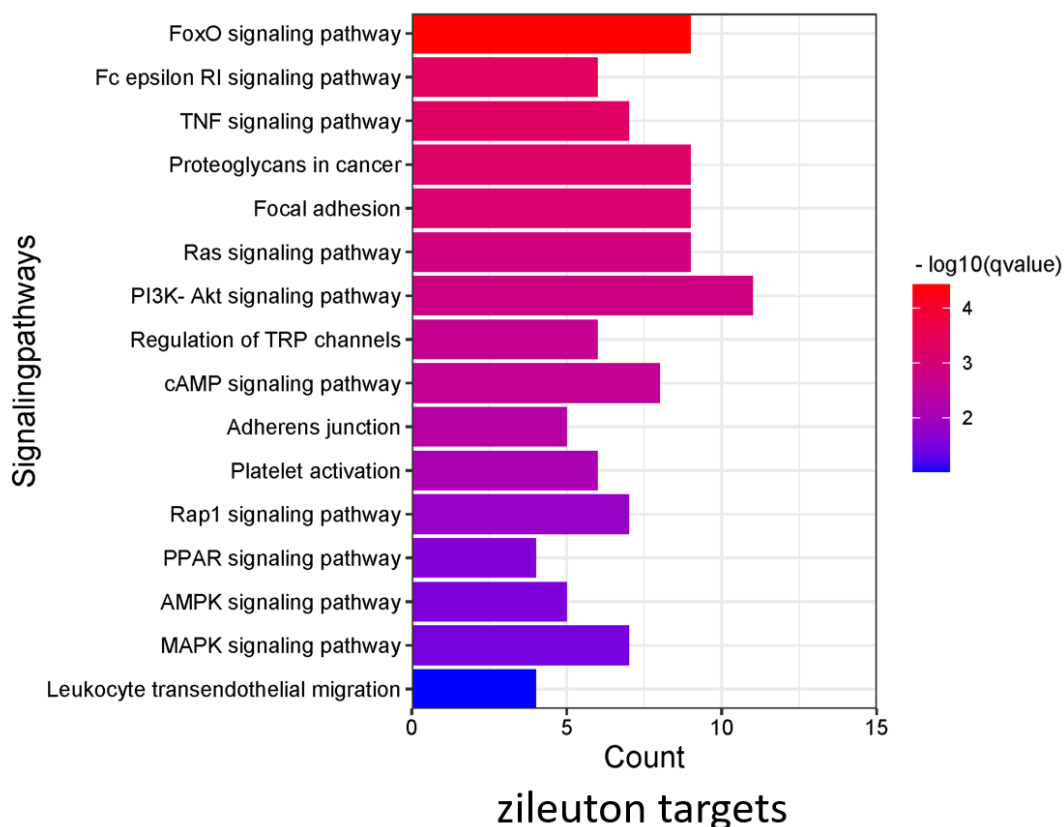


Figure-30: Signaling pathway involved with zileuton.

The x-axis indicates the number of genes in each category, and the y-axis indicates different signaling pathways. The q-value is a corrected p-value ranging from 0 to 1. The color of the bars represents the range of the q-value mapped to the indicated pathways. The heatmap was plotted by <https://www.bioinformatics.com.cn>, a free online data analysis and visualization platform.

We are particularly interested in the chemokine pathway because we have shown that montelukast and zileuton can affect the gene expression of chemokines, including CXCL2/3, TNF- α , and IL-6. Hence, we wanted to determine which proteins and biosynthetic pathways montelukast may be involved in that influencing chemokine synthesis. We rendered the potential target proteins and the intensity of their effects on the chemokine signaling pathway map by Pathview, which is a pathway-based data integration and visualization toolset. As shown in Figure-31, eight proteins are enriched in the chemokine pathway: protein kinase A (PKA), Src, PI3K, Akt, Glycogen synthase kinase-3 (GSK3), Wiskott-Aldrich Syndrome protein (WASP), Raf, and extracellular signal-regulated kinase 1/2 (ERK1/2). ERK1/2 is one of the end-loop proteins of cytokine products and cell migration.

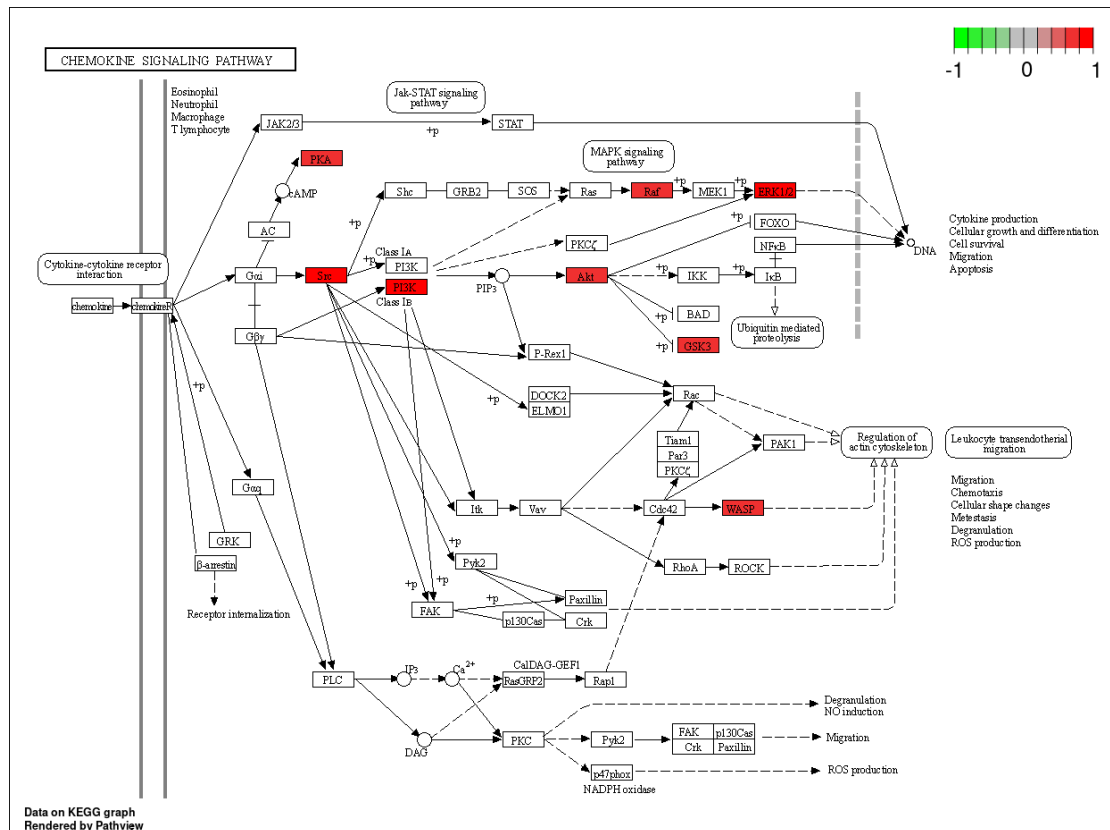


Figure-31: Chemokine signaling pathway from the Kyoto Encyclopedia of Genes and Genomes (KEGG).

The chemokine signaling pathway was generated using graphs from KEGG. The intensity of the red color is based on the Norm Fit value (0–1). The figure was rendered by Pathview.

These findings are consistent with the pathway enrichment results that montelukast and zileuton affect the ERK1/2 pathway. Therefore, we examined the gene expression of MAPK1 (ERK2) and MAPK3 (ERK1) in lung tissue, and found that montelukast and zileuton significantly suppressed the gene expression of ERK1/2. To validate our results at the protein level, the expression of ERK1/2 and its downstream protein pCREB at the protein level on the lung tissue PMNs were detected by immunofluorescence assays. The results showed that montelukast and zileuton significantly suppressed ERK1/2 and pCREB protein expression on lung tissue PMNs (Figure-32).

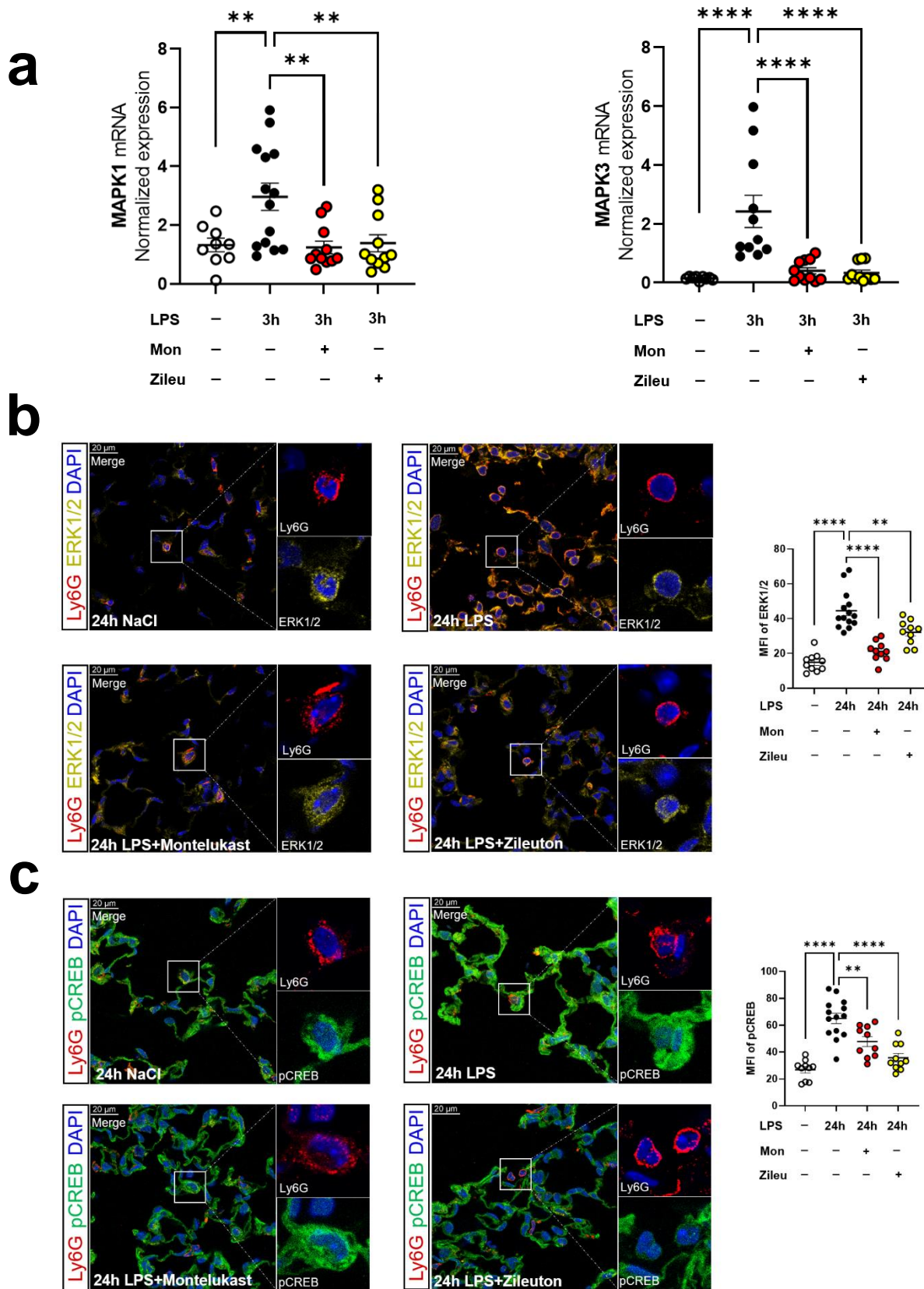


Figure-32: Expression of the ERK1/2 and pCREB on murine PMNs.

Gene expression of MAPK1 (ERK2) and MAPK3 (ERK1) was detected by real-time quantitative polymerase chain reaction (RT-qPCR) in murine lung tissue. Immunofluorescence staining of ERK1/2 (yellow) and pCREB (green) on murine PMNs in the lung 24h after NaCl or LPS exposure with or without montelukast or zileuton (original magnification x63, cell zoomed; one representative image of five from two independent experiments is shown). Ly6G (red) was used as a PMN marker. DAPI (blue) was used as a DNA marker. The scale bar is 20 μ m. The mean fluorescence intensity (MFI) of pCREB was measured at indicated conditions by ImageJ. The data are presented as mean \pm SEM, (n = 10–14); ** p < 0.01; **** p < 0.0001. Multiple group comparisons were analyzed by one-way analysis of variance with the Bonferroni post hoc test.

Since pCREB appeared to be expressed on both endothelium and epithelium, we did the same immunofluorescence assay for pCREB on both endothelium and epithelium. As is shown in Figure-33, the protein levels of pCREB significantly increased 24 hours after LPS stimulation and could be decreased significantly by montelukast or zileuton.

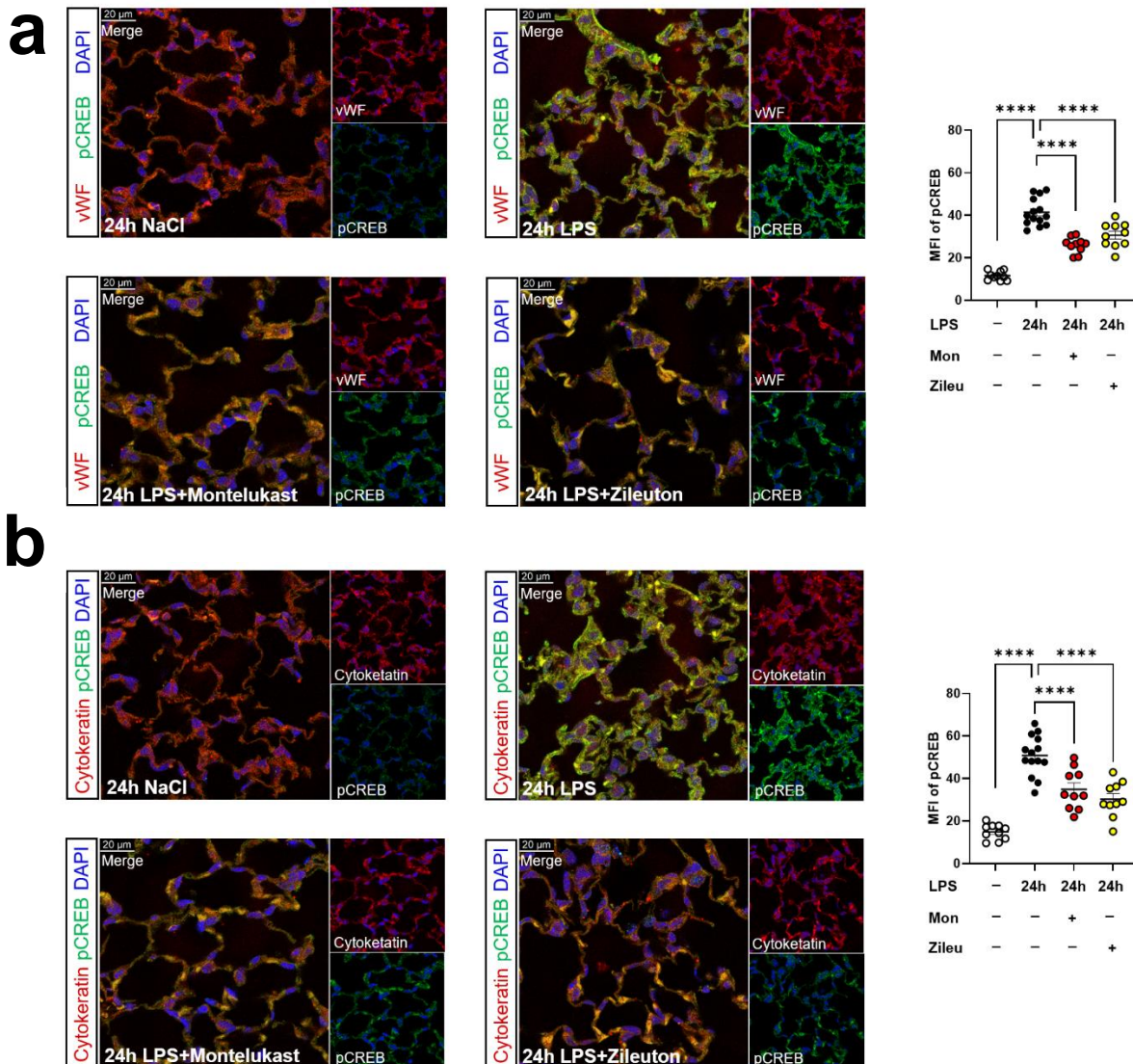


Figure-33: Expression of the pCREB on murine lung endothelium and epithelium.

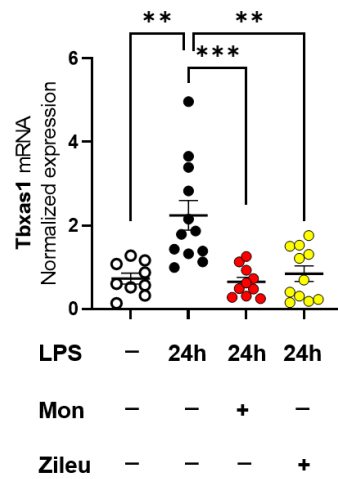
Immunofluorescence staining of pCREB (green) on murine endothelium(**a**) or epithelium(**b**) in the lung 24h after NaCl or lipopolysaccharide (LPS) exposure with or without montelukast or zileuton (original magnification $\times 63$, cell zoomed; one representative image of five from two independent experiments is shown). vWF (red) was used as an endothelium marker (**a**). Cytokeratin (red) was used as an epithelium marker (**b**). DAPI (blue) was used as a DNA marker. The scale bar is 20 μm . The mean fluorescence intensity (MFI) of pCREB was measured at indicated conditions by ImageJ. The data are presented as mean \pm SEM, ($n = 10-14$); **** $p < 0.0001$. Multiple group comparisons were analyzed by one-way analysis of variance with the Bonferroni post hoc test.

3.5.4 Platelet activation is inhibited by montelukast and zileuton

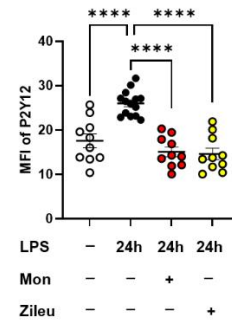
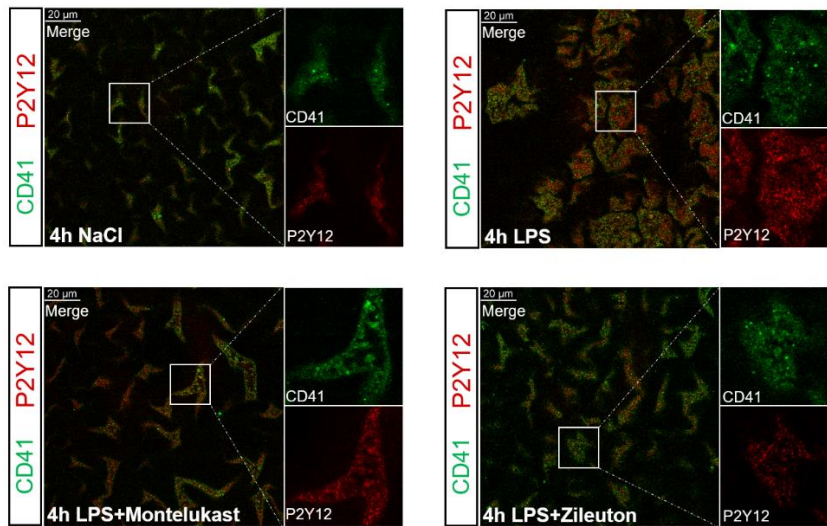
GO enrichment analysis revealed that montelukast and zileuton might interfere with platelet activation (Figure-27 and Figure-28). We know that montelukast and zileuton inhibit the formation of PNCs and ROS production. A commonality of these pathways is the involvement of thromboxane A2 (TXA2), a potent element for platelet aggregation and activation. Adhesion between platelets and neutrophils is regulated by TXA2 (Chlopicki et al., 2003). TXA2 enhances ROS production by neutrophils (Chlopicki et al., 2004). Thus, we hypothesized that montelukast and zileuton inhibit PNC formation and ROS generation by inhibiting TXA2 production. To test our hypothesis, we determined the gene expression of thromboxane A synthase 1 (Tbxas1), a key enzyme for TXA2 synthesis. The result was consistent with our conjecture that Tbxas1 gene expression was repressed by montelukast and zileuton (as shown in Figure-34a).

Tbxas1 is a key enzyme for TXA2 synthesis and interferes with P2Y receptor signaling (Tintinger et al., 2010). Among the P2Y receptors, P2Y12 is the crucial receptor that synergizes with TXA2 to accomplish platelet activation (Dorsam and Kunapuli, 2004). We isolated murine and human platelets for *ex vivo* experiments. Montelukast and zileuton exhibited powerful inhibitory effects on murine (Figure-34b) and human (Figure-34c) P2Y12 receptor.

a



b



c

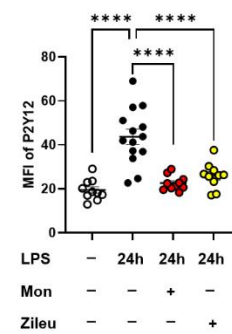
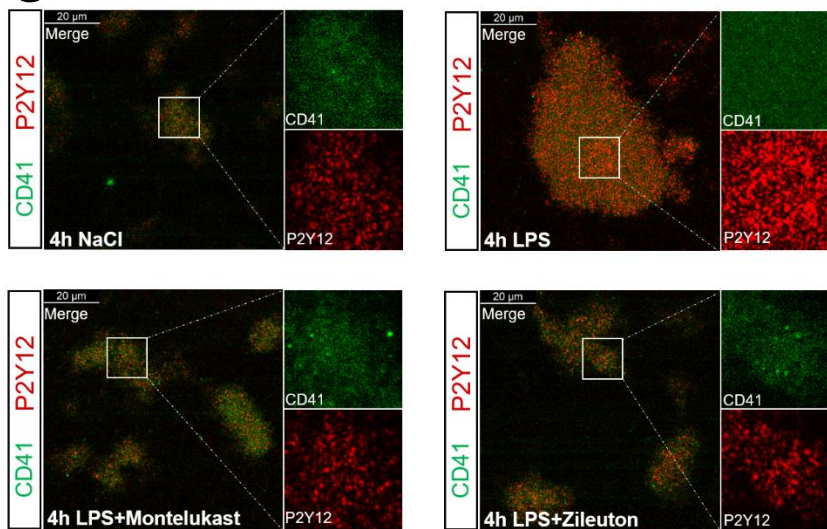


Figure-34: Gene expression of *Tbxas1* in murine lung and protein expression of P2Y12 on isolated platelets.

Gene expression of *Tbxas1* of murine lung tissue was detected by real-time quantitative polymerase chain reaction (RT-qPCR) (a). Immunofluorescence staining of P2Y12 (red) on murine (b) and human (c) platelets isolated from blood 4h after NaCl or lipopolysaccharide (LPS) exposure with or without montelukast or zileuton (original magnification $\times 63$, cell zoomed; one representative image of five from two independent experiments is shown). CD41 (green) was used as a PMN marker. The scale bar is 20 μm . The mean fluorescence intensity (MFI) of P2Y12 was measured at indicated conditions by ImageJ. The data are presented as mean \pm SEM, (n = 10–14); ** $p < 0.01$; *** $p < 0.001$; **** $p < 0.0001$. Multiple group comparisons were analyzed by one-way analysis of variance with the Bonferroni post hoc test.

3.5.5 Other features of montelukast and zileuton

We want to do more verification of the results of our drug target findings. Since montelukast and zileuton were shown to act on metalloproteins and caspase proteins (Figure-26), we determined the gene expression of MMP3 and MMP9 and the protein expression of caspase-1 in lung tissue. Montelukast and zileuton inhibited MMP3 and MMP9 gene expression (Figure-35a). The caspase-1 protein expression significantly decreased in response to both drugs (Figure-35b). Caspase-1 is the key enzyme that catalyzes the production of Interleukin-1 β (IL-1 β) (Lopez-Castejon and Brough, 2011) and the metalloproteases MMP-3 and MMP-9 process IL-1 β precursor (pro-IL-1 β) into the biologically active form IL-1 β as well (Schönbeck et al., 1998). To confirm the result of caspase-1 and MMPs, we measured the protein level of IL-1 β in BAL. Both montelukast and zileuton significantly inhibited IL-1 β production (Figure-35c).

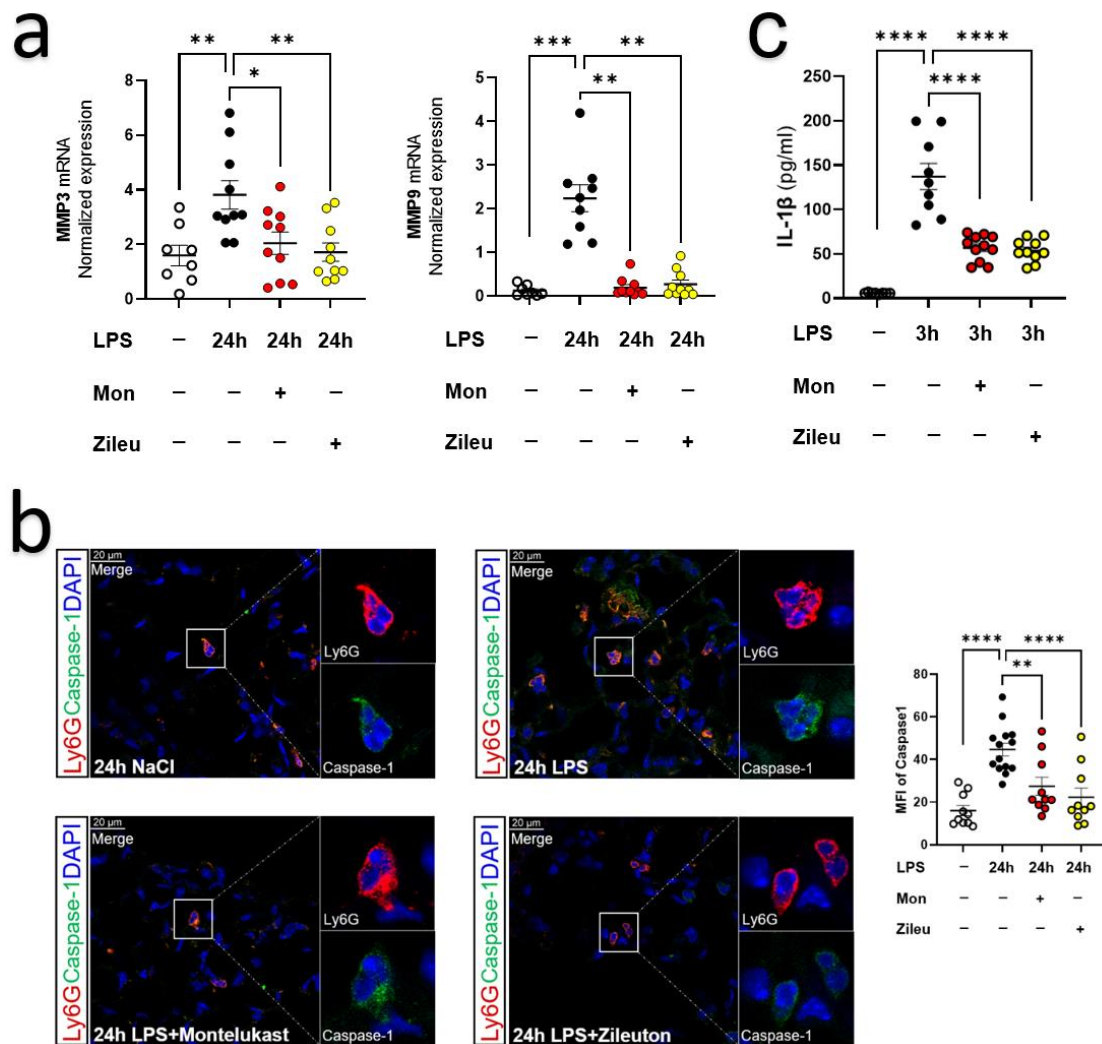


Figure-35: Gene expression of MMP3 and MMP9 and protein level of caspase-1 and IL-1 β on murine PMNs.

Gene expression of MMP3 and MMP9 were detected by real-time quantitative polymerase chain reaction (RT-qPCR). The protein level of IL-1 β in BAL was determined by ELISA. Immunofluorescence staining of caspase-1 (green) on murine PMNs in the lung 24h after NaCl or LPS exposure with or without montelukast or zileuton (original magnification 63 \times , cell zoomed; one representative image from two independent experiments is shown). Ly6G (red) was used as a PMN marker. DAPI (blue) was used as a DNA marker. The scale bar is 20 μ m. The mean fluorescence intensity (MFI) of pCREB was measured at indicated conditions by ImageJ. The data are presented as mean \pm SEM, ($n = 10-14$); * $p < 0.05$; ** $p < 0.01$; *** $p < 0.001$; **** $p < 0.0001$. Multiple group comparisons were analyzed by one-way analysis of variance with the Bonferroni post hoc test.

4 Discussion

4.1 Montelukast and Zileuton impair neutrophil migration mechanisms

The accumulation of neutrophils in the lung tissue and the ensuing excessive inflammatory response are essential factors in lung tissue injury and ARDS progression (Matthay et al., 2018). Moreover, the expression and sequential alteration of neutrophil adhesion molecules are among the most essential and fundamental parts of neutrophil motility (Ley et al., 2007).

Three steps are involved in the extravasation of neutrophils from the blood: rolling and tethering, firm adhesion, and diapedesis. The first step involves the expression of selectins on PMNs and endothelial cells. Integrins, such as LFA-1, Mac-1, and VLA-4, in conjunction with their counter receptors ICAMs and VCAM-1 on the endothelium, are involved in the second step. Subsequently, diapedesis occurs.

4.1.1 Adhesion patterns

P-selectin (CD62P) – Formerly known as GM140, P-selection was first discovered in 1989 (Hamburger and McEver, 1990). P-selectin was previously thought to be mainly expressed on platelets and activated endothelial cells (Pan et al., 1998) and to contribute to PNC formation and neutrophil rolling steps. Since the P-selectin receptor PSGL-1 is expressed on endothelial cells and neutrophils, P-selectin on neutrophils may be involved in the adhesion and rolling of neutrophils on endothelial cells and the neutrophil-neutrophil interactions. It has been reported that leukocytes can roll on activated endothelial cells as well as monolayers of leukocytes adsorbed on an activated endothelium and that P-selectin plays a vital role in this process (Bargatze et al., 1994; Jutila and Kurk, 1996).

Besides, we observed a significant elevation of P-selectin on neutrophils upon entry into the inflamed lung (Figure-16a), suggesting that P-selectin may be involved in either neutrophil function in inflamed tissues or neutrophil interaction with other immune cells. For example, soluble or cellular P-selectin can promote the formation of neutrophil extracellular traps (Etulain et al., 2015). It has been

reported that P-selectin-dependent leukocyte kinetics can be activated by histamine, LTC₄, LTD₄, and many other substances (Kanwar et al., 1995). Montelukast reduced P-selectin expression on the surface of neutrophils at various compartments, whereas zileuton inhibited it in BAL. This dissimilarity in different spaces is difficult to give a reasonable explanation simply from the perspective of leukotriene. Montelukast has a broader pharmacological spectrum (to be discussed later). It may promote the internalization or degradation of P-selectin on neutrophils through an unknown pathway. Compared with other selectins family members that have been well studied, P-selectin on neutrophils and its functions still requires additional studies.

L-selectin (CD62L) – L-selection is an essential member of the selectin family and an integral part of neutrophil migration; it was first identified in 1983. L-selectin is significantly expressed on circulating neutrophils and has been shown to play a crucial role in the adhesion of cells during migration, especially during tethering and rolling (Rahman et al., 2021). Under normal conditions, around 51% of the total blood granulocytes are located in the marginal pool (Athens et al., 1961). The lung is the leading site of neutrophil marginalization, and most marginalized neutrophils are found in the alveolar capillaries (Doerschuk et al., 1987). Although controversial (De Filippo and Rankin, 2020), L-selectin is thought to play a role in marginalization (Anthony J, 2015).

Under conditions of lung inflammation, neutrophil L-selectin expression increases rapidly, allowing for a significant increase in neutrophils adhering to the pulmonary vascular endothelium. However, L-selectin is quickly cleaved and shed once in contact with activated vascular endothelium, a process called "shedding" (Bruce Walcheck et al., 1996). As "shedding" occurs, neutrophils rolling along the endothelium slowly, allowing tight adhesion to facilitate subsequent cell migration (Ivetic, 2018; Venturi et al., 2003). In addition, through L-selectin, neutrophils can roll on neutrophils bound to activated endothelial cells (Bargatze et al., 1994). L-selectin is also involved in PNC formation (Konstantopoulos et al., 1998).

We found that L-selectin in blood neutrophils was not exceptionally high 24 hours after LPS stimulation. This phenomenon may be related to the time point of our measurements. Alveolar PMNs migration peaks 24 hours after stimulation (Reutershan et al., 2005). L-selectin-mediated adhesion and rolling occur mainly in the early process (Rainer, 2002). Montelukast and zileuton did not affect the expression of L-selectin in blood and lung tissue. However, they significantly reduced neutrophil L-selectin expression on alveolar PMNs (Figure-16b).

PSGL-1 (CD162) – This glycoprotein on leukocytes and endothelial cells is a receptor for P-selectin, L-selectin, and E-selectin. Given its ability to bind multiple selectins, it mediates adhesion between different cells. PSGL-1, a functional ligand for L-selectin, mediates neutrophil attachment to the neutrophil monolayer formed on inflamed endothelial cells and rolling them. (B. Walcheck et al., 1996). PSGL-1 has a significant role in the initial tethering of neutrophils to the endothelium (Zou et al., 2005). PSGL-1 on neutrophils binds to platelet P-selectin and enhances PNC formation (Abou-Saleh et al., 2005), and PSGL-1 on the endothelium can also form adhesions with activated platelet P-selectin (Rivera-Nieves et al., 2006). Besides, PSGL-1 appears to have a unique role in activating $\beta 2$ integrins (Yago et al., 2010). Activation of LFA-1 requires PSGL-1–L-selectin complexes, not just L-selectin (Stadtman et al., 2013). P-selectin binds to PSGL-1, inducing an intermediate state of Mac-1 ($\alpha M\beta 2$ integrin) activation (Frenette et al., 2000).

In this investigation, PSGL-1 showed extremely high expression on neutrophils in the blood, with a subsequent decrease in expression when neutrophils entered lung tissue and alveoli (Figure-16c). This finding indicates that PSGL-1 has an influential role in the initial steps of neutrophil migration, such as tethering, rolling (Zou et al., 2005), and firm adhesion (da Costa Martins et al., 2007) on the endothelium. We suggest that montelukast and zileuton impair the initial phase of neutrophil aggregation and adhesion by significantly inhibiting PSGL-1 expression.

LFA-1 (CD11a/CD18, $\alpha L\beta 2$ integrin) – This molecule is expressed on all leukocytes and has a crucial role in cell migration, especially in LFA-1-dependent

vascular adhesion to endothelial cells during trans-endothelial movement (Phillipson et al., 2006). ICAMs are the main ligands (Ley, 2007). PSGL-1 triggers and leads to LFA-1 activation in neutrophils (Zarbock et al., 2011, 2009). We observed a high PSGL-1 signal on blood neutrophils (Figure-16d). Chemokines can stimulate neutrophils to bring LFA-1 to its high-affinity state and mediate arrest (Shamri et al., 2005). These changes may explain the high expression of LFA-1 that we observed on inflamed blood neutrophils (Figure-16d). LFA-1 and Mac-1 have been reported to compete for binding to ICAM-1 (Lub et al., 1996). Although this idea remains controversial (Ding et al., 1999), we did observe opposite expression trends between LFA-1 and Mac-1 in blood and lung tissue (Figure-16d,e).

In an integrin-dependent manner, immunoglobulins can activate Fc receptors and promote phagocytosis. Antibody-dependent cellular cytotoxicity (ADCC) is a process used by neutrophils to annihilate large targets that cannot be phagocytosed (Gómez Román et al., 2014). $\beta 2$ integrins regulate ADCC via inside-out or outside-in mechanisms (Ortiz-Stern and Rosales, 2003). Further, the interaction of CD11a/CD18 and CD11b/CD18 with ICAM-1 is vital in regulating cytolytic granule release and conjugate formation (Dongfang Liu et al., 2009; Steblyanko et al., 2015). It also explains the high expression of LFA-1 and Mac-1 in the alveolar lavage fluid (Figure-16d,e).

LTB₄ induces conformational changes and activation in the human neutrophil CD11a adhesion receptor (Shames and Goetzl, 1993). LTD₄ activates neutrophil $\beta 2$ integrin adhesion, as demonstrated in an *in vitro* study (Meliton et al., 2010). In BAL, the LTB₄ synthesis inhibitor zileuton and the LTD₄ receptor inhibitor montelukast exhibited inhibition of LFA-1 expression.

Mac-1 (CD11b/CD18, $\alpha M\beta 2$ integrin) – This cell surface receptor is widely present on immune cells and plays an essential role in cell adhesion migration (Erdei et al., 2019). Mac-1 has a wide range of binding capabilities with over 40 ligands, including ICAMs, fibrinogen, iC3b, and other extracellular matrix proteins, suggesting that it can affect many cellular processes (Bouti et al., 2021). During neutrophil migration, Mac-1 mainly mediates the crawling step along the

blood vessels (Phillipson et al., 2006). In our study, a certain amount of Mac-1 expression was observed on neutrophils in the blood, significantly increased after exposure to the endothelium (Figure-16e).

Mac-1 is one of the significant receptors mediating leukocyte–platelet interactions. Platelet activation by PMN-derived, leukocyte-derived microparticles is dependent on the presence of Mac-1 (Pluskota et al., 2008). In a study involving CysLTs, Mac-1 expression could be significantly increased at 1 and 10 nM CysLTs, respectively (Fregonese et al., 2002). Our results also showed that montelukast and zileuton have an inhibitory effect on Mac-1 expression in the lung (Figure-16e).

VLA-4 (CD49d/CD29, $\alpha4\beta1$ -integrin) – This protein is one of the critical factors for cell adhesion. The primary ligands of VLA-4 are VCAM-1 and fibronectin (Imai et al., 2010). CD49 is expressed by various immune inflammatory cells, including monocytes, lymphocytes, mast cells, eosinophils, and neutrophils (Lobb and Hemler, 1994). Despite the absence of CD49 on human neutrophils, they can readily move CD49d/CD29 subunits to the membrane surface after endothelial transfer or exogenous stimulation (Kubes et al., 1995).

Under different stimulus conditions, such as TNF- α , neutrophils do not depend on the $\beta2$ integrin pathway for endothelial adhesion, and inhibiting $\beta2$ integrins does not thoroughly prevent neutrophil inflammatory recruitment. $\alpha4\beta1$ integrin adhesion is an alternative pathway to the $\beta2$ integrin-dependent pathway (Bowden et al., 2002; Chuluyan and Issekutz, 1993; Reinhardt et al., 1997).

It has been reported that VLA-4 cannot bind to the appropriate ligand until chemokines activate leukocytes or come into contact with activated endothelial cells (Bowden et al., 2002; Imai et al., 2010). That verifies our flow cytometry results that VLA-4 has a certain level of expression on PMNs in the blood, but once PMNs adhere to the endothelium and enter the lung tissue, the expression of VLA-4 on PMNs increases markedly (Figure-16f).

It has been proved that VLA-4($\alpha 4\beta 1$)-mediated adhesion is supported by the CysLT1 ligand leukotriene D4 (Boehmler et al., 2009). Thus, not surprisingly, both montelukast and zileuton inhibited VLA-4 very well in lung tissue (Figure-16f). Other physiological activities of VLA-4 involved in inflammatory terminals are not well elucidated. From our observations, zileuton, but not montelukast, significantly reduces VLA-4 expression in alveolar lavage fluid.

4.1.2 SDF-1/CXCR4 and bone marrow neutrophil release

SDF-1, also known as CXCL12, is one of the crucial endogenous chemotactic factors. Its main receptors are CXCR4 and CXCR7 (Cruz-Orengo et al., 2011; Nagasawa, 2015). Although SDF-1 is also expressed to some extent in inflammatory tissues and is involved in the recruitment of neutrophils under inflammatory conditions (Konrad et al., 2017), unlike other chemokines, SDF-1 has the highest expression in the body (bone marrow stroma) under normal physiological conditions (Figure-15c).

Neutrophil homeostasis is maintained by the balance of neutrophil production, bone marrow release, and circulation clearance (Christopher and Link, 2007). The bone marrow is the leading site of neutrophil production (Petrides and Dittmann, 1990). Under normal physiological conditions, no more than 2% of mature neutrophils are in circulation (Semerad et al., 2002). The SDF-1–CXCR4 axis is the main factor regulating the transport of mouse neutrophils between bone marrow and blood (Martin et al., 2003). CXCR2 expression is progressively upregulated in the bone marrow with neutrophil maturation (Capucetti et al., 2020). It binds to and is activated by the chemokines CXCL1, CXCL2, CXCL3, CXCL5, CXCL7, and CXCL8, and recruits CXCR2-positive neutrophils into circulation. It has been shown that neutrophils lacking CXCR2 are preferentially retained in the bone marrow (Eash et al., 2010). Therefore, there is a tug-of-war effect of SDF-1/CXCR4 versus inflammatory chemokines/CXCR2 on bone marrow neutrophils. It has been demonstrated that SDF-1 significantly attenuates the chemotactic response of newly isolated human and murine neutrophils to CXCR2 (Martin et al., 2003). Our findings confirm this view. Montelukast and zileuton keep neutrophils in the bone marrow by maintaining the concentration of

SDF-1 in the bone marrow. Meanwhile, after treatment with the agents, the retention effect was more potent for CXCR4+ neutrophils than for CXCR2+ neutrophils (Figure-15a.b).

However, in blood smears, montelukast or zileuton administration reduced more segmented neutrophils than banded neutrophils in the inflammatory state (Figure-15d). And we did not find a significant change in the ratio of banded/segmented PMNs in the blood. There are several possible reasons for this outcome. First, there is no very clear distribution criteria for CXCR4 and CXCR2 between the banded and segmented neutrophils (McKenna et al., 2021). Second, while SDF-1 retains neutrophils through CXCR4, it suppresses CXCR2 mediated neutrophil responses as well (Martin et al., 2003).

4.2 Montelukast and zileuton weaken inflammatory responses

4.2.1 Chemokine release

The severity of ARDS depends on the interaction of pro-inflammatory and anti-inflammatory mediators. The intervention of the pro-inflammatory process in the early stages of ARDS enables the treatment to curb the progression of the disease.

CXCL1, also known as keratinocyte-derived chemokine (KC) or growth-related oncogene α (GRO α), is secreted by many kinds of cells, including neutrophils, macrophages, and epithelial cells (Ley et al., 2007). CXCL1 has a strong chemotactic effect on many immune cells, especially neutrophils. First, it binds to glycosaminoglycans in the endothelium, epithelium, and extracellular matrix, forming a chemotactic gradient to direct peripheral neutrophils toward the site of infection. Second, it releases proteases and ROS into tissues for microbial destruction (Sawant et al., 2016). Third, CXCL1 stimulates calcium influx flow, an essential signaling mediator by which β 2 integrins are activated (Bouti et al., 2021).

CXCL2, also known as macrophage inflammatory protein 2 (MIP-2), is produced by monocytes, neutrophils, and macrophages, and its prominent role is in

chemotactic hematopoietic stem cells and polymorphonuclear leukocytes. Moreover, CXCL2 plays a vital role in breaching endothelial junctions (Girbl et al., 2018).

CXCR2 is a G protein-coupled receptor family member and is a significant receptor for CXCL1 and CXCL2, mediating neutrophil recruitment. CXCR2 activates many G-protein-induced signaling pathways that affect cell function, induce cell migration, and promote cell proliferation and survival (Cheng et al., 2019).

TNF- α is one of the most critical cytokines in the inflammatory process, which acts as an initial step for neutrophil activation (Kolaczkowska and Kubes, 2013). Macrophages and mast cells are typical tissue-resident cells that play an essential role in the inflammatory response. CXCL1 induces TNF- α production by acting on CXCR2 receptors in macrophages and mast cells (Vieira et al., 2009). LTD4 can cause the release of large amounts of TNF- α from macrophages in the alveoli (Ménard and Bissonnette, 2000).

IL-6 is mainly produced by macrophages during inflammation and is rapidly produced in response to tissue damage or infection (Tanaka et al., 2014). Apart from immune cells, endothelial, mesenchymal, fibroblast, and other cells are also responsible for producing IL-6 in response to various stimuli (Akira et al., 1993). IL-6 production promotes the transcription of TNF- α and IL-1 β , which further activate transcription factors that promote the production of IL-6, forming a forward loop. IL-6 also induces excessive vascular endothelial growth factor (VEGF) production, leading to increased vascular permeability (Tanaka et al., 2014). Furthermore, when IL-6 enters the bone marrow, it promotes megakaryocyte maturation and platelet release. LTB4 has been shown to activate IL-6 production by monocytes (Brach et al., 1992; Rola-Pleszczynski and Stankova, 1992).

IL-1 β is a critical mediator of the host response and resistance to pathogens. Various immune cells can produce IL-1 β (Lopez-Castejon and Brough, 2011). pro-IL-1 β is an inactive precursor of IL-1 β with a size of 31 kDa. This precursor is

not secreted and can be cleaved by the pro-inflammatory protease called caspase-1 (Thornberry et al., 1992). Numerous cellular stimuli are recognized by pattern recognition receptors (PRRs), leading to the recruitment and activation of inactive inflammatory caspase-1. Activated caspase-1 cleaves pro-IL-1 β , which promotes the secretion of IL-1 β , leading to inflammation (McIlwain et al., 2013). Besides, the metalloproteases MMP-3 and MMP-9 can process IL-1 β precursor (pro-IL-1 β) into the IL-1 β as well (Schönbeck et al., 1998). IL-1 β -induced neutrophil migration depends on the release of LTB₄ from macrophages (Oliveira et al., 2008). Cysteine leukotriene D₄ can trigger the production and release of IL-1 β from smooth muscle cells of vascular smooth muscle cells (Porreca et al., 1995). The inhibition of caspase-1 and MMPs by montelukast and zileuton (Figure-35a, b) impedes the synthesis of inflammatory factor IL-1 β (Figure-35c). The inhibition of caspase proteins and MMPs by montelukast (Erşahin et al., 2012; Dezhi Liu et al., 2009) and zileuton (Shi et al., 2013; Tu et al., 2009) has been mentioned long ago, but the mechanisms involved have not been elucidated.

Chemokines and their receptors are characterized by pleiotropic effects. Applying multiple antagonists against multiple receptors or multi-targeted agents is a potential research direction (Puneet et al., 2005). Montelukast and zileuton have inhibitory effects on CXCL1, CXCL2/3, TNF- α , and IL-6 (Figure-19a). We also determined the expression of CXCL1, CXCL2, TNF- α , and IL-6 at the protein level. CXCL2, TNF- α , and IL-6 protein expression were markedly reduced by montelukast and zileuton (Figure-19b). However, CXCL1 protein expression was not altered (Figure-19b). It has been demonstrated that some CXCL1 is pre-stored in endothelial cells and can be rapidly released into the blood in response to specific stimuli (Øynebråten et al., 2005). This phenomenon could explain why montelukast and zileuton suppress CXCL1 gene expression without altering the protein level.

By their target proteins analysis, montelukast and zileuton are found to affect the transcription of inflammatory chemokines via intervention in the ERK1/2–pCREB signaling pathway and caspase proteins (Figure-25 and Figure-26). And phosphorylation of CREB has been shown to promote the transcription of several

chemokines, including CXCL1 (Zhang et al., 2002) and IL-6 (Nijnik et al., 2012). The inhibitory effects of montelukast and zileuton on the ERK1/2–pCREB pathway partially explain their repression of chemokine transcription.

ERK1/2 is involved in the inflammatory response in ARDS (Fang et al., 2017). Under inflammatory states, ERK1/2 is activated (Arthur and Ley, 2013), inducing the expression of multiple genes that regulate the inflammatory response (Kyriakis and Avruch, 2001). LTD4 has been reported to induce phosphorylation of ERK 1/2 (Yuan et al., 2009), and arachidonic acid has been shown to activate ERK through a 5-lipoxygenase-dependent pathway (Capodici et al., 1998). LPS-induced lung inflammation can be reduced *in vivo* by inhibiting ERK signaling pathways (Chen et al., 2020). These evidences support our findings that gene and protein expression of ERK1/2 and phosphorylation of the downstream protein CREB were inhibited by montelukast and zileuton.

However, although there have been many studies on pCREB, the up or down regulation of pCREB expression by LPS is still controversial, even with completely opposite opinions. In *in vivo* experiments, the expression of pCREB elevated when the LPS administration time was within one to four days (Chen et al., 2014; Illario et al., 2008). Whereas, the expression of pCREB in tissues was decreased when multiple consecutive dosing times were more than 5 days (Guo et al., 2014; Sun et al., 2021). In *in vitro* experiments, the expression of pCREB increased when the LPS administration time is within 30 minutes to 2 hours (Boulting et al., 2021; Choi et al., 2009; Kreckler et al., 2009; Lee et al., 2015; Park et al., 2005), while it decreased when stimulation time over 8 to 24 hours (Huang et al., 2016). It has been found that there is a time gap of approximately 10 hours between TNF α and IL-10 expression peaks in LPS-stimulated RAW264.7 macrophages (Hobbs et al., 2018).

It has been shown that montelukast inhibits the Ca²⁺ oscillations evoked by the interaction of CysLTs with CysLTR1, thereby reducing CREB activation. The decrease in pCREB is associated with depression (Koch et al., 2009), which may be one of the reasons for the Food and Drug Administration (FDA)'s warning about the neuropsychiatric side effects of montelukast (US Food and Drug

Administration, 2020). In a study on peripheral inflammation and acute pain in mice, LTB₄-LTB₄R1 signaling was shown to promote CREB phosphorylation, which was consistent with our study's results that zileuton caused a decrease in pCREB.

4.2.2 PNC formation

In whole blood, it has long been known that platelets aggregate around neutrophils (Bauer, 1975). Montelukast and zileuton interfere with the formation of PNCs in the blood (Figure-17), perhaps resulting from the inhibition of leukocyte P-selectin (Figure-16a) and PSGL-1 (Figure-16c) and platelet-activated receptor P2Y₁₂ (Figure-34b,c).

PNCs in the blood play a role in various inflammatory diseases involving different body organs (Page and Pitchford, 2013). Inhibition of PNCs contributes significantly to suppressing the progression of ARDS.

PNC formation facilitates neutrophil migration to inflammatory tissues – Upregulation of platelet-activated neutrophil integrins and enhanced responsiveness to chemokines allow adequate adhesion of neutrophils to the vascular endothelium (Page and Pitchford, 2013). Platelets activated by neutrophils promote the release of CXCL8 and CXCL1 from the endothelium upon contact with the endothelium (Mine et al., 2001).

PNCs enhance the production of leukotrienes and platelet activation – The platelet-specific enzyme 12-lipoxygenase produces 12-hydroxyeicosatetraenoic acid (12-HETE), which is taken up by neutrophils to generate 12,20-diHETE, a chemoattractant that neutrophils cannot produce on their own and must from activated platelets (Marcus et al., 1988, 1984). Leukotriene production is also augmented by increasing 12-HETE, which stimulates neutrophil 5-lipoxygenase (Maclouf and Murphy, 1988). In addition, platelets have been reported to acquire arachidonic acid from neutrophils through a subset of membrane-bound molecules called extracellular vesicles (EVs), promoting TXA₂ synthesis and platelet activation (Rossaint et al., 2016).

Hence, the inhibition of PNCs in the blood by montelukast and zileuton could improve the inflammatory response in several ways, including inhibition of neutrophil–endothelial cell interactions and reduction of leukotriene synthesis.

4.2.3 ROS production

A significant contributor to ARDS progression and lung damage is the production of excessive ROS by an injured endothelium/epithelium and recruited leukocytes. When the endothelial and epithelial barriers break down under oxidative stress, neutrophils can penetrate the barrier, releasing cytotoxic agents (Kellner et al., 2017).

We found that montelukast and zileuton could inhibit the production of oxidative stress products in the lung tissue (Figure-18). One possible reason is that leukotriene B₄ stimulates the Rac–ERK cascade to produce ROS (Woo et al., 2002), and CysLTR1 activation promotes the release of ROS (Al Saadi et al., 2011), whereas montelukast and zileuton have a repressive effect on the expression of LTB₄R1 (Figure-20f, 21).

However, flow cytometry and MPO results showed that neither agent ameliorates the oxidative stress response in BAL but significantly inhibits the onset of the oxidative burst in lung tissue.

4.3 Application of montelukast and zileuton

As shown in Figure-36, montelukast and zileuton exhibit potent anti-inflammatory effects that are multidimensional and different from their “official” roles, CysLTR1 antagonist and inhibitor of arachidonate-5-Lipoxygenase. In addition to their officially described functions, montelukast and zileuton act at different sites (bone marrow, intravascular, lung interstitium, alveolar compartment) on multiple functions (PNC formation, ROS generation, and chemokine release) of multiple cells (neutrophils and platelets).

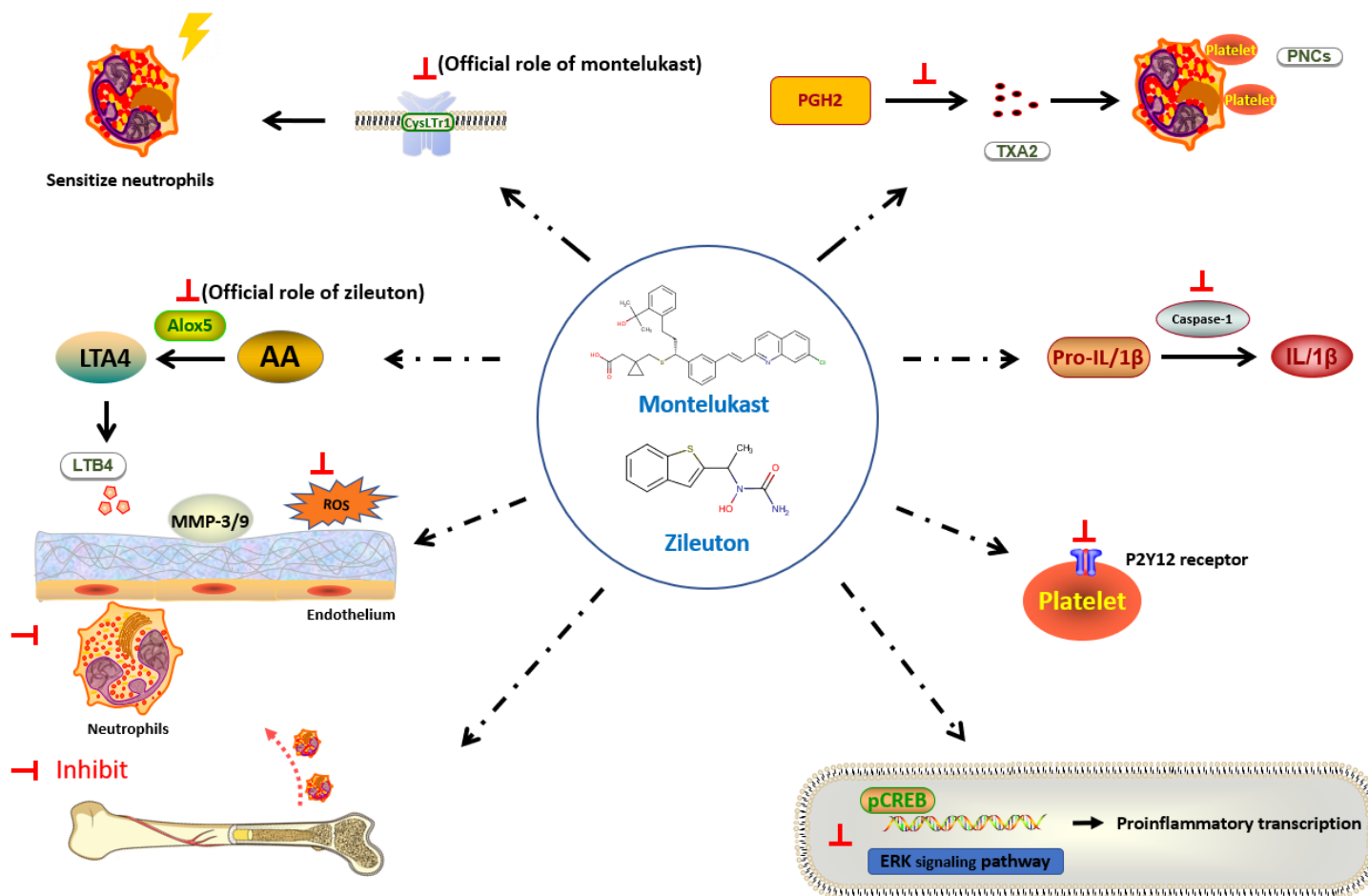


Figure-36: Anti-inflammatory functions of montelukast and zileuton in this study.

AA = Arachidonic acid; ERK = Extracellular signal-regulated kinase; LTA4 = Leukotriene A4; LTB4 = Leukotriene B4; MMP = Matrix metalloproteinase; PGH2 = Prostaglandin H2; PNCs = Platelet-neutrophil complexes; ROS = Reactive oxygen specie; TXA2 =Thromboxane A2
 The figure was created with Edrawsoft (version 12.0.1).

5 Summary

The hallmark of acute lung inflammation is neutrophil infiltration in inflamed lung tissue, and leukotrienes are important mediators that drive immune cell migration. However, the effects of leukotriene modifiers on acute lung inflammation and the mechanisms of their effects are unclear.

Flow cytometry revealed that the leukotriene modifiers montelukast and zileuton inhibited the migration of neutrophils and the expression of the adhesion molecules P-selectin, L-selectin and PSGL-1, as well as the integrins LFA-1, Mac-1 and VLA-4 during migration in each lung compartment. Combined ELISA and blood smear analysis confirmed that both agents reduced the release of bone marrow CXCR4+ neutrophils into the blood by maintaining bone marrow SDF-1 concentrations. The application of montelukast and zileuton resulted in a significant reduction in gene and protein expression of the lung inflammatory factors TNF- α , IL6, and CXCL2/3, but only a reduction in CXCL1 at the gene expression level, which may be related to the rapid release of CXCL1 from endothelial cell preexisting. Further studies confirmed that both agents inhibited the expression of the ERK1/2 pathway and downstream pCREB, which are involved in the transcription of inflammatory chemokines. Montelukast and zileuton also inhibited the production of oxidative bursts in the lung interstitium and the formation of neutrophil-platelet complexes in the vasculature, which promote neutrophil migration. RT-qPCR and immunofluorescence confirmed the key enzymes of the leukotriene synthesis pathway and CysLTR1, LTB4R1 expression on neutrophils, lung endothelial and epithelial cells were inhibited by both modifiers. We observed that montelukast and zileuton exhibited different functions in addition to the classical effects of CysLTR1 antagonist and inhibitor of arachidonate-5-Lipoxygenase. As has been demonstrated: both agents inhibited caspase-1 protein expression and reduced IL-1 β production; They inhibited gene expression of MMP-3 and MMP-9 in lung tissue and protein expression of platelet-activated receptor P2Y12 as well.

In summary, montelukast and zileuton have multitargeted, multidimensional, and potent anti-inflammatory functions during acute pulmonary inflammation.

6 Zusammenfassung

Das Kennzeichen einer akuten Lungenentzündung ist die Infiltration von Neutrophilen in das entzündete Lungengewebe, und Leukotriene sind wichtige Mediatoren, die die Migration von Immunzellen steuern. Die Auswirkungen von Leukotrien-Modifikatoren auf die akute Lungenentzündung und die Mechanismen ihrer Wirkung sind jedoch unklar.

Die Durchflusszytometrie ergab, dass die Leukotrien-Modifikatoren Montelukast und Zileuton die Migration von Neutrophilen und die Expression der Adhäsionsmoleküle P-Selektin, L-Selektin und PSGL-1 sowie der Integrine LFA-1, Mac-1 und VLA-4 während der Migration in jedem Lungenkompartiment hemmten. Kombinierte ELISA- und Blutausrichanalysen bestätigten, dass beide Wirkstoffe die Freisetzung von CXCR4+ Neutrophilen aus dem Knochenmark in das Blut verringerten, indem sie die SDF-1-Konzentrationen im Knochenmark aufrechterhielten. Die Verabreichung von Montelukast und Zileuton führte zu einer signifikanten Verringerung der Gen- und Proteinexpression der Entzündungsfaktoren TNF- α , IL6 und CXCL2/3 in der Lunge, aber nur zu einer Verringerung von CXCL1 auf der Ebene der Genexpression, was mit der raschen Freisetzung von CXCL1 aus Endothelzellen zusammenhängen könnte. Weitere Untersuchungen ergaben, dass beide Wirkstoffe die Expression des ERK1/2-Signalwegs und des nachgeschalteten pCREB hemmten, die an der Transkription von entzündlichen Chemokinen beteiligt sind. Montelukast und Zileuton hemmten auch die Produktion von oxidativen Bursts im Lungeninterstitium und die Bildung von Neutrophilen-Plättchen-Komplexen im Gefäßsystem, die die Migration von Neutrophilen fördern. RT-qPCR und Immunfluoreszenz bestätigten, dass die Schlüsselenzyme des Leukotrien-Synthesewegs und die Expression von CysLTR1 und LTB4R1 auf Neutrophilen, Lungenendothel- und Epithelzellen durch beide Modifikatoren gehemmt wurden. Wir beobachteten, dass Montelukast und Zileuton neben den klassischen Wirkungen eines CysLTR1-Antagonisten und eines Inhibitors der Arachidonat-5-Lipoxygenase unterschiedliche Funktionen aufweisen. Wie gezeigt wurde, hemmten beide

Wirkstoffe die Caspase-1-Proteinexpression und verringerten die IL-1 β -Produktion; sie hemmten auch die Genexpression von MMP-3 und MMP-9 im Lungengewebe und die Proteinexpression des plättchenaktivierten Rezeptors P2Y₁₂.

Zusammenfassend lässt sich sagen, dass Montelukast und Zileuton während einer akuten Lungenentzündung eine vielseitige, mehrdimensionale und starke entzündungshemmende Wirkung haben.

7 Bibliography

- Abou-Saleh, H., Théorêt, J.-F., Yacoub, D., Merhi, Y., 2005. Neutrophil P-selectin-glycoprotein-ligand-1 binding to platelet P-selectin enhances metalloproteinase 2 secretion and platelet-neutrophil aggregation. *Thromb Haemost* 94, 1230–1235. <https://doi.org/10.1160/TH05-05-0344>
- Afonso, P.V., Janka-Junttila, M., Lee, Y.J., McCann, C.P., Oliver, C.M., Aamer, K.A., Losert, W., Cicerone, M.T., Parent, C.A., 2012. LTB4 is a signal-relay molecule during neutrophil chemotaxis. *Developmental Cell* 22, 1079–1091. <https://doi.org/10/f3zp9k>
- Akira, S., Taga, T., Kishimoto, T., 1993. Interleukin-6 in Biology and Medicine. *Adv Immunol* 54, 1–78. [https://doi.org/10.1016/s0065-2776\(08\)60532-5](https://doi.org/10.1016/s0065-2776(08)60532-5)
- Al Saadi, M.M., Meo, S.A., Mustafa, A., Shafi, A., Tuwajri, A.S.A., 2011. Effects of Montelukast on free radical production in whole blood and isolated human polymorphonuclear neutrophils (PMNs) in asthmatic children. *Saudi Pharmaceutical Journal* 19, 215–220. <https://doi.org/10/cc7xrs>
- American lung association, 2020. Recovering from ARDS [WWW Document]. URL <https://www.lung.org/lung-health-diseases/lung-disease-lookup/ards/ards-treatment-and-recovery> (accessed 11.9.22).
- Araz, O., 2020. Current Pharmacological Approach to ARDS: The Place of Bosentan. *Eurasian J Med* 52, 81–85. <https://doi.org/10.5152/eurasianjmed.2020.19218>
- ARDS Definition Task Force, Ranieri, V.M., Rubenfeld, G.D., Thompson, B.T., Ferguson, N.D., Caldwell, E., Fan, E., Camporota, L., Slutsky, A.S., 2012. Acute respiratory distress syndrome: the Berlin Definition. *JAMA* 307, 2526–2533. <https://doi.org/10/gdgtvr>
- ARDS network, Brower, R.G., Matthay, M.A., Morris, A., Schoenfeld, D., Thompson, B.T., Wheeler, A., 2000. Ventilation with lower tidal volumes as compared with traditional tidal volumes for acute lung injury and the acute respiratory distress syndrome. *N Engl J Med* 342, 1301–1308. <https://doi.org/10/c4xj8q>
- Arthur, J.S.C., Ley, S.C., 2013. Mitogen-activated protein kinases in innate immunity. *Nat Rev Immunol* 13, 679–692. <https://doi.org/10.1038/nri3495>
- Ashbaugh, D., Bigelow, D.B., Petty, T., Levine, B., 1967. ACUTE RESPIRATORY DISTRESS IN ADULTS. *The Lancet* 290, 319–323. <https://doi.org/10/c9p4h3>
- Athens, J.W., Haab, O.P., Raab, S.O., Mauer, A.M., Ashenbrucker, H., Cartwright, G.E., Wintrobe, M.M., 1961. Leukokinetic studies. IV. The total blood, circulating and marginal granulocyte pools and the granulocyte turnover rate in normal subjects. *J Clin Invest* 40, 989–995. <https://doi.org/10.1172/JCI104338>
- Aulakh, G.K., 2018. Neutrophils in the lung: “the first responders.” *Cell Tissue Res* 371, 577–588. <https://doi.org/10.1007/s00441-017-2748-z>
- Bargatze, R.F., Kurk, S., Butcher, E.C., Jutila, M.A., 1994. Neutrophils roll on adherent neutrophils bound to cytokine-induced endothelial cells via L-selectin on the rolling cells. *J Exp Med* 180, 1785–1792. <https://doi.org/10.1084/jem.180.5.1785>
- Bauer, H.M., 1975. In-vitro Platelet–Neutrophil Adherence. *Am J Clin Pathol* 63, 824–827. <https://doi.org/10.1093/ajcp/63.6.824>
- Bellani, G., Laffey, J.G., Pham, T., Fan, E., Brochard, L., Esteban, A., Gattinoni, L., van Haren, F., Larsson, A., McAuley, D.F., Ranieri, M., Rubenfeld, G., Thompson, B.T., Wrigge, H., Slutsky, A.S., Pesenti, A., LUNG SAFE Investigators, ESICM Trials Group, 2016. Epidemiology, Patterns of Care, and Mortality for Patients With Acute Respiratory Distress Syndrome in Intensive Care Units in 50 Countries. *JAMA* 315, 788–800. <https://doi.org/10/f3pwt9>
- Bernard, G.R., Artigas, A., Brigham, K.L., Carlet, J., Falke, K., Hudson, L., Lamy, M., Legall, J.R., Morris, A., Spragg, R., 1994. The American-European Consensus

- Conference on ARDS. Definitions, mechanisms, relevant outcomes, and clinical trial coordination. *Am J Respir Crit Care Med* 149, 818–824. <https://doi.org/10/ggc7hp>
- Bersten, A.D., Edibam, C., Hunt, T., Moran, J., Australian and New Zealand Intensive Care Society Clinical Trials Group, 2002. Incidence and mortality of acute lung injury and the acute respiratory distress syndrome in three Australian States. *Am J Respir Crit Care Med* 165, 443–448. <https://doi.org/10/gfspbb>
- Boehmler, A.M., Drost, A., Jaggy, L., Seitz, G., Wiesner, T., Denzlinger, C., Kanz, L., Möhle, R., 2009. The CysLT1 Ligand Leukotriene D4 Supports $\alpha 4\beta 1$ - and $\alpha 5\beta 1$ -Mediated Adhesion and Proliferation of CD34+ Hematopoietic Progenitor Cells. *J Immunol* 182, 6789–6798. <https://doi.org/10.4049/jimmunol.0801525>
- Boulting, G.L., Durreesi, E., Ataman, B., Sherman, M.A., Mei, K., Harmin, D.A., Carter, A.C., Hochbaum, D.R., Granger, A.J., Engreitz, J.M., Hrvatin, S., Blanchard, M.R., Yang, M.G., Griffith, E.C., Greenberg, M.E., 2021. Activity-dependent regulome of human GABAergic neurons reveals new patterns of gene regulation and neurological disease heritability. *Nat Neurosci* 24, 437–448. <https://doi.org/10.1038/s41593-020-00786-1>
- Bouti, P., Webbers, S.D.S., Fagerholm, S.C., Alon, R., Moser, M., Matlung, H.L., Kuijpers, T.W., 2021. $\beta 2$ Integrin Signaling Cascade in Neutrophils: More Than a Single Function. *Front. Immunol.* 11. <https://doi.org/10.3389/fimmu.2020.619925>
- Bowden, R.A., Ding, Z.-M., Donnachie, E.M., Petersen, T.K., Michael, L.H., Ballantyne, C.M., Burns, A.R., 2002. Role of $\alpha 4$ Integrin and VCAM-1 in CD18-Independent Neutrophil Migration Across Mouse Cardiac Endothelium. *Circulation Research* 90, 562–569. <https://doi.org/10.1161/01.RES.0000013835.53611.97>
- Brach, M.A., De Vos, S., Arnold, C., Größ, H.-J., Mertelsmann, R., Herrmann, F., 1992. Leukotriene B4 transcriptionally activates interleukin-6 expression involving NK- κ B and NF-IL6. *Eur. J. Immunol.* 22, 2705–2711. <https://doi.org/10.1002/eji.1830221034>
- Brazil, J.C., Parkos, C.A., 2016. Pathobiology of neutrophil–epithelial interactions. *Immunol Rev* 273, 94–111. <https://doi.org/10/f8zbnj>
- Brock, T.G., McNish, R.W., Coffey, M.J., Ojo, T.C., Phare, S.M., Peters-Golden, M., 1996. Effects of granulocyte-macrophage colony-stimulating factor on eicosanoid production by mononuclear phagocytes. *J Immunol* 156, 2522–2527.
- Bux, J., Sachs, U.J.H., 2007. The pathogenesis of transfusion-related acute lung injury (TRALI). *Br J Haematol* 136, 788–799. <https://doi.org/10/d2g2q5>
- Capodici, C., Pillinger, M.H., Han, G., Philips, M.R., Weissmann, G., 1998. Integrin-dependent homotypic adhesion of neutrophils. Arachidonic acid activates Raf-1/Mek/Erk via a 5-lipoxygenase-dependent pathway. *J Clin Invest* 102, 165–175.
- Capucetti, A., Albano, F., Bonocchi, R., 2020. Multiple Roles for Chemokines in Neutrophil Biology. *Front. Immunol.* 11. <https://doi.org/10/gk44pq>
- Casey, J.D., Semler, M.W., Rice, T.W., 2019. Fluid Management in Acute Respiratory Distress Syndrome. *Semin Respir Crit Care Med* 40, 57–65. <https://doi.org/10/gpb3nq>
- Chen, Shenglin, Xie, J., Zhao, K., Ren, L., Deng, Y., Xie, X., Chen, Shiyi, Xu, H., Long, X., Liu, E., 2020. LPS aggravates lung inflammation induced by RSV by promoting the ERK-MMP-12 signaling pathway in mice. *Respir Res* 21, 193. <https://doi.org/10.1186/s12931-020-01453-6>
- Chen, Y., Junger, W.G., 2012. Measurement of Oxidative Burst in Neutrophils. *Methods Mol Biol* 844, 115–124. <https://doi.org/10/fx9xnd>
- Chen, Z., Jalabi, W., Hu, W., Park, H.-J., Gale, J.T., Kidd, G.J., Bernatowicz, R., Gossman, Z.C., Chen, J.T., Dutta, R., Trapp, B.D., 2014. Microglial displacement of inhibitory synapses provides neuroprotection in the adult brain. *Nat Commun* 5, 4486. <https://doi.org/10.1038/ncomms5486>

- Cheng, Y., Ma, X., Wei, Y., Wei, X.-W., 2019. Potential roles and targeted therapy of the CXCLs/CXCR2 axis in cancer and inflammatory diseases. *Biochimica et Biophysica Acta (BBA) - Reviews on Cancer* 1871, 289–312. <https://doi.org/10.1016/j.bbcan.2019.01.005>
- Chensue, S.W., Kunkel, S.L., 1983. Arachidonic acid metabolism and macrophage activation. *Clin Lab Med* 3, 677–694.
- Chlopicki, S., Lomnicka, M., Gryglewski, R.J., 2003. Obligatory role of lipid mediators in platelet-neutrophil adhesion. *Thromb Res*, 287–292. <https://doi.org/10.1016/j.throm.2003.08.003>
- Chlopicki, S., Olszanecki, R., Janiszewski, M., Laurindo, F., Panz, T., Miedzobrodzki, J., 2004. Functional Role of NADPH Oxidase in Activation of Platelets. *Antioxidants & redox signaling* 6, 691–8. <https://doi.org/10.1089/ars.2004.16.691>
- Choi, Y., Lee, M., Lim, S., Sung, S., Kim, Y., 2009. Inhibition of inducible NO synthase, cyclooxygenase-2 and interleukin-1 β by torilin is mediated by mitogen-activated protein kinases in microglial BV2 cells. *Br J Pharmacol* 156, 933–940. <https://doi.org/10.1111/j.1476-5381.2009.00022.x>
- Christopher, M.J., Link, D.C., 2007. Regulation of neutrophil homeostasis. *Current Opinion in Hematology* 14, 3–8. <https://doi.org/10.1097/00062752-200701000-00003>
- Chuluyan, H.E., Issekutz, A.C., 1993. VLA-4 integrin can mediate CD11/CD18-independent transendothelial migration of human monocytes. *J Clin Invest* 92, 2768–2777. <https://doi.org/10.1172/JCI117442>
- Cruz-Orengo, L., Holman, D.W., Dorsey, D., Zhou, L., Zhang, P., Wright, M., McCandless, E.E., Patel, J.R., Luker, G.D., Littman, D.R., Russell, J.H., Klein, R.S., 2011. CXCR7 influences leukocyte entry into the CNS parenchyma by controlling abluminal CXCL12 abundance during autoimmunity. *J Exp Med* 208, 327–339. <https://doi.org/10.1084/jem.20102010>
- da Costa Martins, P., García-Vallejo, J.-J., van Thienen, J.V., Fernandez-Borja, M., van Gils, J.M., Beckers, C., Horrevoets, A.J., Hordijk, P.L., Zwaginga, J.-J., 2007. P-Selectin Glycoprotein Ligand-1 Is Expressed on Endothelial Cells and Mediates Monocyte Adhesion to Activated Endothelium. *ATVB* 27, 1023–1029. <https://doi.org/10.1161/ATVBAHA.107.140442>
- De Filippo, K., Rankin, S.M., 2020. The Secretive Life of Neutrophils Revealed by Intravital Microscopy. *Frontiers in Cell and Developmental Biology* 8. <https://doi.org/10.3389/fcell.2020.603230>
- Dholia, N., Sethi, G.S., Naura, A.S., Yadav, U.C.S., 2021. Cysteinyl leukotriene D4 (LTD4) promotes airway epithelial cell inflammation and remodelling. *Inflamm. Res.* 70, 109–126. <https://doi.org/10.1007/s00011-020-01416-z>
- Diacovo, T.G., deFougerolles, A.R., Bainton, D.F., Springer, T.A., 1994. A functional integrin ligand on the surface of platelets: intercellular adhesion molecule-2. *J Clin Invest* 94, 1243–1251. <https://doi.org/10.1172/JCI117442>
- Ding, Z.M., Babensee, J.E., Simon, S.I., Lu, H., Perrard, J.L., Bullard, D.C., Dai, X.Y., Bromley, S.K., Dustin, M.L., Entman, M.L., Smith, C.W., Ballantyne, C.M., 1999. Relative contribution of LFA-1 and Mac-1 to neutrophil adhesion and migration. *J Immunol* 163, 5029–5038.
- Doerschuk, C.M., Allard, M.F., Martin, B.A., MacKenzie, A., Autor, A.P., Hogg, J.C., 1987. Marginated pool of neutrophils in rabbit lungs. *J Appl Physiol* (1985) 63, 1806–1815. <https://doi.org/10.1152/jappl.1987.63.5.1806>
- Dorsam, R.T., Kunapuli, S.P., 2004. Central role of the P2Y12 receptor in platelet activation. *J Clin Invest* 113, 340–345. <https://doi.org/10.1172/JCI22967>
- Doyle, R.L., Szaflarski, N., Modin, G.W., Wiener-Kronish, J.P., Matthay, M.A., 1995. Identification of patients with acute lung injury. Predictors of mortality. *Am J Respir Crit Care Med* 152, 1818–1824. <https://doi.org/10.1164/ajrccm.152.6.1818>

- Dvash, E., Har-Tal, M., Barak, S., Meir, O., Rubinstein, M., 2015. Leukotriene C4 is the major trigger of stress-induced oxidative DNA damage. *Nat Commun* 6, 10112. <https://doi.org/10.1038/ncomms10112>
- Eash, K.J., Greenbaum, A.M., Gopalan, P.K., Link, D.C., 2010. CXCR2 and CXCR4 antagonistically regulate neutrophil trafficking from murine bone marrow. *J Clin Invest* 120, 2423–2431. <https://doi.org/10/fws7s7>
- Erdei, A., Lukácsi, S., Mácsik-Valent, B., Nagy-Baló, Z., Kurucz, I., Bajtay, Z., 2019. Non-identical twins: Different faces of CR3 and CR4 in myeloid and lymphoid cells of mice and men. *Seminars in Cell & Developmental Biology* 85, 110–121. <https://doi.org/10.1016/j.semcdb.2017.11.025>
- Erşahin, M., Çevik, Ö., Akakin, D., Şener, A., Özbay, L., Yegen, B.C., Şener, G., 2012. Montelukast inhibits caspase-3 activity and ameliorates oxidative damage in the spinal cord and urinary bladder of rats with spinal cord injury. *Prostaglandins & Other Lipid Mediators* 99, 131–139. <https://doi.org/10.1016/j.prostaglandins.2012.09.002>
- Etulain, J., Martinod, K., Wong, S.L., Cifuni, S.M., Schattner, M., Wagner, D.D., 2015. P-selectin promotes neutrophil extracellular trap formation in mice. *Blood* 126, 242–246. <https://doi.org/10.1182/blood-2015-01-624023>
- Fan, E., Del Sorbo, L., Goligher, E.C., Hodgson, C.L., Munshi, L., Walkey, A.J., Adhikari, N.K.J., Amato, M.B.P., Branson, R., Brower, R.G., Ferguson, N.D., Gajic, O., Gattinoni, L., Hess, D., Mancebo, J., Meade, M.O., McAuley, D.F., Pesenti, A., Ranieri, V.M., Rubenfeld, G.D., Rubin, E., Seckel, M., Slutsky, A.S., Talmor, D., Thompson, B.T., Wunsch, H., Uleryk, E., Brozek, J., Brochard, L.J., 2017. An Official American Thoracic Society/European Society of Intensive Care Medicine/Society of Critical Care Medicine Clinical Practice Guideline: Mechanical Ventilation in Adult Patients with Acute Respiratory Distress Syndrome. *Am J Respir Crit Care Med* 195, 1253–1263. <https://doi.org/10.1164/rccm.201703-0548ST>
- Fang, W., Cai, S.-X., Wang, C.-L., Sun, X.-X., Li, K., Yan, X.-W., Sun, Y.-B., Sun, X.-Z., Gu, C.-K., Dai, M.-Y., Wang, H.-M., Zhou, Z., 2017. Modulation of mitogen-activated protein kinase attenuates sepsis-induced acute lung injury in acute respiratory distress syndrome rats. *Molecular Medicine Reports* 16, 9652–9658. <https://doi.org/10.3892/mmr.2017.7811>
- Fein, A.M., Lippmann, M., Holtzman, H., Eliraz, A., Goldberg, S.K., 1983. The risk factors, incidence, and prognosis of ARDS following septicemia. *Chest* 83, 40–42. <https://doi.org/10/bqt23n>
- Filippi, M.-D., 2019. Neutrophil transendothelial migration: updates and new perspectives. *Blood* 133, 2149–2158. <https://doi.org/10.1182/blood-2018-12-844605>
- Fowler, A.A., Hamman, R.F., Good, J.T., Benson, K.N., Baird, M., Eberle, D.J., Petty, T.L., Hyers, T.M., 1983. Adult respiratory distress syndrome: risk with common predispositions. *Ann Intern Med* 98, 593–597. <https://doi.org/10/gn8sc7>
- Fregonese, L., Silvestri, M., Sabatini, F., Rossi, G.A., 2002. Cysteinyl leukotrienes induce human eosinophil locomotion and adhesion molecule expression via a CysLT1 receptor-mediated mechanism. *Clin Exp Allergy* 32, 745–750. <https://doi.org/10/fmmbck>
- Frenette, P.S., Denis, C.V., Weiss, L., Jurk, K., Subbarao, S., Kehrel, B., Hartwig, J.H., Vestweber, D., Wagner, D.D., 2000. P-Selectin Glycoprotein Ligand 1 (Psgl-1) Is Expressed on Platelets and Can Mediate Platelet–Endothelial Interactions in Vivo. *J Exp Med* 191, 1413–1422.
- Girbl, T., Lenn, T., Perez, L., Rolas, L., Barkaway, A., Thiriot, A., del Fresno, C., Lynam, E., Hub, E., Thelen, M., Graham, G., Alon, R., Sancho, D., von Andrian, U.H., Voisin, M.-B., Rot, A., Nourshargh, S., 2018. Distinct Compartmentalization of the

- Chemokines CXCL1 and CXCL2 and the Atypical Receptor ACKR1 Determine Discrete Stages of Neutrophil Diapedesis. *Immunity* 49, 1062-1076.e6. <https://doi.org/10.1016/j.immuni.2018.09.018>
- Goldsmith, H.L., Spain, S., 1984a. Radial distribution of white cells in tube flow. *Kroc Found Ser* 16, 131–146.
- Goldsmith, H.L., Spain, S., 1984b. Margination of leukocytes in blood flow through small tubes. *Microvasc Res* 27, 204–222. [https://doi.org/10.1016/0026-2862\(84\)90054-2](https://doi.org/10.1016/0026-2862(84)90054-2)
- Gómez Román, V.R., Murray, J.C., Weiner, L.M., 2014. Antibody-Dependent Cellular Cytotoxicity (ADCC), in: Ackerman, M.E., Nimmerjahn, F. (Eds.), *Antibody Fc*. Academic Press, Boston, pp. 1–27. <https://doi.org/10.1016/B978-0-12-394802-1.00001-7>
- Griffin, G.K., Newton, G., Tarrío, M.L., Bu, D., Maganto-Garcia, E., Azcutia, V., Alcaide, P., Grabie, N., Luscinskas, F.W., Croce, K.J., Lichtman, A.H., 2012. IL-17 and TNF- α sustain neutrophil recruitment during inflammation through synergistic effects on endothelial activation. *J Immunol* 188, 6287–6299. <https://doi.org/10.4049/jimmunol.1200385>
- Griffiths, M.J.D., McAuley, D.F., Perkins, G.D., Barrett, N., Blackwood, B., Boyle, A., Chee, N., Connolly, B., Dark, P., Finney, S., Salam, A., Silversides, J., Tarmey, N., Wise, M.P., Baudouin, S.V., 2019. Guidelines on the management of acute respiratory distress syndrome. *BMJ Open Res* 6, e000420. <https://doi.org/10.1136/bmjresp-2019-000420>
- Guo, J., Lin, P., Zhao, X., Zhang, J., Wei, X., Wang, Q., Wang, C., 2014. Etazolate abrogates the lipopolysaccharide (LPS)-induced downregulation of the cAMP/pCREB/BDNF signaling, neuroinflammatory response and depressive-like behavior in mice. *Neuroscience* 263, 1–14. <https://doi.org/10.1016/j.neuroscience.2014.01.008>
- Haendeler, J., Hoffmann, J., Diehl, J.F., Vasa, M., Spyridopoulos, I., Zeiher, A.M., Dimmeler, S., 2004. Antioxidants Inhibit Nuclear Export of Telomerase Reverse Transcriptase and Delay Replicative Senescence of Endothelial Cells. *Circulation Research* 94, 768–775. <https://doi.org/10.1161/01.RES.0000121104.05977.F3>
- Hamburger, S.A., McEver, R.P., 1990. GMP-140 mediates adhesion of stimulated platelets to neutrophils. *Blood* 75, 550–554.
- Haribabu, B., Verghese, M.W., Steeber, D.A., Sellars, D.D., Bock, C.B., Snyderman, R., 2000. Targeted disruption of the leukotriene B(4) receptor in mice reveals its role in inflammation and platelet-activating factor-induced anaphylaxis. *J Exp Med* 192, 433–438. <https://doi.org/10.1084/jem.192.3.433>
- Hedi, H., Norbert, G., 2004. 5-Lipoxygenase Pathway, Dendritic Cells, and Adaptive Immunity. *Journal of Biomedicine and Biotechnology* 2004, 99–105. <https://doi.org/10.1155/S1110724304310041>
- Hobbs, S., Reynoso, M., Geddis, A.V., Mitrophanov, A.Y., Matheny, R.W., 2018. LPS-stimulated NF- κ B p65 dynamic response marks the initiation of TNF expression and transition to IL-10 expression in RAW 264.7 macrophages. *Physiol Rep* 6, e13914. <https://doi.org/10.14814/phy2.13914>
- Hoover, R.L., Karnovsky, M.J., Austen, K.F., Corey, E.J., Lewis, R.A., 1984. Leukotriene B4 action on endothelium mediates augmented neutrophil/endothelial adhesion. *Proc. Natl. Acad. Sci. U.S.A.* 81, 2191–2193. <https://doi.org/10.1073/pnas.81.7.2191>
- Huang, H., Hong, Q., Tan, H., Xiao, C., Gao, Y., 2016. Ferulic acid prevents LPS-induced up-regulation of PDE4B and stimulates the cAMP/CREB signaling pathway in PC12 cells. *Acta Pharmacol Sin* 37, 1543–1554. <https://doi.org/10.1038/aps.2016.88>

- Hudson, L.D., Milberg, J.A., Anardi, D., Maunder, R.J., 1995. Clinical risks for development of the acute respiratory distress syndrome. *Am J Respir Crit Care Med* 151, 293–301. <https://doi.org/10/gn8rr4>
- Hurd, T.R., DeGennaro, M., Lehmann, R., 2012. Redox regulation of cell migration and adhesion. *Trends in Cell Biology* 22, 107–115. <https://doi.org/10.1016/j.tcb.2011.11.002>
- Illario, M., Giardino-Torchia, M.L., Sankar, U., Ribar, T.J., Galgani, M., Vitiello, L., Masci, A.M., Bertani, F.R., Ciaglia, E., Astone, D., Maulucci, G., Cavallo, A., Vitale, M., Cimini, V., Pastore, L., Means, A.R., Rossi, G., Racioppi, L., 2008. Calmodulin-dependent kinase IV links Toll-like receptor 4 signaling with survival pathway of activated dendritic cells. *Blood* 111, 723–731. <https://doi.org/10.1182/blood-2007-05-091173>
- Imai, Y., Shimaoka, M., Kurokawa, M., 2010. Essential roles of VLA-4 in the hematopoietic system. *Int J Hematol* 91, 569–575. <https://doi.org/10/ds52r9>
- Iribarren, C., Jacobs, D.R., Sidney, S., Gross, M.D., Eisner, M.D., 2000. Cigarette smoking, alcohol consumption, and risk of ARDS: a 15-year cohort study in a managed care setting. *Chest* 117, 163–168. <https://doi.org/10/fmxx73>
- Ivetic, A., 2018. A head-to-tail view of L-selectin and its impact on neutrophil behaviour. *Cell Tissue Res* 371, 437–453. <https://doi.org/10/gc4wqj>
- Jutila, M.A., Kurk, S., 1996. Analysis of bovine gamma delta T cell interactions with E-, P-, and L-selectin. Characterization of lymphocyte on lymphocyte rolling and the effects of O-glycoprotease. *J Immunol* 156, 289–296.
- Kanwar, S., Johnston, B., Kubes, P., 1995. Leukotriene C4/D4 Induces P-Selectin and Sialyl Lewisx-Dependent Alterations in Leukocyte Kinetics In Vivo. *Circulation Research* 77, 879–887. <https://doi.org/10.1161/01.RES.77.5.879>
- Katzenstein, A.A., Askin, F.B., 1982. Surgical pathology of non-neoplastic lung disease. *Major Probl Pathol* 13, 1–430.
- Katzenstein, A.L., Myers, J.L., Mazur, M.T., 1986. Acute interstitial pneumonia. A clinicopathologic, ultrastructural, and cell kinetic study. *Am J Surg Pathol* 10, 256–267.
- Kellner, M., Noonepalle, S., Lu, Q., Srivastava, A., Zemskov, E., Black, S.M., 2017. ROS Signaling in the Pathogenesis of Acute Lung Injury (ALI) and Acute Respiratory Distress Syndrome (ARDS). *Adv Exp Med Biol* 967, 105–137. <https://doi.org/10/gm97q9>
- Kinkade, J.M., Pember, S.O., Barnes, K.C., Shapira, R., Spitznagel, J.K., Martin, L.E., 1983. Differential distribution of distinct forms of myeloperoxidase in different azurophilic granule subpopulations from human neutrophils. *Biochemical and Biophysical Research Communications* 114, 296–303. [https://doi.org/10.1016/0006-291x\(83\)91627-3](https://doi.org/10.1016/0006-291x(83)91627-3)
- Koch, J.M., Hinze-Selch, D., Stingele, K., Huchzermeier, C., Göder, R., Seeck-Hirschner, M., Aldenhoff, J.B., 2009. Changes in CREB Phosphorylation and BDNF Plasma Levels during Psychotherapy of Depression. *Psychother Psychosom* 78, 187–192. <https://doi.org/10.1159/000209350>
- Kolaczowska, E., Kubes, P., 2013. Neutrophil recruitment and function in health and inflammation. *Nat Rev Immunol* 13, 159–175. <https://doi.org/10.1038/nri3399>
- Konrad, F.M., Meichssner, N., Bury, A., Ngamsri, K.-C., Reutershan, J., 2017. Inhibition of SDF-1 receptors CXCR4 and CXCR7 attenuates acute pulmonary inflammation via the adenosine A2B-receptor on blood cells. *Cell Death Dis* 8, e2832–e2832. <https://doi.org/10/gnhcwf>
- Konrad, F.M., Wohlert, J., Gamper-Tsigaras, J., Ngamsri, K.C., Reutershan, J., 2019. How adhesion molecule patterns change while neutrophils traffic through the lung during inflammation. *Mediators of Inflammation* 2019, 1–16. <https://doi.org/10/gkgwxf>

- Konstantopoulos, K., Neelamegham, S., Burns, A.R., Hentzen, E., Kansas, G.S., Snapp, K.R., Berg, E.L., Hellums, J.D., Smith, C.W., McIntire, L.V., Simon, S.I., 1998. Venous Levels of Shear Support Neutrophil-Platelet Adhesion and Neutrophil Aggregation in Blood via P-Selectin and β 2-Integrin. *Circulation* 98, 873–882. <https://doi.org/10.1161/01.CIR.98.9.873>
- Krauss, A.H.-P., Nieves, A.L., Spada, C.S., Woodward, D.F., 1994. Determination of leukotriene effects on human neutrophil chemotaxis in vitro by differential assessment of cell motility and polarity. *J Leukoc Biol* 55, 201–208. <https://doi.org/10.1002/jlb.55.2.201>
- Kreckler, L.M., Gizewski, E., Wan, T.C., Auchampach, J.A., 2009. Adenosine Suppresses Lipopolysaccharide-Induced Tumor Necrosis Factor- α Production by Murine Macrophages through a Protein Kinase A- and Exchange Protein Activated by cAMP-Independent Signaling Pathway. *J Pharmacol Exp Ther* 331, 1051–1061. <https://doi.org/10.1124/jpet.109.157651>
- Ku, S.-K., Zhou, W., Lee, W., Han, M.-S., Na, M., Bae, J.-S., 2015. Anti-inflammatory effects of hyperoside in human endothelial cells and in mice. *Inflammation* 38, 784–799. <https://doi.org/10.1007/s10753-014-9989-8>
- Kubes, P., Niu, X.F., Smith, C.W., Kehrl, M.E., Reinhardt, P.H., Woodman, R.C., 1995. A novel beta 1-dependent adhesion pathway on neutrophils: a mechanism invoked by dihydrocytochalasin B or endothelial transmigration. *FASEB J* 9, 1103–1111.
- Kyriakis, J.M., Avruch, J., 2001. Mammalian Mitogen-Activated Protein Kinase Signal Transduction Pathways Activated by Stress and Inflammation. *Physiological Reviews* 81, 807–869. <https://doi.org/10.1152/physrev.2001.81.2.807>
- Lee, D.-K., Kim, J.-H., Kim, W.-S., Jeoung, D., Lee, H., Ha, K.-S., Won, M.-H., Kwon, Y.-G., Kim, Y.-M., 2015. Lipopolysaccharide induction of REDD1 is mediated by two distinct CREB-dependent mechanisms in macrophages. *FEBS Letters* 589, 2859–2865. <https://doi.org/10.1016/j.febslet.2015.08.004>
- Ley, K., 2007. *Adhesion molecules : function and inhibition*. Basel ; Boston : Birkhäuser.
- Ley, K., Laudanna, C., Cybulsky, M.I., Nourshargh, S., 2007. Getting to the site of inflammation: the leukocyte adhesion cascade updated. *Nat Rev Immunol* 7, 678–689. <https://doi.org/10/d3w6pn>
- Liaqat, A., Mason, M., Foster, B.J., Kulkarni, S., Barlas, A., Farooq, A.M., Patak, P., Liaqat, H., Basso, R.G., Zaman, M.S., Pau, D., 2022. Evidence-Based Mechanical Ventilatory Strategies in ARDS. *JCM* 11, 319. <https://doi.org/10.3390/jcm11020319>
- Liu, Dongfang, Bryceson, Y.T., Meckel, T., Vasiliver-Shamis, G., Dustin, M.L., Long, E.O., 2009. Integrin-Dependent Organization and Bidirectional Vesicular Traffic at Cytotoxic Immune Synapses. *Immunity* 31, 99–109. <https://doi.org/10.1016/j.immuni.2009.05.009>
- Liu, Dezhi, Ge, S., Zhou, G., Xu, G., Zhang, R., Zhu, W., Liu, Z., Cheng, S., Liu, X., 2009. Montelukast Inhibits Matrix Metalloproteinases Expression in Atherosclerotic Rabbits. *Cardiovasc Drugs Ther* 23, 431–437. <https://doi.org/10.1007/s10557-009-6211-6>
- Liu, X., Ouyang, S., Yu, B., Liu, Y., Huang, K., Gong, J., Zheng, S., Li, Z., Li, H., Jiang, H., 2010. PharmMapper server: a web server for potential drug target identification using pharmacophore mapping approach. *Nucleic Acids Res* 38, W609-614. <https://doi.org/10/fts4bn>
- Lobb, R.R., Hemler, M.E., 1994. The pathophysiologic role of alpha 4 integrins in vivo. *J. Clin. Invest.* 94, 1722–1728. <https://doi.org/10.1172/JCI117519>
- Lopez-Castejon, G., Brough, D., 2011. Understanding the mechanism of IL-1 β secretion. *Cytokine & Growth Factor Reviews* 22, 189–195. <https://doi.org/10.1016/j.cytogfr.2011.10.001>

- Lorenz, E., Jones, M., Wohlford-Lenane, C., Meyer, N., Frees, K.L., Arbour, N.C., Schwartz, D.A., 2001. Genes other than TLR4 are involved in the response to inhaled LPS. *Am J Physiol Lung Cell Mol Physiol* 281, L1106-1114. <https://doi.org/10.1152/ajplung.2001.281.5.L1106>
- Los, M., Schenk, H., Hexel, K., Baeuerle, P.A., Dröge, W., Schulze-Osthoff, K., 1995. IL-2 gene expression and NF-kappa B activation through CD28 requires reactive oxygen production by 5-lipoxygenase. *The EMBO Journal* 14, 3731–3740. <https://doi.org/10.1002/j.1460-2075.1995.tb00043.x>
- Lub, M., van Kooyk, Y., Figdor, C.G., 1996. Competition between lymphocyte function-associated antigen 1 (CD11a/CD18) and Mac-1 (CD11b/CD18) for binding to intercellular adhesion molecule-1 (CD54). *J Leukoc Biol* 59, 648–655. <https://doi.org/10.1002/jlb.59.5.648>
- Luo, W., 2022. pathview: a tool set for pathway based data integration and visualization. <https://doi.org/10.18129/B9.bioc.pathview>
- Maclouf, J.A., Murphy, R.C., 1988. Transcellular metabolism of neutrophil-derived leukotriene A4 by human platelets. A potential cellular source of leukotriene C4. *J Biol Chem* 263, 174–181.
- Mannes, G.P., Boersma, W.G., Baur, C.H., Postmus, P.E., 1991. Adult respiratory distress syndrome (ARDS) due to bacteraemic pneumococcal pneumonia. *Eur Respir J* 4, 503–504.
- Marcus, A.J., Safier, L.B., Ullman, H.L., Broekman, M.J., Islam, N., Oglesby, T.D., Gorman, R.R., 1984. 12S,20-dihydroxyicosatetraenoic acid: a new icosanoid synthesized by neutrophils from 12S-hydroxyicosatetraenoic acid produced by thrombin- or collagen-stimulated platelets. *Proc. Natl. Acad. Sci. U.S.A.* 81, 903–907. <https://doi.org/10.1073/pnas.81.3.903>
- Marcus, A.J., Safier, L.B., Ullman, H.L., Islam, N., Broekman, M.J., Falck, J.R., Fischer, S., von Schacky, C., 1988. Platelet-neutrophil interactions. (12S)-hydroxyeicosatetraen-1,20-dioic acid: a new eicosanoid synthesized by unstimulated neutrophils from (12S)-20-dihydroxyeicosatetraenoic acid. *J Biol Chem* 263, 2223–2229.
- Martin, C., Burdon, P.C.E., Bridger, G., Gutierrez-Ramos, J.-C., Williams, T.J., Rankin, S.M., 2003. Chemokines Acting via CXCR2 and CXCR4 Control the Release of Neutrophils from the Bone Marrow and Their Return following Senescence. *Immunity* 19, 583–593. <https://doi.org/10/bjq8rx>
- Matthay, M.A., Zemans, R.L., Zimmerman, G.A., Arabi, Y.M., Beitler, J.R., Mercat, A., Herridge, M., Randolph, A.G., Calfee, C.S., 2018. Acute respiratory distress syndrome. *Nature Reviews Disease Primers* 5. <https://doi.org/10/gg6czt>
- Matute-Bello, G., Matthay, M., 2008. Animal Models of Acute Lung Injury [WWW Document]. URL <https://www.thoracic.org/professionals/clinical-resources/critical-care/critical-care-research/animal-models-of-acute-lung-injury.php> (accessed 7.29.22).
- McIntyre, T.M., Zimmerman, G.A., Prescott, S.M., 1986. Leukotrienes C4 and D4 stimulate human endothelial cells to synthesize platelet-activating factor and bind neutrophils. *Proc Natl Acad Sci U S A* 83, 2204–2208.
- McKenna, E., Mhaonaigh, A.U., Wubben, R., Dwivedi, A., Hurley, T., Kelly, L.A., Stevenson, N.J., Little, M.A., Molloy, E.J., 2021. Neutrophils: Need for Standardized Nomenclature. *Front. Immunol.* 12. <https://doi.org/10.3389/fimmu.2021.602963>
- Meliton, A.Y., Muñoz, N.M., Osan, C.M., Meliton, L.N., Leff, A.R., 2010. Leukotriene D4 activates β 2-integrin adhesion in human polymorphonuclear leukocytes. *European Respiratory Journal* 35, 402–409. <https://doi.org/10/bmk4px>

- Ménard, G., Bissonnette, E.Y., 2000. Priming of Alveolar Macrophages by Leukotriene D4 Potentiation of Inflammation. *Am J Respir Cell Mol Biol* 23, 572–577. <https://doi.org/10.1165/ajrcmb.23.4.4152>
- Metzemaekers, M., Gouwy, M., Proost, P., 2020. Neutrophil chemoattractant receptors in health and disease: double-edged swords. *Cell Mol Immunol* 17, 433–450. <https://doi.org/10.1038/s41423-020-0412-0>
- Mine, S., FUJISAKI, T., SUEMATSU, M., TANAKA, Y., 2001. Activated Platelets and Endothelial Cell Interaction with Neutrophils under Flow Conditions. *Intern. Med.* 40, 1085–1092. <https://doi.org/10.2169/internalmedicine.40.1085>
- Moore, F.A., Moore, E.E., Read, R.A., 1993. Postinjury multiple organ failure: role of extrathoracic injury and sepsis in adult respiratory distress syndrome. *New Horiz* 1, 538–549.
- Nagasawa, T., 2015. CXCL12/SDF-1 and CXCR4. *Front. Immunol.* 6. <https://doi.org/10.3389/fimmu.2015.00301>
- Nakamura, M., Shimizu, T., 2011. Leukotriene receptors. *Chem Rev* 111, 6231–6298. <https://doi.org/10.1021/cr100392s>
- Nijnik, A., Pistolic, J., Filewod, N.C.J., Hancock, R.E.W., 2012. Signaling Pathways Mediating Chemokine Induction in Keratinocytes by Cathelicidin LL-37 and Flagellin. *J Innate Immun* 4, 377–386. <https://doi.org/10.1159/000335901>
- Oliveira, S.H.P., Canetti, C., Ribeiro, R.A., Cunha, F.Q., 2008. Neutrophil Migration Induced by IL-1 β Depends upon LTB₄ Released by Macrophages and upon TNF- α and IL-1 β Released by Mast Cells. *Inflammation* 31, 36–46. <https://doi.org/10.1007/s10753-007-9047-x>
- Ortiz-Stern, A., Rosales, C., 2003. Cross-talk between Fc receptors and integrins. *Immunology Letters* 90, 137–143. <https://doi.org/10.1016/j.imlet.2003.08.004>
- Øynebråten, I., Barois, N., Hagelsteen, K., Johansen, F.-E., Bakke, O., Haraldsen, G., 2005. Characterization of a novel chemokine-containing storage granule in endothelial cells: evidence for preferential exocytosis mediated by protein kinase A and diacylglycerol. *J Immunol* 175, 5358–5369. <https://doi.org/10/gpgb8t>
- Page, C., Pitchford, S., 2013. Neutrophil and platelet complexes and their relevance to neutrophil recruitment and activation. *International Immunopharmacology* 17, 1176–1184. <https://doi.org/10/f5m85h>
- Palmblad, J., Lerner, R., Larsson, S.H., 1994. Signal transduction mechanisms for leukotriene B₄ induced hyperadhesiveness of endothelial cells for neutrophils. *J Immunol* 152, 262–269.
- Pan, J., Xia, L., McEver, R.P., 1998. Comparison of promoters for the murine and human P-selectin genes suggests species-specific and conserved mechanisms for transcriptional regulation in endothelial cells. *J Biol Chem* 273, 10058–10067. <https://doi.org/10.1074/jbc.273.16.10058>
- Park, J.M., Greten, F.R., Wong, A., Westrick, R.J., Arthur, J.S.C., Otsu, K., Hoffmann, A., Montminy, M., Karin, M., 2005. Signaling Pathways and Genes that Inhibit Pathogen-Induced Macrophage Apoptosis— CREB and NF- κ B as Key Regulators. *Immunity* 23, 319–329. <https://doi.org/10.1016/j.immuni.2005.08.010>
- Patricia, M.K., Kim, J.A., Harper, C.M., Shih, P.T., Berliner, J.A., Natarajan, R., Nadler, J.L., Hedrick, C.C., 1999. Lipoxygenase Products Increase Monocyte Adhesion to Human Aortic Endothelial Cells. *ATVB* 19, 2615–2622. <https://doi.org/10.1161/01.atv.19.11.2615>
- Pedersen, K.E., Bochner, B.S., Undem, B.J., 1997. Cysteinyl Leukotrienes Induce P-Selectin Expression in Human Endothelial Cells via a Non-CysLT₁ Receptor-Mediated Mechanism. *J Pharmacol Exp Ther* 281, 655–662.
- Pepe, P.E., Potkin, R.T., Reus, D.H., Hudson, L.D., Carrico, C.J., 1982. Clinical predictors of the adult respiratory distress syndrome. *Am J Surg* 144, 124–130. <https://doi.org/10/bkgnp6>

- Petrides, P.E., Dittmann, K.H., 1990. How do normal and leukemic white blood cells egress from the bone marrow? *Blut* 61, 3–13. <https://doi.org/10.1007/BF01739426>
- Pfeifer, R., Heussen, N., Michalewicz, E., Hilgers, R.-D., Pape, H.-C., 2017. Incidence of adult respiratory distress syndrome in trauma patients: A systematic review and meta-analysis over a period of three decades. *J Trauma Acute Care Surg* 83, 496–506. <https://doi.org/10/gpbrx6>
- Phillipson, M., Heit, B., Colarusso, P., Liu, L., Ballantyne, C.M., Kubes, P., 2006. Intraluminal crawling of neutrophils to emigration sites: a molecularly distinct process from adhesion in the recruitment cascade. *J Exp Med* 203, 2569–2575. <https://doi.org/10.1084/jem.20060925>
- Pluskota, E., Woody, N.M., Szpak, D., Ballantyne, C.M., Soloviev, D.A., Simon, D.I., Plow, E.F., 2008. Expression, activation, and function of integrin $\alpha\text{M}\beta\text{2}$ (Mac-1) on neutrophil-derived microparticles. *Blood* 112, 2327–2335. <https://doi.org/10.1182/blood-2007-12-127183>
- Porreca, E., Conti, P., Feliciani, C., Di Febbo, C., Reale, M., Mincione, G., Neri, M., Amerio, P., Cuccurullo, F., 1995. Cysteinyl-leukotriene D4 induced IL-1 β expression and release in rat vascular smooth muscle cells. *Atherosclerosis* 115, 181–189. [https://doi.org/10.1016/0021-9150\(94\)05510-P](https://doi.org/10.1016/0021-9150(94)05510-P)
- PubChem, n.d. PubChem [WWW Document]. URL <https://pubchem.ncbi.nlm.nih.gov/> (accessed 12.15.21).
- Puneet, P., Mochhala, S., Bhatia, M., 2005. Chemokines in acute respiratory distress syndrome. *Am J Physiol Lung Cell Mol Physiol* 288, L3-15. <https://doi.org/10/c56xk2>
- Rahman, I., Collado Sánchez, A., Davies, J., Rzeniewicz, K., Abukssem, S., Joachim, J., Hoskins Green, H.L., Killock, D., Sanz, M.J., Charras, G., Parsons, M., Ivetic, A., 2021. L-selectin regulates human neutrophil transendothelial migration. *Journal of Cell Science* 134, jcs250340. <https://doi.org/10/gjv7xx>
- Rainer, T.H., 2002. L-selectin in health and disease. *Resuscitation* 52, 127–141. [https://doi.org/10.1016/S0300-9572\(01\)00444-0](https://doi.org/10.1016/S0300-9572(01)00444-0)
- Ramos, B.F., Zhang, Y., Qureshi, R., Jakschik, B.A., 1991. Mast cells are critical for the production of leukotrienes responsible for neutrophil recruitment in immune complex-induced peritonitis in mice. *J Immunol* 147, 1636–1641.
- Reinhardt, P.H., Elliott, J.F., Kubes, P., 1997. Neutrophils can adhere via $\alpha\text{4}\beta\text{1}$ -integrin under flow conditions. *Blood* 89, 3837–3846.
- Reutershan, J., Basit, A., Galkina, E.V., Ley, K., 2005. Sequential recruitment of neutrophils into lung and bronchoalveolar lavage fluid in LPS-induced acute lung injury. *American Journal of Physiology-Lung Cellular and Molecular Physiology* 289, L807–L815. <https://doi.org/10/fpd98b>
- Rivera-Nieves, J., Burcin, T.L., Olson, T.S., Morris, M.A., McDuffie, M., Cominelli, F., Ley, K., 2006. Critical role of endothelial P-selectin glycoprotein ligand 1 in chronic murine ileitis. *J Exp Med* 203, 907–917. <https://doi.org/10.1084/jem.20052530>
- Riviello, E.D., Kiviri, W., Twagirumugabe, T., Mueller, A., Banner-Goodspeed, V.M., Officer, L., Novack, V., Mutumwinka, M., Talmor, D.S., Fowler, R.A., 2016. Hospital Incidence and Outcomes of the Acute Respiratory Distress Syndrome Using the Kigali Modification of the Berlin Definition. *Am J Respir Crit Care Med* 193, 52–59. <https://doi.org/10/f753bd>
- Rola-Pleszczynski, M., Stankova, J., 1992. Leukotriene B4 enhances interleukin-6 (IL-6) production and IL-6 messenger RNA accumulation in human monocytes in vitro: transcriptional and posttranscriptional mechanisms. *Blood* 80, 1004–1011. <https://doi.org/10.1182/blood.V80.4.1004.1004>

- Rossaint, J., Herter, J.M., Van Aken, H., Napirei, M., Döring, Y., Weber, C., Soehnlein, O., Zarbock, A., 2014. Synchronized integrin engagement and chemokine activation is crucial in neutrophil extracellular trap-mediated sterile inflammation. *Blood* 123, 2573–2584. <https://doi.org/10.1182/blood-2013-07-516484>
- Rossaint, J., Kühne, K., Skupski, J., Van Aken, H., Looney, M.R., Hidalgo, A., Zarbock, A., 2016. Directed transport of neutrophil-derived extracellular vesicles enables platelet-mediated innate immune response. *Nat Commun* 7, 13464. <https://doi.org/10/f9bz5m>
- Roy, B., Paul, L., 2004. Higher versus Lower Positive End-Expiratory Pressures in Patients with the Acute Respiratory Distress Syndrome. *N Engl J Med* 351, 327–336. <https://doi.org/10.1056/NEJMoa032193>
- Rubinfeld, G.D., Caldwell, E., Granton, J., Hudson, L.D., Matthay, M.A., 1999. Interobserver variability in applying a radiographic definition for ARDS. *Chest* 116, 1347–1353. <https://doi.org/10/b8cknd>
- Rubinfeld, G.D., Caldwell, E., Peabody, E., Weaver, J., Martin, D.P., Neff, M., Stern, E.J., Hudson, L.D., 2005. Incidence and outcomes of acute lung injury. *N Engl J Med* 353, 1685–1693. <https://doi.org/10/dnhsfd>
- Sadik, C.D., Kim, N.D., Luster, A.D., 2011. Neutrophils cascading their way to inflammation. *Trends Immunol* 32, 452–460. <https://doi.org/10.1016/j.it.2011.06.008>
- Samuelsson, B., Borgeat, P., Hammarström, S., Robert, M., 1980. Leukotrienes: a new group of biologically active compounds. *Advances in prostaglandin and thromboxane research* 6, 1–18.
- Sasaki, F., Yokomizo, T., 2019. The leukotriene receptors as therapeutic targets of inflammatory diseases. *Int Immunol* 31, 607–615. <https://doi.org/10/gpcbh9>
- Sawant, K.V., Poluri, K.M., Dutta, A.K., Sepuru, K.M., Troshkina, A., Garofalo, R.P., Rajarathnam, K., 2016. Chemokine CXCL1 mediated neutrophil recruitment: Role of glycosaminoglycan interactions. *Sci Rep* 6, 33123. <https://doi.org/10/f83rkm>
- Schenkel, A.R., Mamdouh, Z., Muller, W.A., 2004. Locomotion of monocytes on endothelium is a critical step during extravasation. *Nat Immunol* 5, 393–400. <https://doi.org/10.1038/ni1051>
- Schönbeck, U., Mach, F., Libby, P., 1998. Generation of biologically active IL-1 beta by matrix metalloproteinases: a novel caspase-1-independent pathway of IL-1 beta processing. *J Immunol* 161, 3340–3346.
- Semerad, C.L., Liu, F., Gregory, A.D., Stumpf, K., Link, D.C., 2002. G-CSF Is an Essential Regulator of Neutrophil Trafficking from the Bone Marrow to the Blood. *Immunity* 17, 413–423. [https://doi.org/10.1016/s1074-7613\(02\)00424-7](https://doi.org/10.1016/s1074-7613(02)00424-7)
- Shames, R.S., Goetzl, E.J., 1993. Activation of human neutrophil LFA-1 (CD11a) by leukotriene B4. *Inflammation* 17, 371–382. <https://doi.org/10.1007/BF00918998>
- Shamri, R., Grabovsky, V., Gauguier, J.-M., Feigelson, S., Manevich, E., Kolanus, W., Robinson, M.K., Staunton, D.E., von Andrian, U.H., Alon, R., 2005. Lymphocyte arrest requires instantaneous induction of an extended LFA-1 conformation mediated by endothelium-bound chemokines. *Nat Immunol* 6, 497–506. <https://doi.org/10.1038/ni1194>
- Shi, S., Yang, W., Tu, X., Wang, C., Chen, C., Chen, Y., 2013. 5-Lipoxygenase inhibitor zileuton inhibits neuronal apoptosis following focal cerebral ischemia. *Inflammation* 36, 1209–1217. <https://doi.org/10/f5gg97>
- Showell, H.J., Conklyn, M.J., Alpert, R., Hingorani, G.P., Wright, K.F., Smith, M.A., Stam, E., Salter, E.D., Scampoli, D.N., Meltzer, S., Reiter, L.A., Koch, K., Piscopio, A.D., Cortina, S.R., Lopez-Anaya, A., Pettipher, E.R., Milici, A.J., Griffiths, R.J., 1998. The preclinical pharmacological profile of the potent and selective leukotriene B4 antagonist CP-195543. *J Pharmacol Exp Ther* 285, 946–954.

- Siegel, M., 2019. Acute respiratory distress syndrome: Clinical features, diagnosis, and complications in adults. Waltham, MA: UpToDate.[Google Scholar].
- Siegel, M.D., 2016. Acute respiratory distress syndrome: Epidemiology, pathophysiology, pathology, and etiology in adults. UpToDate. Waltham, MA.
- Simon, D.I., Chen, Z., Xu, H., Li, C.Q., Dong, J. f, McIntire, L.V., Ballantyne, C.M., Zhang, L., Furman, M.I., Berndt, M.C., López, J.A., 2000. Platelet glycoprotein Ibalpha is a counterreceptor for the leukocyte integrin Mac-1 (CD11b/CD18). *J Exp Med* 192, 193–204. <https://doi.org/10.1084/jem.192.2.193>
- Smith, P.K., Krohn, R.I., Hermanson, G.T., Mallia, A.K., Gartner, F.H., Provenzano, M.D., Fujimoto, E.K., Goeke, N.M., Olson, B.J., Klenk, D.C., 1985. Measurement of protein using bicinchoninic acid. *Analytical Biochemistry* 150, 76–85. [https://doi.org/10.1016/0003-2697\(85\)90442-7](https://doi.org/10.1016/0003-2697(85)90442-7)
- Soberman, R.J., Christmas, P., 2003. The organization and consequences of eicosanoid signaling. *J Clin Invest* 111, 1107–1113. <https://doi.org/10.1172/JCI18338>
- Stadtman, A., Germena, G., Block, H., Boras, M., Rossaint, J., Sundd, P., Lefort, C., Fisher, C.I., Buscher, K., Gelschefarth, B., Urzainqui, A., Gerke, V., Ley, K., Zarbock, A., 2013. The PSGL-1–L-selectin signaling complex regulates neutrophil adhesion under flow. *J Exp Med* 210, 2171–2180. <https://doi.org/10.1084/jem.20130664>
- Standiford, T.J., Ward, P.A., 2016. Therapeutic Targeting of Acute Lung Injury and ARDS. *Transl Res* 167, 183–191. <https://doi.org/10/f752dc>
- Steblyanko, M., Anikeeva, N., Campbell, K.S., Keen, J.H., Sykulev, Y., 2015. Integrins Influence the Size and Dynamics of Signaling Microclusters in a Pyk2-dependent Manner. *Journal of Biological Chemistry* 290, 11833–11842. <https://doi.org/10.1074/jbc.M114.614719>
- Steiner, D.R.S., Gonzalez, N.C., Wood, J.G., 2001. Leukotriene B4 promotes reactive oxidant generation and leukocyte adherence during acute hypoxia. *Journal of Applied Physiology* 91, 1160–1167. <https://doi.org/10.1152/jappl.2001.91.3.1160>
- Sun, Y., Zhang, H., Wu, Z., Yu, X., Yin, Y., Qian, S., Wang, Z., Huang, J., Wang, W., Liu, T., Xue, W., Chen, G., 2021. Quercitrin Rapidly Alleviated Depression-like Behaviors in Lipopolysaccharide-Treated Mice: The Involvement of PI3K/AKT/NF- κ B Signaling Suppression and CREB/BDNF Signaling Restoration in the Hippocampus. *ACS Chem. Neurosci.* 12, 3387–3396. <https://doi.org/10.1021/acschemneuro.1c00371>
- Sutyak, J.P., Wohltmann, C.D., Larson, J., 2007. Pulmonary contusions and critical care management in thoracic trauma. *Thorac Surg Clin* 17, 11–23, v. <https://doi.org/10/ffjt63>
- Swenson, K.E., Swenson, E.R., 2021. Pathophysiology of Acute Respiratory Distress Syndrome and COVID-19 Lung Injury. *Critical Care Clinics* 37, 749–776. <https://doi.org/10.1016/j.ccc.2021.05.003>
- Tager, A.M., Dufour, J.H., Goodarzi, K., Bercury, S.D., von Andrian, U.H., Luster, A.D., 2000. BLTR mediates leukotriene B(4)-induced chemotaxis and adhesion and plays a dominant role in eosinophil accumulation in a murine model of peritonitis. *J Exp Med* 192, 439–446. <https://doi.org/10.1084/jem.192.3.439>
- Tanaka, T., Narazaki, M., Kishimoto, T., 2014. IL-6 in Inflammation, Immunity, and Disease. *Cold Spring Harb Perspect Biol* 6, a016295. <https://doi.org/10.1101/cshperspect.a016295>
- Thornberry, N.A., Bull, H.G., Calaycay, J.R., Chapman, K.T., Howard, A.D., Kostura, M.J., Miller, D.K., Molineaux, S.M., Weidner, J.R., Aunins, J., Elliston, K.O., Ayala, J.M., Casano, F.J., Chin, J., Ding, G.J.-F., Egger, L.A., Gaffney, E.P., Limjuco, G., Palyha, O.C., Raju, S.M., Rolando, A.M., Salley, J.P., Yamin, T.-T., Lee, T.D., Shively, J.E., MacCross, M., Mumford, R.A., Schmidt, J.A., Tocci, M.J., 1992. A novel heterodimeric cysteine protease is required for interleukin-

- 1 β processing in monocytes. *Nature* 356, 768–774. <https://doi.org/10.1038/356768a0>
- Tietjen, P.A., Kaner, R.J., Quinn, C.E., 1994. Aspiration emergencies. *Clin Chest Med* 15, 117–135.
- Tintinger, G.R., Feldman, C., Theron, A.J., Anderson, R., 2010. Montelukast: More than a Cysteinyl Leukotriene Receptor Antagonist? *The Scientific World JOURNAL* 10, 2403–2413. <https://doi.org/10/c824vk>
- Tomashefski, J.F., 1990. Pulmonary pathology of the adult respiratory distress syndrome. *Clin Chest Med* 11, 593–619.
- Tu, X.-K., Yang, W.-Z., Shi, S.-S., Chen, C.-M., Wang, C.-H., 2009. 5-lipoxygenase inhibitor zileuton attenuates ischemic brain damage: involvement of matrix metalloproteinase 9. *Neurol Res* 31, 848–852. <https://doi.org/10/b7nhjf>
- Tzotzos, S.J., Fischer, B., Fischer, H., Zeitlinger, M., 2020. Incidence of ARDS and outcomes in hospitalized patients with COVID-19: a global literature survey. *Crit Care* 24, 516. <https://doi.org/10/gh294r>
- US Food and Drug Administration, 2020. FDA requires Boxed Warning about serious mental health side effects for asthma and allergy drug montelukast (Singulair); advises restricting use for allergic rhinitis. FDA.
- Vaddi, K., Newton, R.C., 1994. Regulation of monocyte integrin expression by beta-family chemokines. *J Immunol* 153, 4721–4732.
- Venturi, G.M., Tu, L., Kadono, T., Khan, A.I., Fujimoto, Y., Oshel, P., Bock, C.B., Miller, A.S., Albrecht, R.M., Kubes, P., Steeber, D.A., Tedder, T.F., 2003. Leukocyte migration is regulated by L-selectin endoproteolytic release. *Immunity* 19, 713–724. [https://doi.org/10.1016/s1074-7613\(03\)00295-4](https://doi.org/10.1016/s1074-7613(03)00295-4)
- Vieira, S., Lemos, H., Grespan, R., Napimoga, M., Dal-Secco, D., Freitas, A., Cunha, T., Verri Jr, W., Souza-Junior, D., Jamur, M., Fernandes, K., Oliver, C., Silva, J., Teixeira, M., Cunha, F., 2009. A crucial role for TNF- α in mediating neutrophil influx induced by endogenously generated or exogenous chemokines, KC/CXCL1 and LIX/CXCL5. *Br J Pharmacol* 158, 779–789. <https://doi.org/10.1111/j.1476-5381.2009.00367.x>
- Walcheck, Bruce, Kahn, J., Fisher, J.M., Wang, B.B., Fisk, R.S., Payan, D.G., Feehan, C., Betageri, R., Darlak, K., Spatola, A.F., Kishimoto, T.K., 1996. Neutrophil rolling altered by inhibition of L-selectin shedding in vitro. *Nature* 380, 720–723. <https://doi.org/10.1038/380720a0>
- Walcheck, B., Moore, K.L., McEver, R.P., Kishimoto, T.K., 1996. Neutrophil-neutrophil interactions under hydrodynamic shear stress involve L-selectin and PSGL-1. A mechanism that amplifies initial leukocyte accumulation of P-selectin in vitro. *J Clin Invest* 98, 1081–1087. <https://doi.org/10.1172/JCI118888>
- Wang, X., Shen, Y., Wang, S., Li, S., Zhang, W., Liu, X., Lai, L., Pei, J., Li, H., 2017. PharmMapper 2017 update: a web server for potential drug target identification with a comprehensive target pharmacophore database. *Nucleic Acids Res* 45, W356–W360. <https://doi.org/10/gbmz37>
- Winterbourn, C.C., Hampton, M.B., Livesey, J.H., Kettle, A.J., 2006. Modeling the Reactions of Superoxide and Myeloperoxidase in the Neutrophil Phagosome. *Journal of Biological Chemistry* 281, 39860–39869. <https://doi.org/10.1074/jbc.M605898200>
- Woo, C.-H., Eom, Y.-W., Yoo, M.-H., You, H.-J., Han, H.J., Song, W.K., Yoo, Y.J., Chun, J.-S., Kim, J.-H., 2000. Tumor Necrosis Factor- α Generates Reactive Oxygen Species via a Cytosolic Phospholipase A2-linked Cascade. *Journal of Biological Chemistry* 275, 32357–32362. <https://doi.org/10.1074/jbc.M005638200>
- Woo, C.-H., You, H.-J., Cho, S.-H., Eom, Y.-W., Chun, J.-S., Yoo, Y.-J., Kim, J.-H., 2002. Leukotriene B4 Stimulates Rac-ERK Cascade to Generate Reactive Oxygen

- Species That Mediates Chemotaxis. *Journal of Biological Chemistry* 277, 8572–8578. <https://doi.org/10.1074/jbc.M104766200>
- World Health Organization, 2022. WHO Coronavirus (COVID-19) Dashboard [WWW Document]. URL <https://covid19.who.int> (accessed 1.13.22).
- Xue, L., Fergusson, J., Salimi, M., Panse, I., Ussher, J.E., Hegazy, A.N., Vinall, S.L., Jackson, D.G., Hunter, M.G., Pettipher, R., Ogg, G., Klenerman, P., 2015. Prostaglandin D2 and leukotriene E4 synergize to stimulate diverse TH2 functions and TH2 cell/neutrophil crosstalk. *Journal of Allergy and Clinical Immunology* 135, 1358–1366.e11. <https://doi.org/10.1016/j.jaci.2014.09.006>
- Yago, T., Shao, B., Miner, J.J., Yao, L., Klopocki, A.G., Maeda, K., Coggeshall, K.M., McEver, R.P., 2010. E-selectin engages PSGL-1 and CD44 through a common signaling pathway to induce integrin $\alpha\text{L}\beta\text{2}$ -mediated slow leukocyte rolling. *Blood* 116, 485–494. <https://doi.org/10.1182/blood-2009-12-259556>
- Yang, S.-C., Chen, P.-J., Chang, S.-H., Weng, Y.-T., Chang, F.-R., Chang, K.-Y., Chen, C.-Y., Kao, T.-I., Hwang, T.-L., 2018. Luteolin attenuates neutrophilic oxidative stress and inflammatory arthritis by inhibiting Raf1 activity. *Biochem Pharmacol* 154, 384–396. <https://doi.org/10.1016/j.bcp.2018.06.003>
- Yokomizo, T., Nakamura, M., Shimizu, T., 2018. Leukotriene receptors as potential therapeutic targets. *Journal of Clinical Investigation* 128, 2691–2701. <https://doi.org/10/gkgwxb>
- Yuan, Y.-M., Fang, S.-H., Qian, X.-D., Liu, L.-Y., Xu, L.-H., Shi, W.-Z., Zhang, L.-H., Lu, Y.-B., Zhang, W.-P., Wei, E.-Q., 2009. Leukotriene D4 stimulates the migration but not proliferation of endothelial cells mediated by the cysteinyl leukotriene cyslt(1) receptor via the extracellular signal-regulated kinase pathway. *J Pharmacol Sci* 109, 285–292. <https://doi.org/10/c92w4c>
- Zarbock, A., Ley, K., McEver, R.P., Hidalgo, A., 2011. Leukocyte ligands for endothelial selectins: specialized glycoconjugates that mediate rolling and signaling under flow. *Blood* 118, 6743–6751. <https://doi.org/10.1182/blood-2011-07-343566>
- Zarbock, A., Müller, H., Kuwano, Y., Ley, K., 2009. PSGL-1-dependent myeloid leukocyte activation. *Journal of Leukocyte Biology* 86, 1119–1124. <https://doi.org/10.1189/jlb.0209117>
- Zarbock, A., Singbartl, K., Ley, K., 2006. Complete reversal of acid-induced acute lung injury by blocking of platelet-neutrophil aggregation. *Journal of Clinical Investigation* 116, 3211–3219. <https://doi.org/10/bq67bk>
- Zemans, R.L., Matthay, M.A., 2017. What drives neutrophils to the alveoli in ARDS? *Thorax* 72, 1–3. <https://doi.org/10/gmps5v>
- Zhang, Y., Zhai, Q., Luo, Y., Dorf, M.E., 2002. RANTES-mediated Chemokine Transcription in Astrocytes Involves Activation and Translocation of p90 Ribosomal S6 Protein Kinase (RSK). *Journal of Biological Chemistry* 277, 19042–19048. <https://doi.org/10.1074/jbc.M112442200>
- Zhou, M.-T., Chen, C.-S., Chen, B.-C., Zhang, Q.-Y., Andersson, R., 2010. Acute lung injury and ARDS in acute pancreatitis: Mechanisms and potential intervention. *World J Gastroenterol* 16, 2094–2099. <https://doi.org/10/b9z3hm>
- Zhou, X., Dai, Q., Huang, X., 2012. Neutrophils in acute lung injury. *Front Biosci (Landmark Ed)* 17, 2278–2283. <https://doi.org/10.2741/4051>
- Zou, X., Shinde Patil, V.R., Dagia, N.M., Smith, L.A., Wargo, M.J., Interliggi, K.A., Lloyd, C.M., Tees, D.F.J., Walcheck, B., Lawrence, M.B., Goetz, D.J., 2005. PSGL-1 derived from human neutrophils is a high-efficiency ligand for endothelium-expressed E-selectin under flow. *American Journal of Physiology-Cell Physiology* 289, C415–C424. <https://doi.org/10.1152/ajpcell.00289.2004>

8 Declaration of Contributions

This work was performed at the Research Center of Anesthesiology and Critical Care Medicine of Tübingen University under the supervision of PD Dr. Franziska Konrad. The study was designed in collaboration with PD Dr. Franziska Konrad, Dr. Kristian-Christos Ngamsri, and Anika Fuhr.

Animal operations were performed in collaboration with Dr. Kristian-Christos Ngamsri or Anika Fuhr. Other experiments were carried out by myself independently after training by Dr. Kristian-Christos Ngamsri, Anika Fuhr, and qualified technician assistant Ms. Jutta Gamper-Tsigaras.

The statistical analysis was carried out independently by myself.

I assure you that the manuscript was written by myself.

9 Acknowledgements

First of all, I would like to thank my supervisor, PD. Dr. Franziska Konrad sincerely for providing me with the opportunity to do research in her group. I am very grateful for her guidance, patience, and continuous support. She helped me develop the right attitude toward scientific research.

Thanks to Kristian for his patience in guiding me at the beginning of my research and for his encouragement when I encountered setbacks, telling me the truth that the road to science is full of ups and downs, twists and turns.

During these years, I spent more time working or in the same office with Anika than with my family and other friends, which gave me a feeling of family. I am so happy that I have the opportunity to witness the birth of her baby. I wish this new life a healthy and happy growth.

Many thanks to Jutta, who was always patient and detailed in my training. I want to thank Michaela for always going out of her way to help me whenever I could not find something. She is the person who smiled at me the most in the lab and made me feel warm. I would like to extend my sincere thanks to my colleagues Anna, Michelle, Robin, Tobias, Mariana, and Meike. I am a man of few words. But with them, I feel a lot of comfort and joy.

Special thanks to Linyan Tang and her family. During my most challenging time, Linyan comforted, encouraged, and supported me. Without her, I could not have made it this far.

It is high time to express my gratitude to my parents! I grew up with their constant care and love. Although they get older with gray hair and wrinkles, they never lose their dignity in both life and work. I wish they could always be happy and healthy.

Last but not least, I would like to thank the CSC (China Scholarship Council) for their financial support during these three years of my study in Germany. Without this funding, I would not be able to complete my project.